

MECHANICAL PROPERTIES OF
ALPHA-BETA BRASS-STUDIES
ON MODEL SYSTEMS

Thesis for the Degree of Ph. D.
MICHIGAN STATE UNIVERSITY
CHRIS FREDERICK NILSEN
1973



This is to certify that the
thesis entitled
MECHANICAL PROPERTIES OF ALPHA-BETA BRASS-
STUDIES ON MODEL SYSTEMS

presented by
CHRIS FREDERICK NILSEN

has been accepted towards fulfillment
of the requirements for

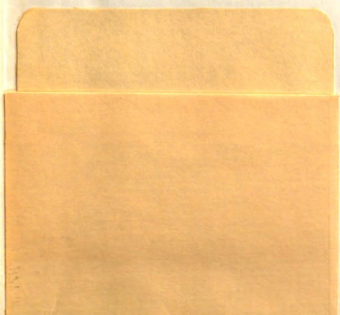
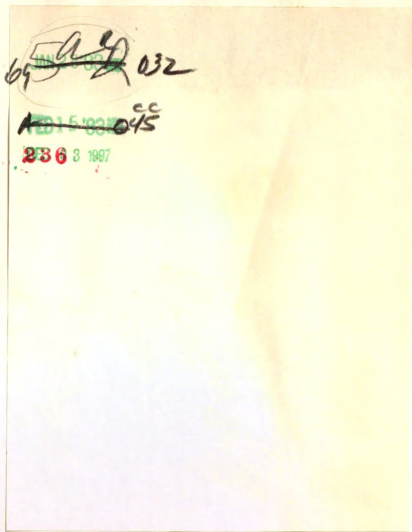
Ph.D. degree in Metallurgy

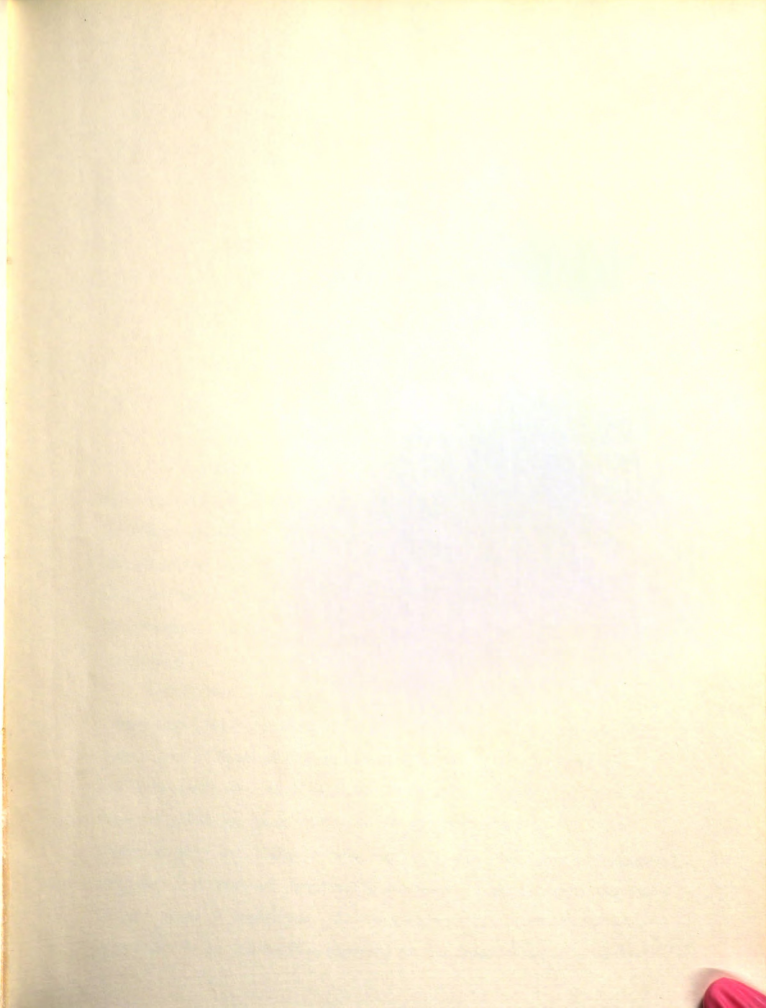
S. N. Subramanian

Major professor

Date June 19, 1973







THE MECHANICAL PROPERTIES OF

ALPHA-BETA BRASS

BY J. W. M. H. VAN DER

W. J. VAN DER

ABSTRACT

THE MECHANICAL PROPERTIES OF

MECHANICAL PROPERTIES OF ALPHA-BETA BRASS

STUDIES ON MODEL SYSTEMS

THE MECHANICAL PROPERTIES OF

THE MECHANICAL PROPERTIES OF

THE MECHANICAL PROPERTIES OF

THE MECHANICAL PROPERTIES OF

THE MECHANICAL PROPERTIES OF

The mechanical properties of two-phase materials are affected by slip interactions at phase boundaries and by the properties of the individual phases. Fundamental studies on two-phase materials can be carried out on a model system that consists of a single crystal of one phase joined to a large single crystal, or a few large crystals, of the second phase. Such specimens may be called bicrystals or multicrystals, respectively.

Indentation testing and strain-rate tests were carried out using alpha-beta brass specimens having four types of boundary geometries. These types of boundaries were oriented duplex, flat, corrugated, and equiaxed (unoriented) duplex. The equiaxed duplex type of interface structure was found to be the strongest in blocking the propagation of slip from alpha to beta regions in the four types of interfaces studied. A strain-rate sensitivity was found in the bicrystal specimens for all types of boundaries. At low strain-rate, all of the boundaries were found to be ineffective barriers to the propagation of slip and

deformation. At high strain-rates, all of the boundaries fully resisted the passage of deformation. At low strain-rates coarse slip was observed, while at high-strain rates fine slip occurred in the alpha phase. Dislocation modelling

ABSTRACT

have been employed to explain the observed mechanical behavior of these model systems. Indentation tests performed on

MECHANICAL PROPERTIES OF ALPHA-BETA BRASS -

STUDIES ON MODEL SYSTEMS

that are slip generated in these tests. Rather, the deformation created by the indentation stress concentration was accommodated in the alpha phase of the microalloy.

by

In the course of the investigation, microstructural changes of deformed specimens were studied using metallographic and scanning electron microscopic techniques.

CHRIS FREDERICK NILSEN

The mechanical properties of two-phase materials are affected by slip interactions at phase boundaries and by the properties of the individual phases. Fundamental studies on two-phase materials can be carried out on a model system that consists of a single crystal of one phase joined to a large single crystal, or a few large crystals, of the second phase. Such specimens may be called bicrystals or multicrystals, respectively.

Indentation testing and strain-rate tests were carried out using alpha-beta brass specimens having four types of boundary geometries. These types of boundaries were oriented duplex, flat, corrugated, and equiaxed (unoriented) duplex. The equiaxed duplex type of interface structure was found to be the strongest in blocking the propagation of slip from alpha to beta regions in the four types of interfaces studied. A strain-rate sensitivity was found in the bicrystal specimens for all types of boundaries. At low strain-rate, all of the boundaries were found to be ineffective barriers to the propagation of slip and

deformation. At high strain-rates, all of the boundaries fully resisted the passage of deformation. At low strain-rates coarse slip was observed, while at high-strain rates fine slip occurred in the alpha phase. Dislocation modelling methods have been employed to explain the observed mechanical behavior of these model systems. Indentation tests performed on three of the types of boundaries indicated that the slip generated in these tests was fine, and it did not effectively react with the boundary. Rather, the deformation created by the indentation stress concentration was accommodated in the alpha phase of the bicrystal.

In the course of the investigation, microstructural studies of deformed specimens were carried out with optical and scanning electron microscopic techniques.

Submitted to
Michigan State University
in partial fulfillment of the requirements
for the degree of

DOCTOR OF PHILOSOPHY

Department of Metallurgy, Mechanics and Materials Science

1973

MECHANICAL PROPERTIES OF ALPHA-BETA BRASS- STUDIES ON MODEL SYSTEMS

Acknowledgements	Page
List of Figures	iv
List of Tables	v
List of Appendices	xi

I INTRODUCTION by CHRIS FREDERICK NILSEN

A. General	1
B. The Cu-Zn System	2

II HISTORICAL REVIEW

A. Two-Phase Material Investigations	3
1. Thin Foils	4
2. Bulk Two-Phase Material	5
B. Related Aspects of Mechanical Behavior	11
1. Strain Hardening of Single Crystals	14
2. Alpha Brass Structure and Properties	15
3. Beta Brass Structure and Properties	19
4. Role of Dislocations	21
5. Strain Rate	26
6. Strain Ageing	30
7. Orientation	32

III OBJECTIVES OF THIS WORK Submitted to 37

IV DESCRIPTION in partial fulfillment of the requirements 39

A. Specimen Preparation for the degree of	39
1. Materials	39
a. Alpha Brass	39
b. Beta	39
c. Two-Phase	40
2. Alpha Brass Single Crystal Growth	41
3. Crystal Preparation	42
4. Specimen Preparation	44
5. Joining Alpha and Beta Brass	46
6. Duplex Interface Region	46
7. Machining	48
8. X-Ray	49

Department of Metallurgy, Mechanics and Materials Science

1973

DOCTOR OF PHILOSOPHY

	Page
B. Mechanical Testing Procedures	
1. Tension Tests	54
2. Strain-Rate Tensile Tests	55
Y TEST RESULTS	
TABLE OF CONTENTS	
A. Identification Tests	57
B. Strain-Rate Tensile Tests	
	Page
Acknowledgements	iv
List of Figures	v
List of Tables	xi
List of Appendices	xii
I INTRODUCTION	
A. General	1
B. The Cu-Zn System	5
II HISTORICAL REVIEW	
A. Two-Phase Material Investigations	6
1. Thin Foils	6
2. Bulk Two-Phase Material	7
B. Related Aspects of Mechanical Behavior	13
1. Strain Hardening of Single Crystals	14
2. Alpha Brass Structure and Properties	15
3. Beta Brass Structure and Properties	19
4. Role of Dislocations	23
5. Strain-Rate	26
6. Strain Ageing and Geometric Softening	30
7. Orientation	32
III OBJECTIVES OF THIS WORK	37
IV DESCRIPTION OF EXPERIMENTAL PROCEDURES	39
A. Specimen Preparation	39
1. Materials	39
a. Alpha Brass	39
b. Beta Brass	39
c. Two-Phase Foil	40
2. Alpha Brass Single Crystal Growth	41
3. Crystal Preparation	43
4. Two-Phase Foil Preparation	45
5. Joining Alpha and Beta Brass	46
6. Duplex Interface Reduction	48
7. Machining	52
8. X-Ray	54

	Page
B. Mechanical Testing Procedures	
1. Indentation Tests	54
2. Strain-Rate Tensile Tests	55
V TEST RESULTS	
A. Indentation Tests	57
B. Strain-Rate Tensile Tests	75
VI Discussion and Analysis of Results	134
A. Roll of the Type of Boundary	134
B. Coarse and Fine Slip in the Alpha Phase	146
C. Stress Concentration and Strain-Rate Effects	146
D. Slip in the Beta Phase	154
VII Summary and Conclusions	158
VIII Suggested Topics for Further Investigation	161
BIBLIOGRAPHY	163
APPENDICES	168

C. W. Ullagaddi.

My gratitude is also due to the members of the Advisory and Guidance Committee, particularly Dr. J. W. Hoffman, whose critical suggestions and consultation were valued. Special thanks are also due to Dr. J. W. Hoffman, Director of Engineering Research, for the awarding of a research assistantship to enable this study to be done.

My very special gratitude is extended to my wife Kathleen, for her sacrifice, patience, and understanding during this work.

ACKNOWLEDGEMENTS

I am greatly indebted to Dr. K. N. Subramanian for his untiring guidance, interest, and assistance, as well as for acting as my major professor. I am also indebted to, and sincerely thank Anil K. Hingwe for his help, consultation and comradeship during the course of this work. I would also like to sincerely thank the other members of the research group who offered their assistance freely when it was most needed, namely Sandra Carr, Mohammed Z. Fahmy, Ali Khezri, and C. B. Ullagaddi.

My gratitude is also extended to all of the members of my guidance committee, particularly Dr. Sean Adams, whose helpful suggestions and consultation were valued. Special thanks are also due to Mr. John Hoffman, Director of Engineering Research, for the awarding of a research assistantship to enable this study to be done.

My very special gratitude is extended to my wife Kathleen, for her sacrifice, patience, and understanding during this work.

8. (Continued)	
c) 0.5 cm/min. Cross-head Speed	60
d) 5.0 cm/min. Cross-head Speed	60
9. Slip Interactions with an Oriented Duplex Interface	
25 kg Load, 0.005 cm/min. Cross-head Speed, Indentation at:	
a) 1.5 mm	62
b) 0.5 mm	62

10. Slip Interactions with an Oriented Duplex Interface.

25 Kg Load, 0.5 cm/min. Cross-head Speed, Inden-

tation at:

a) 1.5 mm

b) 0.5 mm

LIST OF FIGURES

Figure

Page

11. Slip Interactions with an Oriented Duplex Interface.

25 Kg Load, 5.0 cm/min. Cross-head Speed, Inden-

tation at:

1. Schematic of the Assembly used for Growing Single Crystals of Alpha Brass. 42
2. Schematic of the Arrangement used for Growing Single Crystals of Alpha Brass. (Temperature Distribution in the Furnace is also Plotted.) 44
3. Schematic of the Arrangement used for Joining Alpha and Beta Brass 47
4. Schematic of the Lowering Arrangement Utilized for Reducing the Duplex Transition Zone. (Temperature Distribution in the Furnace is also Plotted.) 50
5. a) Schematic of the Local Annealing Arrangement 51
b) Temperature of the Local Annealing Set-up. 51
6. Machined Tensile Specimen Ready for Testing. 53
7. Four Types of Interfaces Studied 58
 - a) Oriented Duplex Interface. 58
 - b) Equiaxed Duplex Interface. 58
 - c) Corrugated Bicrystal Interface 58
 - d) Flat Boundary Interface. 58
8. Slip Interactions With an Oriented Duplex Interface
25 Kg Load, Indentation at a Distance of 1.5 mm
from the Interface at Various Rates of Loading
 - a) 0.005 cm/min. Cross-head Speed 59
 - b) 0.05 cm/min. Cross-head Speed. 59
8. (Continued)
 - c) 0.5 cm/min. Cross-head Speed 60
 - d) 5.0 cm/min. Cross-head Speed 60
9. Slip Interactions with an Oriented Duplex Interface
25 Kg load, 0.005 cm/min. Cross-head Speed, Inden-
tation at:
 - a) 1.5 mm 62
 - b) 0.5 mm 62
- a) Extensive Cross-slip in the Alpha Phase Region 76

10.	Slip Interactions with an Oriented Duplex Interface. 25 Kg Load, 0.5 cm/min. Cross-head Speed, Indentation at:	
a)	1.5 mm	63
b)	0.5 mm	63
11.	Slip Interactions with an Oriented Duplex Interface. 25 Kg Load, 5.0 cm/min. Cross-head Speed, Indentation at:	
a)	1.5 mm	64
b)	0.5 mm	64
12.	Slip Interactions with an Oriented Duplex Interface. 40 Kg Load, 0.005 cm/min. Cross-head Speed, Indentation at 1.5 mm. Compare with Fig. 8a	66
13.	Slip Interactions with an Equiaxed Duplex Interface. 25 Kg Load, 0.05 cm/min. Cross-head Speed, Indentation at 1.5 mm. Compare with Fig. 8b.	67
14.	Slip Interactions with an Equiaxed Duplex Interface. 40 Kg Load, Indentation at 0.5 mm from Interface at various Cross-head Speeds.	
a)	0.005 cm/min. Cross-head Speed	69
b)	0.05 cm/min. Cross-head Speed.	69
14.	(Continued)	
c)	0.5 cm/min. Cross-head Speed	70
d)	5.0 cm/min. Cross-head Speed	70
15.	Slip Interactions with an Equiaxed Duplex Interface. 40 Kg Load, 5.0 cm/min. Cross-head Speed, Indentation at 1.5 mm from Interface. Compare with Fig. 14d.	71
16.	Slip Interactions with a Bicrystal Flat Interface. 25 Kg Load, Indentation at 1.0 mm from Interface at Different Rates of Loading.	
a)	0.005 cm/min. Cross-head Speed	73
b)	5.0 cm/min. Cross-head Speed	73
17.	Slip Interactions with a Bicrystal Flat Interface. 40 Kg Load, Indentation at 1.0 mm from Interface at Different Rates of Loading.	
a)	0.005 cm/min. Cross-head Speed	74
b)	5.0 cm/min. Cross-head Speed	74
18.	Slip Interactions with Equiaxed Duplex Interface. 25 Kg Load, Indentation into the Duplex Interface	
a)	Cross-slip and Slip Propagation Through the Boundaries	76
b)	Extensive Cross-slip in the Alpha Phase Region	76

19.	Four Faces of a Slightly Deformed Strain-Rate Tensile Specimen.	76
	Specimen No. 13, Cross-head Speed 3.0 cm/min.	79
20.	Stress-Strain Curves for Specimens having an Oriented Duplex Interface Structure.	183
	Specimen No. 48, Cross-head Speed 0.2 cm/min.	84
	Specimen No. 50, Cross-head Speed 0.3 cm/min.	84
	Specimen No. 36, Cross-head Speed 2.0 cm/min.	84
21.	Stress-Strain Curves for Specimens having an Equiaxed Interface Structure.	85
	Specimen No. 40, Cross-head Speed 0.1 cm/min.	85
	Specimen No. 42, Cross-head Speed 0.5 cm/min.	85
	Specimen No. 39, Cross-head Speed 0.5 cm/min.	85
	Specimen No. 24, Cross-head Speed 0.5 cm/min.	85
	Specimen No. 38, Cross-head Speed 1.0 cm/min.	85
	Specimen No. 45, Cross-head Speed 2.0 cm/min.	85
	Specimen No. 46, Cross-head Speed 3.0 cm/min.	85
22.	Stress-Strain Curves for Bicrystal Specimens having a Corrugated Interface Structure.	86
	Specimen No. 12, Cross-head Speed 0.01 cm/min.	86
	Specimen No. 43, Cross-head Speed 0.05 cm/min.	86
	Specimen No. 23, Cross-head Speed 0.5 cm/min.	86
	Specimen No. 31, Cross-head Speed 1.0 cm/min.	86
23.	Stress-Strain Curves for Bicrystal Specimens having a Flat Interface Structure.	87
	Specimen No. 37, Cross-head Speed 0.005 cm/min.	87
	Specimen No. 35, Cross-head Speed 0.1 cm/min.	87
	Specimen No. 22, Cross-head Speed 0.2 cm/min.	87
	Specimen No. 21, Cross-head Speed 0.3 cm/min.	87
	Specimen No. 44, Cross-head Speed 0.5 cm/min.	87
	Specimen No. 13, Cross-head Speed 3.0 cm/min.	87
	Specimen No. 14, Cross-head Speed 5.0 cm/min.	87
24.	Slip Interactions with Oriented Duplex Interface. Tests Performed using Cross-head Speeds of 0.2 and 0.3 cm/min.	97
25.	Slip Interactions with Equiaxed Interface Structure. Tests Performed using Cross-head Speeds of 0.1 and 0.5 cm/min.	98
25.	(Continued) Tests Performed using Cross-head Speeds of 1.0 and 2.0 cm/min.	100
26.	Coarse Slip Lines in the Beta Phase Initiated by Slip Interactions with a Flat Bicrystal Boundary Tested using a Cross-head Speed of 0.005 cm/min.	117

26.	Scanning Electron Micrographs of Specimen No. 36 having an Oriented Duplex Interface. Tested using a Cross-head Speed of 2.0 cm/min.	123
a)	500 X	102
b)	1000 X	102
26.	(Continued)	121
	Tested using a Cross-head Speed of 2.0 cm/min.	
c)	2000 X	103
27.	Fine and Rumpled Slip occurred in the Beta Phase in Regions away from the Interface. Tests at Cross-head Speeds of 1.0 and 2.0 cm/min.	104
28.	Cross-slip in Alpha Phase Regions Caused by Beta Island. Test run using a Cross-head Speed of 0.5 cm/min	106
29.	Optical Micrographs Showing Slip Propagation through an Equiaxed Interface Structure. Specimen No. 24, Cross-head Speed 0.5 cm/min.. . . .	107
30.	Scanning Electron Micrographs of an Equiaxed Interface Specimen Showing Fine Slip in the Beta Phase at B. Specimen No. 24, Cross-head Speed 0.5 cm/min.. . . .	108
31.	Scanning Electron Micrograph of a Deformed Specimen with a Corrugated Interface. Specimen No. 23, Cross-head Speed 0.5 cm/min.. . . .	110
32.	Slip Interactions with a Corrugated Interface at Various Strain-rates. Tests Performed using Cross-head Speeds of 0.01 and 0.05 cm/min.	111
32.	(Continued)	130
	Tests Performed using Cross-head Speeds of 0.5 and 1.0 cm/min.. . . .	113
33.	Very Heavy Slip in the Alpha Crystal at Regions away from the Corrugated Duplex Interface. Specimen No. 31, Cross-head Speed 1.0 cm/min.. . . .	114
34.	Fine Slip in the Beta Phase away from the Corrugated Duplex Interface. Tests Performed using Cross-head Speeds of 0.05 and 1.0 cm/min.. . . .	116
35.	Slip Propagation through a Flat Bicrystal Loaded at a Cross-head Speed of 0.005 cm/min. Specimen No. 37	117
36.	Coarse Slip Lines in the Beta Phase Initiated by Slip Interactions with a Flat Bicrystal Boundary Tested using a Cross-head Speed of 0.005 cm/min.	119

37. Cross-slip in the Alpha Phase Occurring Very Near the Phase Boundary. Specimen No. 37, Cross-head Speed 0.005 cm/min	120
38. Multiple Slip in the Alpha Crystal in a Region away from the Phase Boundary. Specimen No. 37, Cross-head Speed 0.005 cm/min.	121
39. Slip Interactions in a Flat Boundary Specimen Tested at 0.1 cm/min. Cross-head Speed	122
40. Coarse Slip in the Beta Phase near the Boundary Initiated in a Direction Drastically Different from the Trace of the Primary Slip System in the Alpha Phase. Specimen No. 35, Cross-head Speed 0.1 cm/min.. . . .	124
41. Scanning Electron Micrographs showing Coarse Slip in the Beta Phase Initiated by Interaction of the Slip in the Alpha Phase with the Interface in a Flat Boundary Bicrystal. Specimen No. 35, Cross-head Speed 0.1 cm/min.. . . .	125
42. Slip Propagation through a Flat Interface. Specimen No. 22, Cross-head Speed 0.2 cm/min.. . . .	126
43. Scanning Electron Micrographs showing Slip Propagation through a Flat Boundary. Specimen No. 22, Cross-head Speed 0.2 cm/min.. . . .	128
44. Slip Interactions with a Flat Boundary at High Strain-rates. Cross-head Speeds of 3.0 and 5.0 cm/min. used.	129
45. Fine Slip in the Beta Phase. Specimen No. 13, Cross-head Speed 3.0 cm/min.. . . .	130
46. Scanning Electron Micrograph showing the Fine Slip in the Alpha Crystal in High Strain-rate Flat Boundary Specimens. Specimen No. 13, Cross-head Speed 3.0 cm/min.. . . .	133
47. Model for the Interaction of Slip with an Oriented Duplex Boundary	136
48. Model for the Interaction of Slip with a Corrugated Boundary.	140
49. Model for Analyzing the Effect of the Slip Orientation Relative to a Corrugated Boundary.	143
50. Zone of Stress Concentration Caused by a Dislocation Pile-up in a Fine Slip Line.	147

Figure	Page
51. Zone of Stress Concentration Caused by Dislocation Pile-ups in a Slip Band.	150
52. Model for Analyzing the Deformation Zone in Beta	155
53. Transmission Electron Micrographs of Deformed Alpha-Beta Bicrystals.	169

Table	Page
I. Crystallographic orientations of the specimens used in strain-rate tests.	160
II. Strain-rate test results for specimens having an oriented duplex type of interface.	161
III. Strain-rate test results for specimens having an equiaxed (unoriented) duplex type of interface.	162
IV. Strain-rate test results for bicrystal specimens having a corrugated alpha-beta interface.	163
V. Strain-rate test results for bicrystal specimens having a flat alpha-beta interface.	164

LIST OF TABLES

Table	Page
I. Crystallographic orientations of the specimens used in strain-rate tests.	80
II. Strain-rate test results for specimens having an oriented duplex type of interface.. . . .	88
III. Strain-rate test results for specimens having an equiaxed (unoriented) duplex type of interface.	90
IV. Strain-rate test results for bicrystal specimens having a corrugated alpha-beta interface.	92
V. Strain-rate test results for bicrystal specimens having a flat alpha-beta interface.	94

LIST OF APPENDICES

A. GENERAL

Appendix Page

A. Transmission Electron Micrographs. 168

A large percentage of engineering materials in use today are two phase materials. These materials are biphase materials. The mechanical properties and the deformation mechanisms of two-phase materials are of great practical importance. The properties of two-phase materials depend on the properties of the individual phases, their distribution, the volume fraction of phases present, and on the phase boundaries.

A polycrystalline aggregate of a single phase material consists of grains which are all of the same crystal structure. Since each grain will have different crystallographical orientations, they will be separated by grain boundaries.

In order to investigate the mechanical properties of single phase materials, an ideal fundamental unit such as a single crystal is used as a means of avoiding the constraints that arise due to the presence of other grains. To study the effect of grain boundaries on the mechanical behavior of a single phase material, either a series or parallel type of bicrystal can be used. A series bicrystal has the grain boundary oriented normal to the loading axis, and a constant stress condition is developed at the boundary during uniaxial loading. A parallel bicrystal having the grain boundary oriented parallel to the loading axis experiences a constant strain condition at the boundary. The stresses in the adjacent portions of a parallel bicrystal will vary according to their relative cross sectional areas normal to the loading axis. This arrangement

CHAPTER I

INTRODUCTION

A. GENERAL

A large percentage of engineering materials in use consist of more than one phase. These materials are inhomogeneous. The mechanical properties and the deformation mechanisms of two-phase materials are of great practical importance. The properties of two-phase materials depend on the properties of the individual phases, their distribution, the volume fraction of phases present, and on the phase boundaries.

A polycrystalline aggregate of a single phase material consists of grains which are all of the same crystal structure. Since these grains will have different crystallographic orientations, they will be separated by grain boundaries.

In order to investigate the mechanical properties of single phase materials, an ideal fundamental unit such as a single crystal is used as a means of avoiding the constraints that arise due to the presence of other grains. To study the effect of grain boundaries on the mechanical behavior of a single phase material, either a series or parallel type of bicrystal can be used. A series bicrystal has the grain boundary oriented normal to the loading axis, and a constant stress condition is developed at the boundary during uniaxial loading. A parallel bicrystal having the grain boundary oriented parallel to the loading axis experiences a constant strain condition at the boundary. The stresses in the adjacent portions of a parallel bicrystal will vary according to their relative cross sectional areas normal to the loading axis. This arrangement

imposes an additional geometrical constrain on the test material, and for this reason the series type bicrystal is preferred in studies of the role of grain boundaries on the mechanical behavior of the materials.

In two-phase alloys, each phase will have a different chemical composition, and may possess a different crystal structure. One phase will have a low relative solute atom concentration, and the other will have a high relative solute atom concentration. Because of their different compositions and crystal structures, the mechanical properties of the various phases will be different. The boundary separating two phase regions in a material is properly termed a phase boundary, which is analogous to a grain boundary in a polycrystalline single phase material.

The ideal fundamental unit for studying the mechanical behavior of a two-phase material should consist of a single crystal of one phase joined to a single crystal of the other phase. Such a model automatically incorporates a phase boundary separating the two single crystals. A variation of this fundamental unit may be constructed so that a single crystal of one phase is joined to a few very large grains of another phase. Such a model unit may be termed a multicrystal. Ideally, this multicrystal would have only one grain at the phase boundary contacting the single crystal of the other phase. An alternate approach is to use duplex crystals. Such duplex crystals will contain two-phase regions, where the phases present will have definite crystallographic orientation relationships. For example, a duplex crystal of alpha-beta brass will have (111) of alpha parallel to (110) of beta, and $\langle 110 \rangle$ of alpha parallel to $\langle 111 \rangle$ of beta.

Some examples of two-phase alloys that are of commercial and engineering importance are alpha-beta brass, alpha-beta titanium, micro-duplex stainless steels, some copper-tin alloys, and various steels. In these materials, one phase is harder by virtue of its higher solute atom

concentration. The mechanical properties of bulk two-phase materials such as these will vary according to the relative compositions of the two phases and with the distribution and volume fraction of the phases present in the material.

Other types of two-phase materials that are of importance consist of alloys with a finely dispersed second phase, composite materials, and unidirectionally solidified eutectic alloys. In dispersion hardenable alloys, the hard second phase present effectively strengthens the matrix. This fine, dispersed second phase may be produced in two different ways. In tool steels, for example, the second phase is obtained by adding small amounts of alloying elements such as titanium and vanadium. These additions react with elements already present in the steel to form fine, stable precipitates that are uniformly dispersed throughout the material. Powder metallurgical techniques may also be used to create these types of two-phase aggregates. In such a technique powders of two different phases are blended, pressed to the desired size, shape and density, and then sintered. The volume fraction and size of second phase particles is easily controlled in this process.

Another means of producing the strength enhancing dispersed second phase is by a precipitation process. The copper-aluminum alloys are the classic examples of this process. Submicroscopic precipitates are obtained by the aging treatment of alloys that have been solution heat treated to produce a super-saturated solid solution. The precipitate formed from age-hardenable copper-aluminum alloys is a hard Cu_2Al_3 phase, which is uniformly dispersed. Such precipitation effectively strengthens the matrix.

Fiber reinforced composites may be constructed by embedding some type of fine fiber in a matrix. In a material like reinforced concrete, the fiber is ductile and the matrix is brittle. In another example, a

composite containing alumina fibers in a silver matrix, the fiber is the brittle phase. Through special processing techniques some eutectic alloys, which are two-phase materials, may be unidirectionally solidified. This process coarsens and aligns the phases in the eutectic in a particular direction to enhance the mechanical properties in that direction.

Dispersion and precipitation hardenable materials, two-phase powder composites, and fiber-reinforced composites, have been investigated extensively to understand their mechanical behavior. However, the deformation mechanisms of bulk two-phase materials, such as alpha-beta brass and alpha-beta titanium are not well understood. Deformation of these types of two-phase alloys can be studied by using different approaches. Although a continuum mechanics approach may be used to analyze an idealized model, solutions are difficult to achieve. Also, by necessity the model used will be so highly idealized that the solutions obtained may not yield realistic results that can be correlated with the practical material behavior.

An alternative approach is to carry out an experimental study on a simple model. In order to understand the basic mechanisms involved in the deformation of two-phase alloys, the number of variables involved must be minimized. This may be accomplished by studying the deformation behavior of two-phase bicrystals and duplex crystals. Response of such bicrystals to an applied stress depends on the ability of the constituents to transfer strain across the phase boundary. Under an applied stress the two participant phases in a bicrystal will differ in their response. This is a direct result of differences in elastic and shear moduli, crystal structures, relative crystallographic orientations, Peierls-Nabarro stresses, and coefficients of work hardening of the phases involved.

B. THE COPPER-ZINC SYSTEM

The copper-zinc system has been chosen for this study for a number of reasons. The alpha-beta brass alloy has found wide technical applications and is a commercially important engineering material. Details of the equilibrium phase diagram and properties of the individual phases are well known. Unlike titanium alloys, specialized equipment such as vacuum melting furnaces are not needed for investigation of this alloy. Further, both alpha and beta phases in the Cu-Zn system have a cubic crystal structure; alpha phase is face-centered cubic and the beta phase has a CsCl structure. The drastically different mechanical behavior of alpha and beta phases in this alloy system provide various interesting possibilities. Alpha-beta brass is typical of a large number of two-phase alloys, and it is hoped that the results of this study may be applicable to various other alloy systems.

As a result of a recent study on the mechanical behavior of two-phase materials, the alpha and beta brass containing thin films of both the phases as a bicrystal or crystal of one phase deposited with a thin film of the other phase, the thin films do not accommodate plastic deformation. For this reason, investigators working with thin films use the modulus of elasticity as a criteria for deformation. Results obtained by using thin films, where the modulus of elasticity are used as the main criteria, do not represent the behavior of the material in the bulk form.

Under a general state of stress in a bicrystal, the macroscopic and microscopic compatibility conditions should be satisfied at the phase boundary. Macroscopic compatibility conditions require that the stresses or strains across the phase boundary in each phase be equal, depending on the loading configuration. This condition requires the operation of a certain number of slip systems in both crystals. On the other hand,

microscopic compatibility conditions must be satisfied at the phase boundary, and have been explained by employing the concepts of dislocation pile-ups, or dislocation density.

CHAPTER II

HISTORICAL REVIEW

A. TWO-PHASE MATERIAL INVESTIGATIONS

1. General

The role of grain boundaries on plastic deformation behavior of single phase materials is investigated by using bulk bicrystals. Chalmers and his coworkers,^{1,2,3} and Hirth and Hook⁴ have carried out extensive studies on the behavior of face-centered cubic bicrystals. However, most of the work related to the influence of a phase boundary on the mechanical behavior of two-phase materials has utilized specimens containing thin films of both the phases or a bulk single crystal of one phase deposited with a thin film of the other phase. The thin films cannot accommodate plastic deformation. For this reason, investigators working with thin films use the modulus of elasticity as a criteria for deformation. Results obtained by using thin films, where the moduli of elasticity are used as the main criteria, do not represent the behavior of the material in the bulk form.

Under a general state of stress in a bicrystal, the macroscopic and microscopic compatibility conditions should be satisfied at the phase boundary. Macroscopic compatibility conditions require that the stresses or strains across the phase boundary in each phase be equal, depending on the loading configuration. This condition requires the operation of a certain number of slip systems in both crystals. On the other hand,

microscopic compatibility conditions must be satisfied at the phase boundary, and have been explained by employing the concepts of dislocation pile-ups, or dislocation density.⁵

In two-phase systems, theoretical studies have been carried out to describe the behavior of dislocations at phase boundaries. Van der Merwe⁶ has considered the case of interfacial misfit between oriented films and their single crystal substrates. The registry between the atoms on either side of the interface is reduced by the formation of interfacial dislocations. The latter hinder the passage of other dislocations. Head,⁷ Connors,⁸ and Yoffe⁹ have considered various geometries of dislocation pile-ups at an interface. Eshelby's¹⁰ concept of image dislocations is used to calculate the force experienced by a dislocation approaching an interface. All of the experimental studies on two-phase materials use either thin two-phase films or thin films coated on single crystal substrates to study their behavior under loading. The behavior of a fundamental unit that will represent bulk materials has not been studied so far because of the lack of availability of such a unit.

2. TWO-PHASE MATERIAL RESEARCH

One of the first systematic investigations of the deformation of polycrystalline two-phase materials was made by Unckel.¹¹ Alloys of copper containing 6% iron, leaded brass, alpha-beta brass, complex brass, alpha-delta bronze, aluminum containing 8% copper, and aluminum containing 12% silicon were deformed by cold rolling. The particle size was measured before and after rolling. For materials in which the second-phase particles were softer and more ductile than the matrix, such as leaded brass, the amount of reduction undergone by the particles on rolling was greater than

the reduction of the specimen as a whole. In all other alloys the inclusions were harder than the matrix, and the particles deformed less than the matrix. It has been shown by several investigations that large brittle precipitates, such as CuAl_2 in overaged aluminum alloys^{12,13}, do not deform with the matrix. Unckel¹¹ reported that, as the amount of deformation is increased, the deformation of the matrix and particle tended to become more homogeneous, i.e., the hard particles deformed more, and the soft particles deformed less. This can be attributed to work-hardening of the softer matrix phase.

Chao and Van Vlack^{14,15} confirmed Unckel's conclusions that the extent of the deformation of the second-phase depends on the relative hardness of the particles compared to the matrix. They compressed steel specimens in which inclusions of manganese sulphide and glass were embedded. The amount of deformation of the particles was measured either from the change in shape of the inclusions or from the movement of tungsten markers adjacent to the inclusions. At elevated test temperatures, where the particles were softer than the matrix, more deformation occurred in the particles than in the matrix.

The first detailed metallographic study was undertaken by Honeycombe and Boas.¹⁶ They deformed alpha-beta brass containing 40% zinc, which is composed of soft face-centered cubic alpha phase, and relatively hard cesium-chloride structure beta phase. Slip first appeared in the alpha grains, which became heavily deformed before slip was seen in the beta grains. When a heavily deformed specimen was repolished and then re-strained, slip lines again started in the alpha grains. Slip traces occasionally crossed the alpha-beta phase boundaries owing to a contiguous grains having parallel slip systems. The orientation relationship between the alpha and beta phases for this to occur was $(110)_\beta \parallel (111)_\alpha$ and $\langle 111 \rangle_\beta \parallel \langle 110 \rangle_\alpha$ which are the conditions for obtaining contiguous grains. More deformation

was seen to occur in the beta phase near an alpha-beta boundary than in the interior of the beta grain.

Honeycombe and Boas attempted to correlate the extent of deformation of individual phases with the recrystallization temperature (on subsequent annealing) of the particular phase. These studies were complicated by precipitation in the alloy at the recrystallization temperature, and by the order-disorder transformation in the beta phase.

Clarebrough¹⁷ subsequently studied silver-magnesium alloys which consisted of soft silver-rich grains of face-centered cubic alpha phase, and grains of hard beta-phase, having a cesium-chloride structure. These alloys deformed in a manner similar to two-phase alpha-beta brass. Measurements of the recrystallization temperature of the alpha and beta phases in alloy specimens that were deformed equal amounts, but that contained varying proportions of the two phases, indicated that below 30 vol. % of beta, the alpha phase deformed more than the beta phase. When the volume fraction of beta phase exceeded 30 vol. %, the extent of deformation in both the phases were the same, equal to that of the alloy specimen as a whole. Clarebrough and Perger¹⁸ observed similar behavior in alloys of copper and zinc.

After a preliminary investigation of the structure and properties of sintered tungsten carbide-cobalt composites, Gurland and Norton¹⁹ concluded that the high strength and low ductility of these alloys were due to the constraint exerted by the hard carbide particles on the cobalt binder phase. The complex residual thermal stresses are attributable to the different thermal expansion coefficient of the two phases.

The mechanical properties of a ductile material containing either hard, or soft particles were determined by Gurland.²⁰ Increases in the

strength of silver containing tungsten, molybdenum, or tungsten carbide, compared with silver containing nickel were studied. Silver containing nickel is softer than the other three second-phase particles, but stronger than silver. All of these alloys were made by powder-metallurgical techniques. The similarity in the properties of silver containing tungsten, molybdenum, or tungsten-carbide led Gurland to suggest that the type of second-phase particle is not an important parameter so long as it does not deform during the deformation of the alloy. The effect of strong second-phase particles on strengthening is usually explained by proposing that the particles restrict the plastic deformation of the softer matrix.²⁰ Slip is initiated in the matrix by stress concentrations created by the presence of hard particles. In tungsten carbide-cobalt alloys the stress required for initiation of slip in the matrix decreased as the amount of carbide particles increased.²¹

A systematic study of the role of the second-phase particles in two-phase materials has been made by Edelson and Baldwin.²² They attempted to identify the parameters that control the mechanical properties of copper-based composites by varying independently the volume fraction and size of the second-phase particles. The composites were made by solid-state sintering. Since theoretical density could not be attained by this technique, the porosity of the composites was standardized at 2%. Voids approximately 1 μm in size were shown to have no influence on the flow stress and ultimate tensile strength of copper; but the fracture stress and ductility decreased markedly with increasing number of voids. Tensile properties were plotted against volume fraction, mean free path, and interparticle spacing of second-phase particles and voids. The latter two parameters are dependent on both volume fraction and particle size. Only particles of iron and chromium, which have some solubility in copper and hence may

be expected to be strongly bonded to copper, produced a strengthening effect. This increase in strength depended on the mean free path between particles, and hence on both volume fraction and particle size of the second phase. The ductility of copper was reduced by the presence of voids, of particles of iron, chromium, or alumina. However, the embrittlement depended only on the volume fraction of the second phase.

The embrittling effect of second-phase additions was thought by Edelson and Baldwin to be caused by the ability of particles to restrict the deformation locally between particles, allowing fracture to occur earlier than if the strains were homogeneous. They further proposed that the same strain concentrations exist in alloys containing a constant volume fraction of second-phase particles; but, with varying particle size a different strain distribution would be obtained in alloys with different volume fractions of constant-sized particles. Thus, the ductility of an alloy would be dependent only on volume fraction of particles and independent of particle size. Confirmation of this model was subsequently claimed by Edelson,²³ who used strain-sensitive birefringent films to observe the strain patterns on copper sheet that contained arrays of drilled holes.

The thermal and elastic properties of a second-phase usually differ from those of the matrix.²⁴ This leads to the important consequence that particles can give rise to dislocation sources when a composite is cooled from an elevated temperature or is deformed. As a result, the substructure in the vicinity of second-phase particles can be considerably modified, and this modification should be accounted for in any theory of plastic deformation of two-phase materials. Dislocations are usually generated near the compounds (frequently carbide) or inclusions. Observations of this effect have become common with the development of thin-film transmission electron microscopy, and dislocation generation near second-phase particles have

been observed in many alloy systems. This ability of particles to increase the density of unlocked dislocations has been cited to explain the results obtained during an investigation of deformation in iron-alumina alloys.²⁵ Values of the dislocation velocity exponent derived from variable strain-rate tests were found to increase with increasing alumina content. To correlate these results with current models of yielding,²⁶ the alumina particles were envisaged as acting as dislocation sources on straining the alloy.

Margolin, Farrar and Greenfield²⁷ have studied the deformation of alpha-beta titanium alloys. In these alloys the alpha phase is distributed as equiaxed alpha in an aged beta matrix, or as Widmanstätten plates and grain boundary alpha (continuous alpha) in an aged beta matrix. For clarity the equiaxed alpha may be termed type 1 alpha, and the Widmanstätten plates and grain boundary alpha may be designated as type 2 alpha phase. At approximately constant yield stress the fracture strength of the type 1 structures was found to be higher than that of type 2 structures of the same grain size. Correspondingly, the reduction of area was higher for the type 1 structure. It would be expected that the alpha phase is softer than the aged beta matrix. Honeycombe and Boas¹⁶ have reported that in an alpha-beta brass, preferential deformation of the softer alpha phase can occur. Examination of the fracture surface of the titanium alloy, after polishing and etching, showed void formation at the alpha-beta interfaces. Void formation has also been reported earlier by Wood, Williams, Ogden and Jaffee.²⁸ The percentage of voids appeared to be independent of grain size, and not directly related to the volume fraction of alpha present. The percentage of voids did appear to be related to the size of the alpha regions, increasing with the size of alpha. The larger the alpha particles, the more easily would the alpha deform. Thus, the difference between the fracture

strength of type 1 alpha and type 2 alpha is related to the greater ease of void formation and link-up in the type 2 alpha structure. In this type 2 alpha structure, void formation tends to be greater at grain boundaries. Link-up of grain boundary and/or intragranular voids would produce a larger crack more easily in the type 2 alpha structure than in type 1 alpha. This would propagate at a lower stress than that needed for the type 1 alpha structure.

All of these studies that have been discussed have been carried out using oriented thin films as one extreme, or bulk polycrystalline two-phase materials as the other extreme. To understand the fundamental mechanisms of plastic deformation in two-phase materials, a model unit between these two extremes must be utilized. Such studies have not yet been carried out. A macroscopic two-phase bicrystal, multicrystal, or duplex crystal provides such an ideal unit. This model unit would allow observation of the plastic deformation progressing across the phase boundary. Understanding the role of the phase boundary in the deformation process is fundamental in developing two-phase materials having specific or superior properties for engineering application.

B. RELATED ASPECTS OF MECHANICAL BEHAVIOR

During the deformation of a two-phase material, there are many factors that have to be considered. In the initial stage of deformation of a single phase crystal, strain hardening plays a major role. In the later stages of deformation of a two-phase material, the behavior of each phase and the influence of their respective crystal structures are of great importance. Slip progresses from one phase into another through a phase boundary, which acts as a barrier. As a result, the behavior of dislocations and slip at such a barrier have to be considered. The effect of strain-rate

upon dislocation motion must also be taken into account. Of fundamental importance in the process of propagating deformation from one phase to another, across a phase boundary, is the relative crystallographic orientation of the phases. The effect of strain-aging upon dislocation motion during the deformation process in a two-phase material may also be an important factor. In the following sections of this chapter, these factors are reviewed briefly, because of their relevance to this investigation.

2. ALPHA BRASS STRUCTURE AND PROPERTIES

Alpha brass is a single phase intermetallic solid solution of zinc

1. STRAIN HARDENING AND RECOVERY OF SINGLE CRYSTALS

Strain-hardening may be defined as the increase in hardness and flow stress with increasing plastic deformation. The slope of the stress-strain curve is used to define the rate of strain-hardening. If the crystal is oriented so that the resolved shear stresses on two or more slip systems are equal, then these systems will slip simultaneously in a multiple slip process.

The face-centered cubic crystals display three stages of hardening; easy glide, in which there is a low strain-hardening rate; linear hardening, over which the slope of the stress-strain curve is high and constant; and dynamic recovery, in which the rate of strain-hardening decreases. These stages of deformation behavior are commonly referred to as Stage I, Stage II and Stage III. The extent of strain in the first two stages is sensitive to crystal orientation and decreases with increasing temperature. The body-centered cubic metals, on the other hand, exhibit a decreasing strain-hardening rate over the entire range of deformation.

The low work hardening rate in Stage I deformation is associated with the fact that there are no interactions between dislocations moving in different slip planes, since deformation takes place by single slip. The

high strain-hardening rate in Stage II, is the result of dislocation interactions due to multiple slip. The decreasing strain-hardening rate in Stage III is the result of dynamic recovery processes occurring simultaneously with strain-hardening. The two major processes by which recovery occurs are cross-slip and dislocation climb.

2. ALPHA BRASS STRUCTURE AND PROPERTIES

Alpha brass is a single phase substitutional solid solution of zinc in copper. The zinc atoms occupy random substitutional atomic positions in the face-centered cubic copper crystal lattice structure. Such a structure accommodates from zero to approximately 38 wt.% of zinc at room temperature. The alpha phase in the copper-zinc alloys is somewhat unusual in that its solubility for zinc increases as the temperature drops from 32.5 wt.% at 903°C to 39 wt.% at 454°C. The solubility trend of zinc in the alpha phase is reversed below 454°C. Alpha brass has a face-centered cubic structure and therefore normally deforms along close packed (111) planes in $\langle 1\bar{1}0 \rangle$ directions.

When a face-centered cubic metal single crystal is deformed in uniaxial tension, the plot of resolved shear stress-shear strain usually exhibits three stages of deformation, Stage I, Stage II, and Stage III. Several work-hardening mechanisms have been proposed for Stages I and II. Guided by Bell's^{29,30} work, Hartman³¹ has investigated the deformation during Stage III using stacking fault energy as a criteria. Bell has shown that Stage III deformations of several face-centered cubic metals exhibit a deformation behavior which can be quantitatively related to the deformation of polycrystalline materials under uniaxial stressing. This generalized behavior is expressed in the form of an empirical, linearly temperature

dependent, parabolic stress-strain relationship whose coefficient is related to the material's elastic properties.

According to the impurity atmosphere theory of the yield point proposed by Cottrell,³² Nabarro,³³ and Cottrell and Bilby,³⁴ dislocations in crystals become anchored by solute atoms. The material will then soften when these dislocations are pulled away from their atmospheres at the beginning of plastic deformation.

In face-centered cubic metals a substitutional solute atom must be roughly the same size as the solvent metal atom. Substitutional solute atoms occupying cube corner, face-centered, or the mainly used cube center substitutional sites do not create a spherically non-symmetrical distortion. However, it might still be possible to anchor the screw dislocations indirectly, as indicated by Heidenreich and Shockley.³⁵ In a face-centered cubic lattice, ordinary unit dislocations in close-packed planes should dissociate into pairs of partial dislocations. These partial dislocations are joined to each other by a stacking fault, and must glide together as a unit in the slip plane. Always, at least one of these partials will have a substantial edge component, and therefore be able to be locked by solute atoms. If one is locked, then the other cannot move either, since they are separated by the stacking fault. While this locking is undoubtedly weaker, in general, than impurity locking in the body-centered cubic lattice, nevertheless the possibility of producing yield points in face-centered cubic crystals cannot be ruled out.

Arndley and Cottrell³⁶ have studied the yielding phenomena in 70%Cu-30%Zn alpha brass crystals at room temperature. Well marked yield points were observed in virgin and strain-aged specimens. The observed yield drop was quite large and was 10-20% of the lower yield stress. Further, both the upper yield stress and the yield drop increased markedly

with increasing zinc content of the alloy. The effect was particularly significant at small zinc concentrations.

Karashima³⁷ has studied the dislocation structure in deformed alpha brass by using electron microscopy. At low strain (1-5%), dislocations piled up against grain boundaries, sub-grain boundaries, and obstacles within a crystal. With increasing degrees of deformation (5-10%), dislocations from 2 or 3 slip systems interact to form dislocation tangles and kinks. The dislocation sub-structure varies according to the degree of deformation, and may be correlated with suggested work-hardening mechanisms in various stages. Work-hardening in the early stages is mainly attributed to the back-stresses caused by dislocations piling up against grain boundaries.³⁸ The formation of Lomer-Cottrell sessile dislocations^{39,40} as well as the formation of jogs⁴¹ caused by interaction at dislocations with vacancies become increasingly important as work-hardening progresses. The prominent characteristic in alpha brass is that most of the dislocations introduced during cold-working are still confined to the primary slip planes. This behavior is quite different from that found in metals having high stacking fault energy like beta brass.

Karashima's studies on alpha brass showed that slip progressed through grain boundaries and twin boundaries, with clear indications that slip was continuous across a boundary into a neighboring grain. This observation supports the view that some dislocations can apparently pass through the boundary,⁴² if adjacent grains are favorably oriented crystallographically. The results of Karashima's work⁴³ provides a model for the deformation of polycrystalline aggregates. Slip can be induced in neighboring grains with the aid of stress concentrations from the pile-up of dislocations against grain boundaries. Such a pile-up can give rise to the following two possibilities: a) Frank-Read⁴⁴ sources present in neighboring grains

begin to operate because of stress concentrations,^{43,45,46} and b) grain boundary dislocation sources can become operative.⁴⁷

Mitchell and Thornton⁴⁸ have investigated the role of secondary slip during the deformation of copper and alpha brass single crystals. Secondary slip, which is a deviation from single glide, is likely to be important, especially in Stage II work hardening, since dislocations moving in primary and secondary slip planes can interact. Various theories for Stage II work-hardening have utilized these interactions. The deviations from single glide caused by secondary slip are much less in alpha brass than in copper crystals. It is possible to conclude that, with increasing zinc content, the amount of secondary slip decreases.

The largest contribution to the flow stress in Stage I of alpha brass is caused by the elastic interaction between nearly parallel dislocations on nearly parallel slip planes. Since this interaction cannot be overcome by thermal activation, it therefore depends on temperature only through the elastic constants. From etch-pit observations on alpha brass, Meakin and Wilsdorf⁵ have postulated that Lomer-Cottrell locks are formed by the reaction of the leading glide dislocation of the pile-up groups with the forest dislocations. Strutt, Kear and Wilsdorf,⁴⁹ have found that the frictional stress for dislocation motion is approximately two-thirds of the easy glide flow stress. This stress remained constant throughout Stages I and II. Further, the frictional stress was found to be rather insensitive to strain rate. The results for alpha brass contrast markedly with those for pure copper crystals. In copper the initial value of frictional stress in Stage I is much lower than the frictional stress in Stage II. This large difference in frictional stress, in the pure metal, has been attributed to dislocations becoming jogged. The constancy of the frictional stress in alpha brass, even after 90% glide strain, is attributed to the fact that in

single crystals of solid solutions there are many dislocation groups on slip planes even in Stage II. *a material having high stacking fault energy.*

In general, stress relaxation in alloys appears to be more complex than in pure metals. The interaction of impurities and alloying elements with dislocations appears to have a significant effect on the mechanism of relaxation. The aim of the work of Feltham and Spears⁵⁰ was to examine the stress relaxation in a homogeneous solid solution of simple structure, using solute content as one of the variables. Experiments showed that in alloys the extent of the relaxation was more pronounced at large strains and at low temperatures. For single crystals at room temperature, within the linear stage of hardening, the relaxation was too small and too sensitive to error for any accurate analysis. *grain atoms become important at*

may be demonstrated by considering the slip process.

The displacement by a slip vector $\frac{a}{2}$ the plane is one layer to move

3. BETA BRASS STRUCTURE AND PROPERTIES *the position. This produces a change*

The beta brass phase is an intermediate solid solution in the Cu-Zn system. The maximum solubility of zinc in beta is 36.9 wt.% at the peritectic temperature, and its solubility increases with temperature to 45% zinc at 454°C. Any copper-zinc alloy containing between 36.9 wt.% zinc (63.1 wt.% copper) and 39 wt.% zinc (61.0 wt.% copper) completes its freezing as homogeneous beta. Subsequently, and with further cooling, because of the solubility change, it forms a two-phase alpha-beta alloy. Above approximately 454°C to 468°C, depending on composition, and beta phase is a disordered body-centered cubic structure. Below this temperature, it becomes an ordered beta prime structure. The ordered beta prime phase has a cesium-chloride type of structure. This cesium-chloride type of atom arrangement is equivalent to two interconnected simple cubic unit cells; one of copper and one of zinc, and is referred to as a B2 type.

superlattice. Beta brass deforms by slip on (110) type planes in $\langle 1\bar{1}1 \rangle$ directions, and in general is a material having high stacking fault energy.

There are some solid solutions, like beta brass, in which a specific distribution of the atom species can be induced. Zinc atoms segregate more or less completely on one set of atomic positions, leaving atoms of copper to the remaining positions. The resulting arrangement can be described as a lattice of copper atoms interpenetrating a lattice of zinc atoms. A random solid solution, or disordered arrangement, is changed to an ordered solid solution (superlattice) below a critical temperature. Beta brass in the disordered state has a body-centered cubic lattice, and the dislocation behavior will be as in any body-centered cubic solid solution alloy. However, in an ordered lattice the positions of the individual atoms become important as may be demonstrated by considering the slip process.

The displacement by a slip vector causes the atoms in one layer to move from one position a unit distance to a new position. This produces a change in the local arrangement of the atoms on the slip plane, thereby creating an antiphase boundary. This boundary has a characteristic energy depending on the degree of order in the lattice. The disorder produced by the slip process can be removed by a second dislocation which restores the original atomic arrangement. Thus, the perfect dislocation in the ordered lattice consists of two ordinary dislocations on the slip plane joined by an antiphase domain boundary. This is similar to an extended dislocation consisting of two partial dislocations joined by a stacking fault.

Since a single unit dislocation produces an antiphase domain boundary, it is energetically favorable for it to be associated with a second unit dislocation which removes the high energy fault. This pair of dislocations is called a superlattice dislocation. These two dislocations should move on the same slip plane in the crystal. However, Brown⁵¹ has shown that,

in general, a high stress will be required to move the dislocation. ³⁶

The yield point in beta brass has been studied by Ardley and Cottrell.³⁶ In their investigation, jerky flow was strongly evident in crystals that were annealed at 200°C for 5 minutes before straining at room temperature. The stress-strain curves showed a serrated flow region, followed by a smoother region. In the serrated flow region, there was practically no rise in the average value of the stress with increasing strain. However, in the smoother region, where smaller and more frequent jerks were observed, work hardening was pronounced. This jerky flow was observed both in crystals grown in an argon atmosphere, which did not exhibit a yield point, and in crystals that were grown in a hydrogen atmosphere and did exhibit a marked yield point. A possible explanation for the jerky flow behavior may stem from the fact that the stress necessary to activate a Frank-Read source is greater than the stress required to continue its operation. Since beta brass has a superlattice structure, it is likely that unit dislocations in the superlattice must move through the crystal in pairs in order to leave a perfect superlattice behind. Under these conditions it would be difficult to initially start a Frank-Read source operating.

Greninger⁵² has studied the plastic deformation of beta brass and found that parallel markings that appear on the surface of a crystal after slight deformation represent lattice transformations. Two apparently distinct structural characteristics appear on a polished surface of beta after slight deformation; sets of fine parallel lines in slip bands, and a corrugated relief which shows up as a light and dark banding effect (deformation bands). Neither slip lines nor deformation bands were observed to continue over a grain boundary without changing direction, and both must be related in some way to the beta lattice. Producing deformation bands does not involve any considerable change in orientation,

and the lattice movement involved in producing them can not be much different from that which produces slip lines. Titchener and Ferguson⁵³ have investigated the dynamic compressive behavior of beta brass single crystals and have observed upper and lower yield points. The upper and lower yield stresses were found to depend on both strain rate, and temperature. The yield stress increases significantly with increasing strain-rate and with decreasing temperature. Flow stress was observed to be insensitive to strain-rate at strains less than approximately 4%. At strains greater than 4% for a given strain, the dynamically deformed material was softer than that deformed statically. The dynamic work-hardening rate was less than the static rate. Deformation bands were observed in Titchener and Ferguson's work, but no twinning or jerky flow was apparent. The slip bands created by dynamic deformation were coarse. Such behavior is representative of disordered alloys. This coarse slip and the reduced rate of work hardening during dynamic deformation of beta brass could be attributed to the movement of $a/2\langle 111 \rangle$ unit dislocations rather than superlattice dislocations. The movement of such dislocations would rapidly disorder the operative slip plane, and the subsequent motion of dislocations would be easier. Thus, the behavior would tend to be typical of disordered alloys. Marcinkowski and Brown⁵⁴ have stated that the dislocations in ordered Fe_3Al (B2 structure) move as unit $a/2\langle 111 \rangle$ dislocations. They have observed the antiphase boundary left behind by the glide of such dislocations. Marcinkowski and Chessin⁵⁵ have postulated similar behavior for the static deformation of ordered FeCo (B2 structure). These authors found that the behavior at high stress levels was similar to disordered FeCo , and they reported observing unit dislocations in electron micrographs.

4. ROLE OF DISLOCATIONS

Plastic deformation of a crystalline material having low dislocation density causes rapid multiplication of dislocations. With increasing plastic strain the dislocation density will increase. In the early stages of deformation, dislocation movement tends to be confined to a single set of (parallel) slip planes. On further deformation, slip occurs in other slip systems and dislocations moving in different slip systems interact. This results in the formation of specific dislocation sub-structures which are characteristic of (1) crystal structure of the material, (2) temperature of deformation, (3) strain, and (4) strain rate. Further, grain boundaries, precipitates, and stacking faults affect the dislocation motion.

In general, five independent modes of deformation are necessary to preserve the compatibility at a grain or a phase boundary. Materials that lack sufficient modes of deformation will be brittle, and when such materials are deformed, cracks and voids are created at their grain or phase boundaries. In the face-centered cubic structure there are four {111} slip planes and each has three independent $\langle 1\bar{1}0 \rangle$ slip directions, which yields twelve possible modes of deformation for a material like alpha brass. In the body-centered cubic structure there are six {110} slip planes, each having two independent $\langle 1\bar{1}1 \rangle$ slip directions, also making a total of twelve modes of deformation for the beta brass phase.

During the plastic deformation of a polycrystalline material, the dislocations must overcome the resistance resulting from obstacles such as impurity atoms, point defects, other dislocations, and the grain boundaries. Dislocations moving on slip planes which are terminated by a boundary will tend to pile up at the boundary. Because of this dislocation pile-up, a back-stress will be created which eventually may stop the dislocation source from operating. Dislocations are stored so as to allow compatible

In the region near a leading dislocation stopped at a boundary, there will be a stress concentration. If the stress concentration is high enough, the dislocation may penetrate the boundary and move on a coherent slip plane in the adjacent region. This condition is most likely to occur when many slip planes in the form of a slip band meet a boundary and if there is a dislocation pile-up on each individual slip plane within the band. Under such condition, the stress can reach sufficient levels to form Lüders bands; slip in one region initiates slip in the adjacent region to form a band. Double cross glide can also cause the band to grow laterally and get thicker.

Various mechanisms have been proposed to explain the continuation of slip through the boundary into an adjacent grain. One possibility is that the high stress concentration preceeding the leading dislocations in the slip band cause dislocations to multiply in the adjacent grain. These newly created dislocations would then, under the applied stress, continue to produce glide in that region. Another theory⁵⁶ predicts that the leading dislocations in the slip band, and the stress concentration produced by them at the boundary, cause some boundary dislocations to move into the adjacent grain. These dislocations multiply and slipping takes place in that grain. Another theory⁵⁷ predicts that the stress concentration produced by a dislocation pile-up at a boundary activates a dislocation source present in the nearby region of the adjacent grain. (assuming that dislocation sources

with According to Ashby,⁵⁸ when a relatively stronger, harder, second-phase is present in a material, the deformation immediately becomes non-uniform. No slip occurs within each second-phase region or in the matrix layer adjacent to the particle, provided this layer is strongly bonded to the particle. Such alloys are "plastically non-homogeneous" because of the gradients of plastic deformation that are imposed by the microstructure. To accommodate the deformation gradients, dislocations are stored so as to allow compatible

deformation of the two phases. These are called "geometrically-necessary" dislocations. The density of these dislocations will be directly related to the gradients of plastic deformation. By contrast, dislocations are not geometrically necessary if deformation is uniform, such as in a simple tension test of a pure single crystal. In spite of this, dislocations do accumulate; their presence causes the crystal to work-harden. There is no simple geometric argument to predict the density of these dislocations; this is one reason that the stress-strain relationship for pure metals is so difficult to calculate. Since their accumulation is probably a result of chance encounters in the crystal resulting in mutual trapping, they are called "statistically-stored" dislocations. Of course, shear within the Geometrically-necessary dislocations control the work hardening of the specimen when their density exceeds that of the statistically-stored ones. They contribute to hardening in two ways: by acting as individual obstacles to slip, and (collectively) by creating along-range back stress with wave length equal to the particle spacing.

Except in the region close to a dislocation core, the largest stresses in a plastically deformed crystal containing strong particles generally occur at the interface between particle and matrix because of the discontinuity of elastic properties there. Nucleation of dislocations with new Burgers vectors will occur there (assuming that dislocation sources with the appropriate Burgers vectors are not available locally in the matrix). Prismatic generation, or local shear, which must now involve non-primary Burgers vectors, will take place. These arrays, though complicated, still satisfy compatibility, a fact which is important in determining the effect of particles on the work-hardening rate.

Studies on generation of new dislocations from an interface,^{59,60,61} have shown the following:

(a) Nucleation of new dislocations from a coherent interface is extremely difficult, and requires local stresses of order $G/6$; where G is the shear modulus; the cross-slip mode therefore is anticipated at such particles.

(b) Nucleation of new dislocations at an incoherent or weak interface is relatively easy, requiring a stress of order $G/100$, decreasing as the particles become larger. This means that at large particles multiple slip should be easier than cross-slip. This is in agreement with the observation that prismatic arrays are found at small particles having diameters less than 1000\AA ^{62,63}; multiple slip arrays are found at large particles having diameters greater than 1000\AA .⁶⁴ Of course, shear within the particle, loss of cohesion at the particle-matrix interface, or fracture of the particle or matrix may intervene at any stage of the deformation process if the local stress exceeds that required to nucleate one of these failure modes.

5. STRAIN RATE EFFECTS

Plastic flow occurs as a result of the motion of dislocations within a solid. Orowan⁶⁵ was the first to point out explicitly that the strain rate depends on the number of dislocations moving and their average velocity as well as on how much displacement is carried by each dislocation. The strain-rate is defined by the basic geometric relation

$$\frac{d\epsilon}{dt} = \dot{\epsilon} = \rho b v$$

Where ρ is the dislocation line length per unit volume, or density of dislocation loops.

mobile dislocations; b is the Burgers vector of the mobile dislocations; and v is the average velocity of the mobile dislocations. For particular conditions of stressing and materials, each of the parameters b , v , and ρ can be dependent on time.

Experimental verification of this mechanical transport equation was first provided by Johnston and Gilman,⁶⁶ and many subsequent verifications have been carried out. Different means for relating the microscopic quantities in the equation to the macroscopic shear stress and the plastic strain have been proposed. The value of this general formula for interpreting plastic phenomena is now well established.

If the mobile dislocations in question may be resolved into edge and screw elements then, $\dot{\epsilon} = b(\rho_e v_e + \rho_s v_s)$ according to Gilman.⁶⁷ Subscripts 'e' and 's' represent the values of ' ρ ' and ' v ' for edge and screw components respectively. Where v_e and v_s differ appreciably, it is important to decide which component makes the major contribution to macroscopic strain-rate so that the correct v can be used in the strain rate equation. Experimental evidence that related velocity measurements to macro flow stresses is currently a topic of considerable research interest and is far from being clearly understood. Stein⁶⁸ believes that v_e is rate-controlling for many metals, and he suggests that the temperature dependencies of the two velocities may be similar. Gilman⁶⁹ has a different view. He uses a loop model to suggest that the strain-rate at all strains is determined by the geometrical mean of the edge and screw dislocation velocities. Christian⁷⁰ assumes that the mean dislocation velocity is uniform when the effective stress is constant and neglects acceleration or deceleration effects. According to this model, the slower moving dislocations control the strain-rate through their influence on the rate of deformation of new dislocation loops.

The empirical power law equation⁷¹ often used to describe the stress dependence of the dislocation velocity is

$$v = v_0 \left(\frac{\tau}{\tau_0} \right)^m$$

where v_0 is taken as 1 cm sec.^{-1} , τ_0 as the stress required to give a velocity $v = 1 \text{ cm sec.}^{-1}$, and τ is the applied stress. The constants m and τ_0 may vary with temperature and structure, and as yet there is some controversy as to the manner of their variation. This empirical expression is based on an experimentally observed linear relation between $\log v$ and $\log \tau$.

The other variable in the strain-rate equation that is also the subject of controversy among investigators is the mobile dislocation density ρ . Mecking and Lücke⁷² have postulated that the dislocation density ρ can be considered to be nearly constant, and that changes in the stress influence only the dislocation velocity. Seeger⁷³ noted that the processes controlling the mobility of a dislocation can be conveniently divided into two categories, intrinsic and extrinsic. The intrinsic processes include various Peierls Models, constriction and recombination (pseudo-Peierls), and jogging of screw dislocations. Extrinsic processes would include impurity and dislocation interaction models. The mathematics of some of these models is so similar that they obey much the same functional relationships, and for this reason it will be difficult to distinguish between the various possibilities on the basis of the temperature or rate dependence of the flow stress.

Adams⁷⁴ has suggested that a strong stress dependence of the mobile dislocation density occurs when the internal stress amplitude is comparable in magnitude to the applied stress. When there is a small, but finite

breakaway stress, and the internal stress amplitude is comparable in magnitude to the applied stress, dislocations will be trapped whenever the total stress drops to the breakaway stress. Very small changes in the applied stress can change the velocity of a significant number of dislocations from zero to a relatively high value corresponding to the breakaway stress. The rate sensitivity of the flow stress is thereby very small.

Gilman⁷⁵ has suggested that the total dislocation density increases because of regenerative processes. The ease of movement decreases with increasing plastic strain because of more frequent interaction. There are, according to Gilman, two equivalent ways to explain this statistically. According to the first explanation, if an average velocity that decreases as a result of plastic strain is used, the drag stress becomes a function of plastic strain ϵ_p . The second explanation considers the moving dislocations continuing at the same speed, but the fraction of the total density that moves decreases continually with plastic strain. Gilman observes that the total dislocation density is a linear function of strain, and that the dislocations can breed, especially by a cross-glide process.

Schadler⁷⁶ did not find the multiplication rate of dislocations to be a function of stress if it is measured on a strain basis. Obviously the dislocation density will increase most rapidly near the yield stress, because at this point the plastic strain-rate is greatly increased, but the increased plastic strain-rate would be a consequence of dislocation mobility. Therefore, it is the rate of dislocation multiplication-per-unit strain that should be examined to determine if the multiplication is stress sensitive. Otherwise, one may confuse dislocation multiplication rate with dislocation mobility.

One ageing parameter that is free of most objections has been developed by Sylwestrowicz and Hall.⁷⁸ If a primary Lüders band is run partway along a specimen and the test stops, then,

6. STRAIN AGEING AND GEOMETRIC SOFTENING

The multiple yield points observed as deformation begins in many materials are the result of interrupted motion of the Lüders band along the specimen.⁷⁷ The movement of dislocations near the band front become locked, a phenomenon known as strain ageing, and as a result the stress has to rise to release the Lüder's front again. The ductility is thereby reduced, a phenomenon known as blue-brittleness, and is the result of simultaneous straining and ageing. If a sample is stressed to a level above the lower yield stress (but below the upper yield stress) and subjected to a low-temperature heat treatment, the phenomenon of strain ageing will occur, and it becomes still more difficult to nucleate the Lüders band. Delayed yielding has been examined in beta brass single crystals by Kramer and Maddin.⁷⁸ If the lower yield stress is grain size controlled, and if the upper yield stress obeys a similar law, then the nucleation of the first Lüders band must depend on deformation occurring before the upper yield point, i.e., there should be some evidence of slight plastic flow in the so called elastic region that is termed micro-strain. For those alloys showing Lüders deformation and undergoing longer periods of ageing, they yield point becomes more obvious until there is a true Lüders extension for the second time. This band is termed a secondary a Lüders band and has a diffuse front in the early stages but progressively sharpens as ageing proceeds. At the same time hardness and yield stress also increase. The study of the kinetics of strain ageing is an important part of the theory of yield points and is rendered more difficult by the variety of parameters employed. One ageing parameter that is free of most objections has been developed by Sylwestrowicz and Hall.⁷⁹ If a primary Lüders band is run partway along a specimen and the test stopped, then,

after ageing, an additional stress must be applied to start the band in motion again. All ageing effects do not increase with time; some, particularly in face-centered cubic metals decrease with ageing. For example, some of the unloading yield points in copper and the effects of serrated yielding in aluminum base alloys are often less in fully aged than in freshly quenched or air-cooled materials. Whatever the physical situation, the appearance of a yield point after straining must mean that dislocations are now more difficult to move than before, i.e., they are locked in position. Several mechanisms have been proposed for this dislocation locking effect; Cottrell-Bilby locking, Suzuki Locking, short-range order locking and precipitation on dislocations. *note the existence of single crystal Lüders type extensions. In place of latter results by Ardley and*

Geometric Softening - Single crystals deform on certain slip planes and directions, the initial system being the one where the Schmid factor ($\sin \psi \cos \lambda$) is the largest⁸⁰ (where ψ and λ are the angles between the tension axis and slip plane and slip direction respectively) is a maximum. As deformation proceeds, the crystal planes will rotate so that the specimen axis tends to coincide with the slip direction. If the initial orientation is within a certain range, and the rate of work-hardening low, this slip plane rotation may cause the Schmid factor to increase, and a lower stress is needed to support the continuing deformation. Geometric softening can also lead to single-crystal Lüders bands developing, where the slipped region spreads into the underformed part of the crystal in a controlled manner. *to Johnston and Feltner,⁸⁵ there are two metals which may be used* In Ardley and Cottrell's³⁶ work, the propagation of a Lüders front in alpha brass single crystals was not necessarily restricted to the crystal orientations exhibiting geometric softening, and it must be concluded that some form of solute locking is present, which in turn must be dependent

on orientation. The evidence is in favor of ordering as the locking mode since Heubner and Schumacher⁸¹ showed that strain ageing is less pronounced at higher ageing temperatures.

In beta brass, which is a superlattice based on a body-centered cubic structure, there are very rapid changes in physical properties with departures from stoichiometry. This is caused in many cases by a high concentration of point defects (vacancies). In general, there is a minimum in strength at the stoichiometric composition, with increases on either side, due on one hand, to vacancies, and on the other to substitutional alloying effects. First investigations on single crystals of the compound beta brass were carried out by Elam.⁸² She has noted the existence of single crystal Luders type extension. In view of later results by Ardley and Cottrell, this yield could well be caused by the presence of dissolved gasses. Other indirect evidence of strain ageing from dissolved nitrogen is provided by the internal friction evidence of Clarebrough,⁸³ and by the work of Kramer and Madden⁷⁸ with delayed yield studies. Other investigations using gas-free crystals have found little evidence of any initial yield or strain ageing. Green and Brown,⁸⁴ for example, showed that ordered beta brass is softer than disordered, which is in agreement with other alloys.

7. ORIENTATION EFFECTS

According to Johnston and Feltner,⁸⁵ there are two models which may be used to give semi-quantitative explanations for experimentally established relationships between grain size and resistance of a polycrystal to plastic deformation.

1.) Pile-up Model.

In a favorably oriented grain, a slip band is formed that terminates at a grain boundary. For the shear displacement associated with the impinging slip band to be accommodated plastically in the adjacent grain, the stress concentration at the grain boundary must be sufficient to nucleate slip along the trace of the shear zone. This condition can be expressed most simply in the form $n(\tau - \tau_0) \geq m\tau_c$, where τ is the applied resolved shear stress, τ_0 is a back stress that depends upon dislocation interactions with the lattice, solute atoms and forest dislocations, and τ_c is the critical resolved shear stress necessary to nucleate slip in the adjacent grain in the neighborhood of the boundary. The average Schmid orientation factor "m" takes into account the differences in the direction and plane of the impinging band and the directions and plane of the accommodation slip bands. The importance of including a term such as m was first emphasized by Armstrong.⁸⁶ The term "n" is a stress concentration factor. Eshelby⁸⁷ assumed that the impinging slip bands can be considered to be a pile-up of n dislocations, where n is proportional to the length of the slip band, and is determined by the grain diameter ℓ . The equation for n is; $n = A[(\tau - \tau_0) \ell / \mu b]$, where μ is the shear modulus, b is the Burgers vector, and A is a constant. More simply, the stress concentration at a distance r ahead of the pile-up is given approximately⁸⁸ by $(\ell/r)^{1/2}$. Therefore $\tau = \tau_0 + m\tau_c \cdot r^{1/2} \cdot \ell^{-1/2}$, or in terms of tensile stress $\sigma = \sigma_0 + (m^2 r^{1/2} \cdot \tau_c) \ell^{-1/2}$. This form leads to the familiar Hall-Petch relationship^{56,89}

$$\sigma = \sigma_0 + k \ell^{-1/2}$$

where, by comparison of the equations, $\kappa \equiv m^2 r^{1/2} \tau_c$, which simply states that the flow stress is a function of the grain diameter.

2.) In the second approach,^{90,91} stress concentrations at grain boundaries are not taken into account explicitly, and the assumption of dislocation pile-ups is avoided. Instead, use is made of the relationship which expresses the flow stress σ in terms of the dislocation density ρ , i.e.,

$$\sigma = \sigma_0 + \alpha \mu b \rho^{1/2}$$

where σ_0 is a constant lattice friction stress perturbed by solid solution effects, and α is a numerical constant. The principal feature of this explanation of the grain size dependence of the flow stress, based on dislocation density, is the experimental finding that ρ is an inverse function of the grain size. This equation also reduces to the Hall-Petch relationship since ρ is proportional to $1/l$ and κ is a function of $\alpha \mu b$.

Any model or explanation for the influence of grain size on the plastic deformation of a polycrystal cannot be divorced from the consequences of strain compatibility that constitute the foundation of grain boundary effects. The need to maintain continuity of plastic strain across grain boundaries between randomly oriented neighbors demands that multiple slip or shear modes be brought into operation when the polycrystal as a whole is deformed.^{57,92,93} In the neighborhood of a boundary between two grains in a randomly oriented polycrystal, deformation occurs through the operation of several different slip systems, a phenomenon examined in detail by Chalmers and co-workers.^{94,95}

The total number of operative slip systems in a given region embracing a boundary will depend on the magnitude of the plastic strain. In the microplastic strain regime of 10^{-5} to 10^{-6} those grains having the most favorable Schmid factors deform initially in a way that approaches free monocrystal

behavior. As the strain level increases, the number of different slip systems necessary to maintain continuity of strain increases up to a maximum of 5, the number anticipated by the macroscopic homogeneous criteria of von Mises⁹⁶ and Taylor.⁹² Kochs⁹⁷ has analyzed the relationship between poly and monocrystal behavior. This analysis showed that the shear stress-shear strain curve of a face-centered cubic monocrystal oriented for "polyslip", where Stage I is essentially missing, i.e., one having a $\langle 111 \rangle$ orientation, can be made to superpose on the tensile stress-tensile strain curve of the corresponding polycrystal. This was done simply by taking into account the average orientation factor m at the Taylor value of 3.1.

Plastically anisotropic crystals exhibit strong grain boundary strengthening effects that reflect the barriers that individual grain present to each other because of insufficient independent slip systems. In other words, the average orientation factor m is high, and dislocations tend to adopt coplanar pile-up configurations. At the other extreme, grain size effects are reduced to a minimum in those solids that are essentially isotropic in a plastic sense (high purity face-centered cubic solids with high stacking energies and high purity body-centered cubic solids). Intermediate degrees of plastic anisotropy represent those situations where there are sufficient independent slip systems to satisfy macroscopically the von Mises-Taylor criteria but where limitations imposed on cross-slip cause dislocations to adopt coplanar arrays. In these cases, the effect of grain size on flow stress is correspondingly intermediate. According to Johnston and Feltner,⁸⁵ the principal source of grain boundary strengthening may be viewed as a heightened strain hardening effect. This stems from the dynamical imbalance (induced by the need for polyslip) in the rates of plastic flow on both sides of individual grain boundaries. The role of solute

elements on the ability of the grain boundaries to increase the flow stress is considered to stem from the effect of such solutes on the mode of deformation rather than from dislocation source interactions.

CHAPTER III

OBJECTIVES OF THIS WORK

Hingwe and Subramanian⁹⁸ have developed experimental techniques for growing fundamental bicrystal and duplex crystal units of alpha-beta brass. Single crystals of alpha brass are carefully grown using a Bridgman method and are joined to large-grain beta brass. The resulting two-phase structure at the interface after joining the alpha phase to beta is reduced to a flat, sharp boundary by a cyclic local annealing technique developed by them. In their work, the phase transformations that take place upon heat-treating the interface structure and the morphology of the structure has been studied. Low strain-rate uniaxial tension behavior of the duplex crystals and bicrystal units was also studied.

The objectives of this work were to produce macroscopic size multicrystal units of alpha brass in series with beta phase with sharp or duplex boundaries. These model units were used to investigate mechanical properties of model systems of alpha-beta brass. Of specific interest were the effects of stress concentration, variable strain-rate, and the crystallographic orientation of the alpha and beta phases upon the propagation of slip and deformation across the phase boundary. Indentation tests were used to study the stress concentration effect upon slip interaction with the phase boundary. Tension tests using various strain-rates, and stress relaxation tests were utilized to study the deformation near and across the phase boundary. Laue back-reflection X-Ray techniques

were used to determine the relative orientation of the alpha and beta phases at the boundary prior to testing.

Optical and electron microscopic techniques were used during and after testing to examine the slip distribution near the phase boundary. Dislocation modelling techniques are employed to explain the observed deformation behavior of image composites.

Since the properties of a two-phase material depend on the properties of the individual phases and on the phase boundary, understanding the role of the phase boundary is fundamental in developing an understanding of the two-phase material behavior. This understanding then may be applied to develop two-phase materials having specific or superior properties for engineering application. The main purpose of this work has been to obtain a better understanding of the role of the phase boundary in the plastic deformation of two-phase materials.

CHAPTER IV

DESCRIPTION OF EXPERIMENTAL PROCEDURES

A. SPECIMEN PREPARATION

1. MATERIALS

a.) Alpha Brass

The alpha brass used in this work had 70% copper and 30% zinc. The material was obtained in the form of 1/4 in. x 1 in. bar stock. Pieces of stock 1/4 in. square and approximately 1 1/2 in. long were cut from the bar stock, and turned to 1/4 in. diameter in a lathe to fit the graphite crucibles for crystal growth.

b.) Beta Brass

The beta brass used for this work was made by adding laboratory purity zinc to Muntz metal (60% copper - 40% zinc). The beta prime phase (having CsCl structure) exists at room temperature between composition limits of approximately 48-50.5 wt.% zinc. Appropriate amounts of pure zinc were weighed and added to the Muntz metal to make approximately 1000 gm. batches of beta brass. Extra zinc, approximately 5%, was also added to each batch to account for the inevitable loss of zinc during melting and pouring.

The 60/40 Muntz metal was first melted in a covered graphite crucible, with a one inch thick layer of carburizing compound covering the top surface

11

to minimize the zinc loss, for approximately 1 1/2 hrs. at a temperature of 925°C. The crucible with the molten 60/40 brass was withdrawn from the furnace and the weighed amount of zinc (with the additional 5%) was added and submerged in the melt quickly to minimize zinc loss. After maintaining the melt at 925°C for 30 min., the melt was quickly stirred to ensure homogenization, and poured into rectangular cast iron ingot molds.

After cooling, the beta brass ingots were cold rolled approximately 15% in a rolling mill, and annealed in closed containers containing a carburizing compound for 2 hrs. at 500°C. This was followed by furnace cooling to room temperature. After cleaning, the ingots were cut, polished and etched with a ferric chloride solution, and examined with an optical microscope for microstructural analysis. Evidence of any alpha phase at the grain boundaries would indicate too low a zinc content, and any gamma phase present in the structure would be indicative of excessive zinc content. Samples of approximately 2 gm. were taken from each ingot by drilling, and analyzed in a Fisher spectrophotometer for copper content. All of the beta brass used for this work had a 51 wt.% copper-49 wt.% zinc composition.

After analysis, the ingots were cut into 1/4 in. square by 1 1/2 in. long pieces and turned in a lathe to 1/4 in. diameter cylinders.

c.) Two-Phase Foil

The two-phase foil used in the joining of the alpha brass single crystal with the beta brass was prepared by cold rolling 60/40 Muntz metal in a rolling mill to a thickness of approximately 0.35 mm. This was accomplished by a sequence of rolling and annealing treatments until the desired thickness was achieved.

2. ALPHA BRASS SINGLE CRYSTAL GROWTH

Alpha brass single crystals of random orientation were grown by the Bridgman technique. The alpha brass stock material cylinders were cleaned in a 50% HNO_3 and water solution, washed in water and alcohol and dried thoroughly. Crucibles were made from high density graphite rod, and a specially made gun drill was used to produce the smooth surface and special shape in the bottom of the crucible cavity, which is shown in Fig. 1. The alpha brass stock was placed in the graphite crucible, which was then sealed in a 15 mm quartz tube using an oxygen-propane torch. A small gas expansion space was left at the top when sealing the tube. Special care was taken not to "pull" the heated quartz tube while sealing, since this would reduce the glass wall thickness and cause its fracture during crystal growth. This sealing procedure is necessary to prevent zinc loss from the alloy during single crystal growth.

After sealing, the quartz tube containing the graphite crucible was placed in a mullite tube, packed with fireclay, and dried thoroughly. The purpose of the tube and surrounding fireclay is to minimize the radial temperature gradient in the assembly. As shown schematically in Fig. 1, the bottom portion of the crystal growing assembly was kept to a minimum thickness to enhance the axial temperature gradient for crystal growth. The smoothly shaped cavity having a sharp tip at the base of the crucible was found to be necessary to grow single crystals of alpha brass. Any sharp corners, as in an ordinary drilled hole, or tool marks in the cavity were found to initiate the growth of other crystals in addition to the single crystal nucleated from the pointed tip of the cavity.

This entire assembly was suspended by a thin metal rod in a vertical tube furnace in which an axial temperature gradient was maintained as shown schematically in Fig. 2. The tube furnace temperature gradient was

Fig. 1 Schematic Of The Assembly Used For Growing Single Crystals
of Alpha Brass.

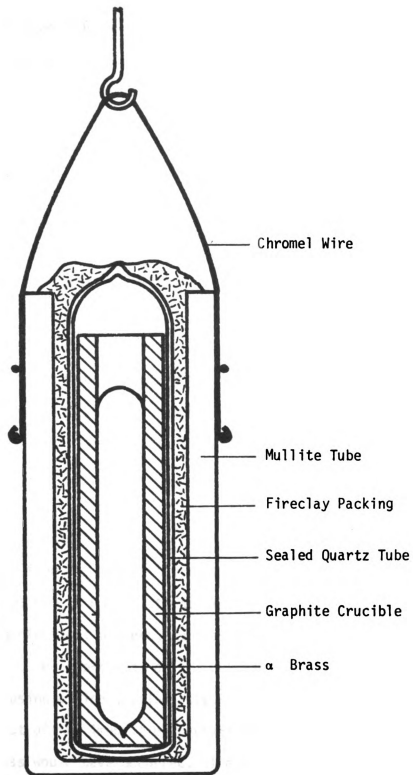


Fig. 1 Schematic Of The Assembly Used For Growing Single Crystals
Of Alpha Brass.

checked by an axial thermocouple probing technique before inserting each crystal growing assembly. The assembly was positioned in the temperature gradient so that the entire length of the alpha brass stock was at a temperature of 1000°C. The assembly was soaked in this position for 2 hrs. before lowering through the temperature gradient.

Lowering was accomplished by means of an independently mounted 1 rph motor and pulley. The motor pulley diameter was sized to give a lowering rate of 1.0 cm./hr. The assembly was lowered for a period 12 hrs. so that the entire alpha brass crystal had solidified and cooled somewhat in the lower temperature region in the furnace. After lowering, the assembly was removed from the furnace, cooled to room temperature, and opened. The zinc loss using this technique was minimal as evidenced by the very clean appearance of the inside of the quartz tube. The alpha brass crystals grown by this method were 9 mm. in diameter and 3-3.5 cm long.

3. TREATMENT OF ALPHA CRYSTALS

After removal from the graphite crucible, the alpha brass crystals were cleaned in a 50% HNO_3 - H_2O solution. This procedure revealed any serious crystal imperfections present, such as lineage structure, or polycrystalline regions. The upper ends of the crystals, approximately 1 cm. long, were cut off using a fine jewelers saw. These discarded ends are regions in which most of the impurities present would be located and where most of the zinc loss would have occurred. The crystals were sealed in 9 mm I.D. quartz tubing and homogenized for 16 hrs. at 800°C to remove any micro-segregation, as suggested by Maddin,⁹⁹ and were furnace cooled.

The cut end of each crystal was ground carefully on a wet belt surfacing machine to produce a flat surface normal to the crystal axis. The

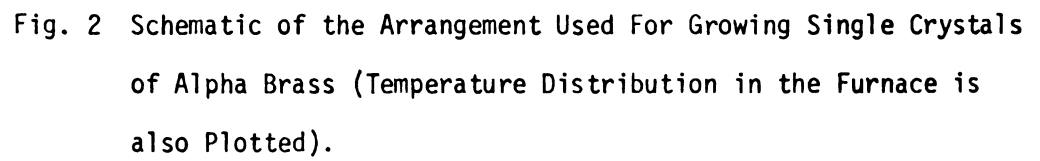


Fig. 2 Schematic of the Arrangement Used For Growing Single Crystals of Alpha Brass (Temperature Distribution in the Furnace is also Plotted).

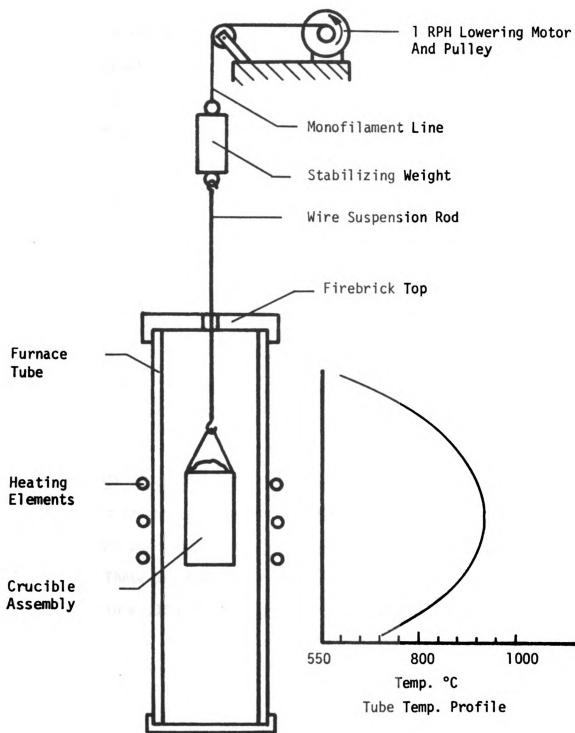


Fig. 2 Schematic Of The Arrangement Used For Growing Single Crystals of Alpha Brass (Temperature Distribution In The Furnace Is Also Plotted)

damaged surface layer from this procedure was removed by polishing with concentrated nitric acid. The ground end then was hand polished on 240, 320, 400 and 600 grit wet metallographic papers. Between each polishing paper the crystal was washed and polished in concentrated nitric acid to remove the damage introduced by grinding with the previous paper. Finally the surface was lapped on a canvas wheel with a 600 grit alumina slurry followed by final polishing on a nylon backed microcloth wheel using 1 μ diamond compound and Metadi fluid. After washing thoroughly, the polished surface was treated with a chemical polish consisting of 17% nitric acid, 17% phosphoric acid, and 66% acetic acid to remove the last traces of damaged surface layer.

Back reflection Laue X-rays of each crystal were taken on the polished end surfaces. In addition to crystal orientation determination, the X-rays were useful in assessing the crystal perfection.

4. TWO-PHASE FOIL PREPARATION

Discs of the two-phase foil material to be used in the joining of the crystals were punched out of the rolled stock to have approximately a 9 mm. diameter. These discs were reduced in thickness to approximately 0.15 mm. by etching in a 50% nitric acid-water solution, followed by thorough washing and drying.

5. JOINING ALPHA AND BETA BRASS

The technique for constructing the two-phase bicrystals for this work has been developed by Hingwe and Subramanian.⁹⁸ This method consists of first enclosing the alpha brass single crystal, two-phase foil, and polycrystalline beta brass stock in a quartz tube. The heating set-up used melted the beta brass and the foil without melting any of the alpha brass substrate. The arrangement is shown schematically in Fig. 3.

The alpha crystal, foil, and beta stock were all chemically polished in a solution of 17% nitric acid-17% phosphoric acid-66% acetic acid, washed thoroughly and dried before insertion in the quartz tube. The graphite crucible diameter in which the alpha single crystals were grown was chosen to match the inside diameter of the 9mm. quartz tubing. This eliminates chemical reduction of the crystal diameter to fit the tubing. The primary purpose of using a two-phase foil in the joining procedure is to inhibit the diffusion process between the alpha brass single crystal and the higher zinc composition beta brass. By blocking the diffusion of zinc a thinner two-phase region is developed at the interface.

A large axial temperature gradient used in solidifying the beta brass on the alpha crystal substrate has been suggested by Greninger.¹⁰⁰ This promotes large coarse grain growth in the beta phase upon solidification. In most cases a large single grain of beta phase developed at the interface. In most of the cases where more than one beta grain formed at the boundary, the cyclic local annealing process promoted grain growth and aided in obtaining a single large beta grain at the boundary.

Seven to eight closely spaced windings of (0.005 in. x 0.125 in.) nichrome ribbon was wound on the quartz tube as a heating element. Approximately 1 1/2 wraps were kept on the alpha brass single crystal to heat the substrate and facilitate the wetting action and bonding to the liquid metal

Fig. 3 Schematic of the Arrangement Used for Joining Alpha and Beta Brass.

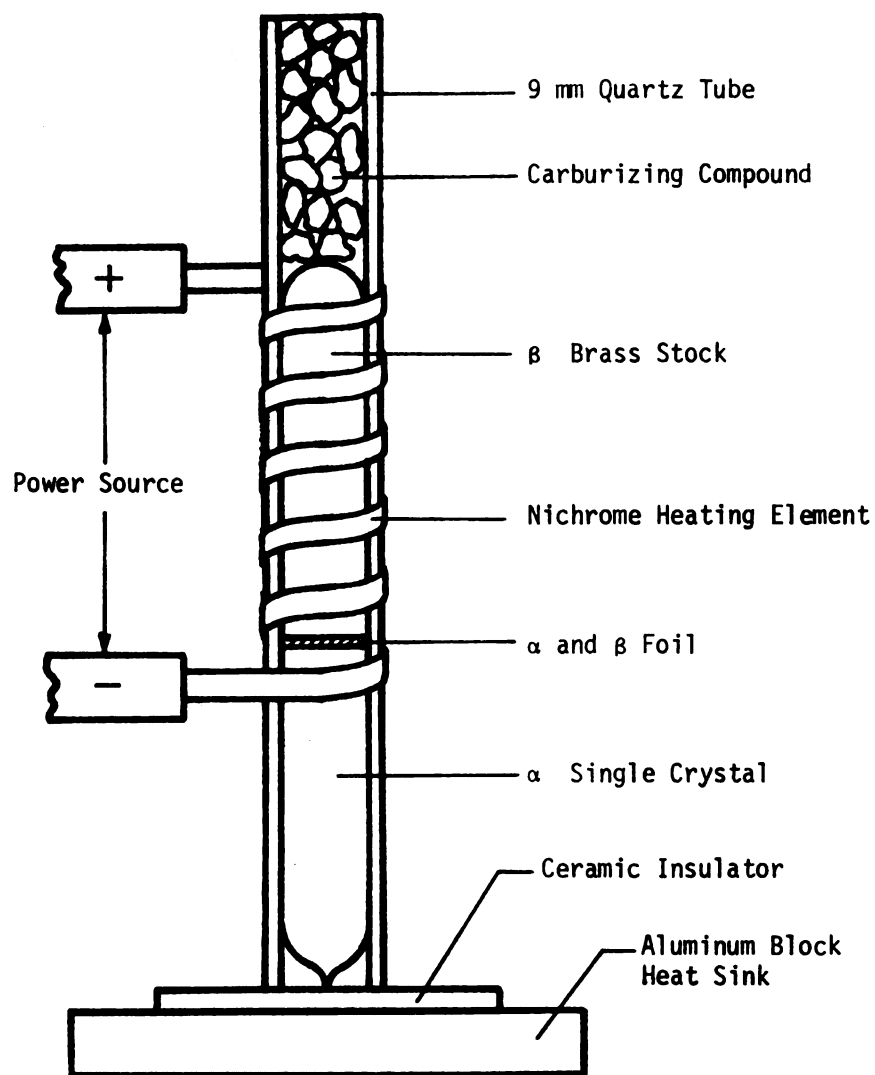


Fig. 3 Schematic Of The Arrangement Used For Joining Alpha And Beta Brass.

17

17

above. This also aided in melting the two-phase foil. Granules of carburizing compound were put in the quartz tube above the beta brass stock to create a non-oxidizing CO_2 atmosphere to minimize zinc loss during melting and cooling. The whole assembly was sitting on a ceramic plate.

Melting was accomplished using a direct current power supply providing approximately 30 volts and 20-23 amperes. After wetting of the alpha substrate by molten beta was seen at the junction, the power was maintained at the same level for another 1-1 1/2 min. and then shut off. The ceramic insulating plate was carefully removed to allow the pointed end of the alpha crystal to come in contact with the aluminum heat sink. This created the large axial temperature gradient desired for the solidification of the beta phase. Upon cooling to room temperature, the bicrystal was removed from the quartz tube, cleaned with chemical polish, and washed.

To inspect the character and extent of the two-phase region developed at the boundary, a longitudinal flat was ground and polished on the specimen. After etching in a solution composed of 5 parts of FeCl_3 , 50 parts of HCl and 100 parts of 50/50 alcohol-water, the two-phase structure at the alpha-beta interface was inspected and photographed on a metallograph for reference while local annealing.

6. DUPLEX INTERFACE REDUCTION

The crystals were either lowered through a sharp temperature gradient in a vertical tube furnace and then received a cyclic local annealing treatment, or were cyclically local annealed directly. The procedure utilized was determined by the character and extent of the duplex, or two-phase region created at the boundary. Samples with wide zones of Widmanstätten structure, particularly if the alpha platelets were not continuous with the alpha crystal,

were lowered two to three times through a temperature gradient as shown in Fig. 4. Thermocouple temperature probing of the vertical tube furnace was used to locate the position of a 760°C temperature zone. The interface of the bicrystal was positioned so as to coincide with the 760°C temperature point and was soaked for 15 minutes in this position before lowering at 8.0 cm/hr. for another 15 minutes.

Lowering through the temperature gradient was found to effectively reduce the extent of the two-phase region and tended to make the Widmanstätten structure alpha phase platelets continuous with the alpha crystal substrate.

The cyclic local annealing treatment reduced the duplex boundary structure to an oriented, equiaxed, corrugated or a sharp flat boundary in the specimens. The arrangement is shown schematically in Fig. 5(a). Local annealing cycles of one hour duration were found to be most effective. The specimen was cooled to room temperature after each cycle. The current used to heat the single wrap of nichrome ribbon was adjusted to give a maximum temperature of approximately 800°C at the boundary, as shown in Fig. 5(b). During the initial local annealing cycles the diffusion of zinc was fairly rapid between the beta phase and the two-phase zone. Later in the heat treating cycles, as the two-phase zone diminished toward a flat boundary, the compositions of the alpha and beta phases approach their equilibrium values and the process slows considerably. Slightly longer, (approximately 1 1/2-2 hrs.) heating cycles were found to be more effective in the final stage of heat treating. The specimens were heat-treated to produce specimens with duplex interface, sharp corrugated interface, and bicrystals.

Periodically during the local annealing cycles the longitudinal flat of the crystal was polished and etched for visual examination with the microscope. This was essential to follow the progress of the reduction of the duplex region. When the two-phase zone had been completely eliminated,

Fig. 4 Schematic of the Lowering Arrangement Utilized for Reducing the Duplex Transition Zone. (Temperature Distribution in the Furnace is also Plotted)

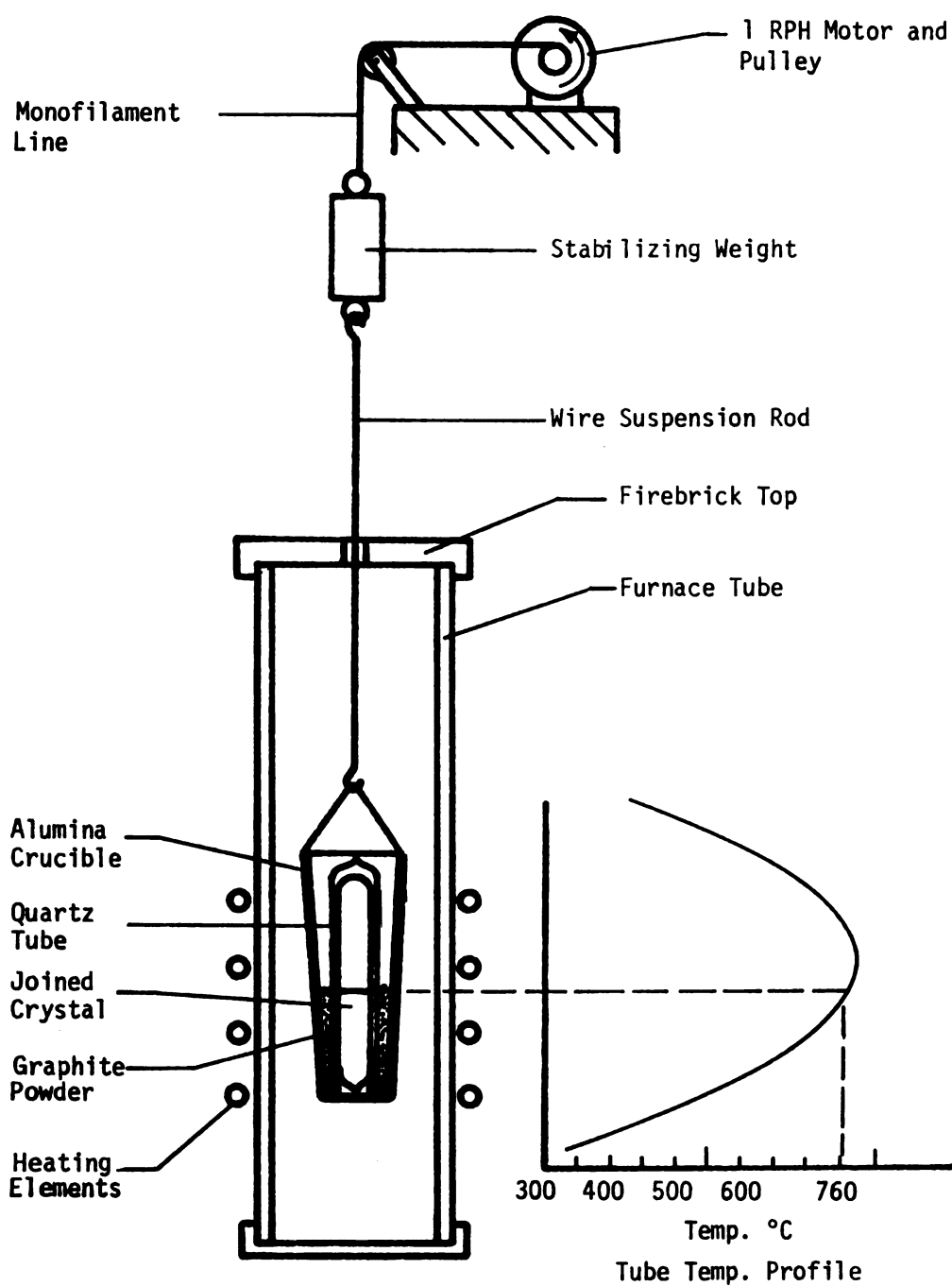


Fig. 4 Schematic Of The Lowering Arrangement Utilized For Reducing Duplex Transition Zone.

Fig. 5 (a) Schematic of the local annealing arrangement.
(b) Temperature of the local annealing set-up.

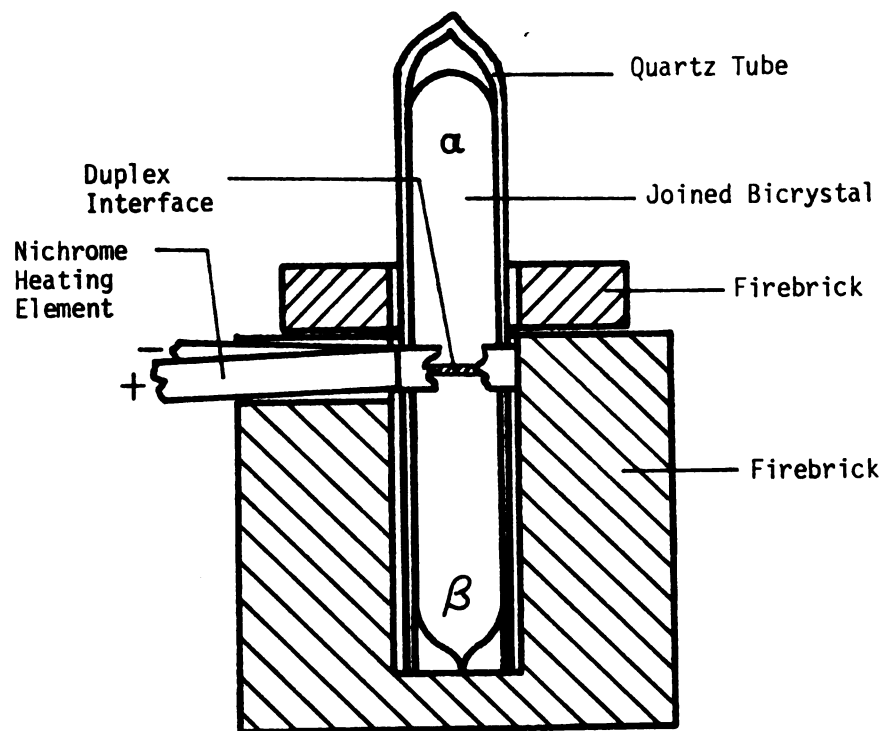


Fig. 5a Local Annealing Arrangement

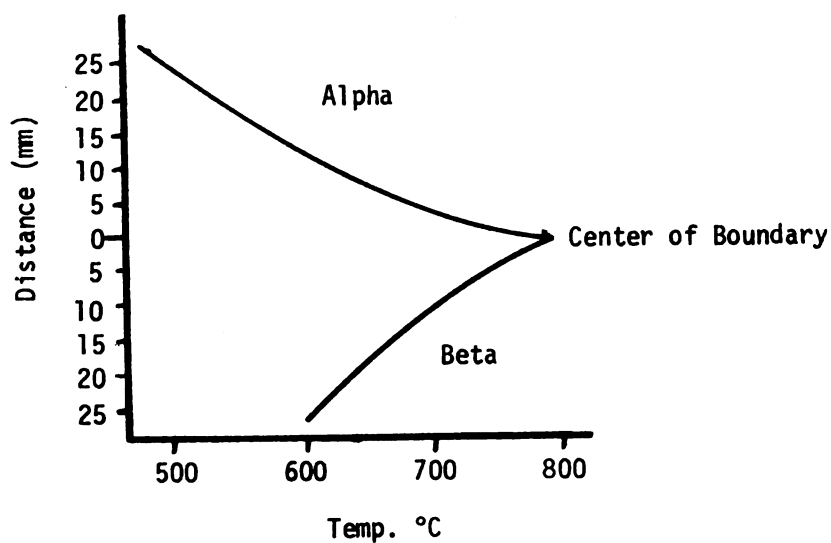


Fig. 5b Local Annealing Temp. Profile

and a sharp flat boundary resulted, the local annealing process was stopped. Such a process produced two-phase bicrystals or multi crystals. The diffusion process, phase transformations, and morphology of the duplex boundary region have been studied in detail by Hingwe and Subramanian.⁹⁸

7. MACHINING

Once the desired boundaries were achieved, the bicrystals were machined to two different configurations on a vertical milling machine. Square specimens were made for indentation testing and reduced section tensile bar shapes were machined for strain-rate tests. Machining was done with a new 11/32 in. diameter, four flute end mill. A table feed rate of 2 in/min. was used. The depth of the initial cuts was 0.003 in., and the last finishing cuts were reduced to 0.001 in. deep to minimize the damage to the crystal surface layer.

When machined to desired dimensions, the specimens were carefully polished on all four sides through 240, 320, 400 and 600 grit wet metallographic papers, 600 grit wheel, and finished on a lapping wheel using 1 μ diamond compound. The specimens were treated with the chemical polish, and were washed thoroughly and dried after immersing in alcohol. Steel nuts, whose threaded holes had been drilled out to 1/4 in. diameter, were silver soldered to the ends of the specimens as shown in Fig. 6 for the strain-rate samples. Special care was taken to keep the samples cool by placing a wet cloth over most of their length while silver soldering the nuts on the ends as suggested by Brindley et al.¹⁰¹

Fig. 6 Machined Tensile Specimen Ready for Testing.

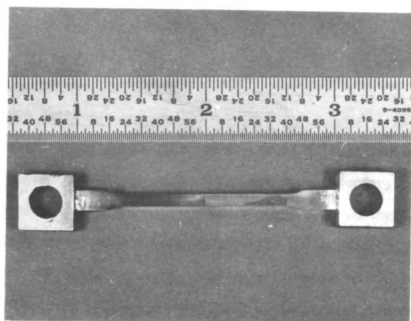


Fig. 6

8. X-RAYS

Laue back reflection X-ray pictures were taken on the alpha brass single crystal on two adjacent faces near the boundary, and on two adjacent faces of a beta single grain in contact with alpha at the phase boundary. These X-rays were taken to determine the relative orientation of the alpha and beta phases in contract at the boundary. Photomicrographs of the boundary region on all four sides were taken to facilitate the comparisons of the deformed structure with the original structure after testing.

B. MECHANICAL TESTING PROCEDURES

1. Indentation Tests

Indentation tests were performed to create a localized region of high stress concentration near the alpha-beta phase boundary. The objective in producing such a stress condition was to determine whether a concentration of stress alone at the boundary would initiate and propagate slip through the barrier of the phase boundary. The tests were performed in an Instron testing machine using a 20 degree included angle conical indenter. The tests were performed on samples that had been machined and polished to have square cross-sections approximately 4 mm. x 4 mm.

The load applied to the indenter, the distance of the indentation in the alpha phase from the phase boundary, and the rate of load application to the indenter were all varied. Three loads were chosen for these tests, 12, 25 and 40 kg., and the cross-head speeds, or rates of load application used were 0.005, 0.05, 0.5, and 5.0 cm/min. Approximate distances of the indentations in the alpha phase from the boundary used were 1.5, 1.0 and 0.5 mm.

Indentation tests were performed on specimens having duplex boundary

regions as well as specimens with flat phase boundaries. Observations of the tested samples were made using an optical microscopy, scanning electron microscope and by the transmission electron microscope with replicas of the deformed region at the phase boundary.

2. STRAIN-RATE TESTS

Reduced section multicrystal specimens having steel nuts silver-soldered on the ends, as previously described, were used for testing in tension at various strain-rates. All specimens were machined and polished to approximately the same dimensions. A specimen ready for testing is shown in Fig. 6. An Instron testing machine was used for these tests. A 35 mm. camera with a copy lens was set up to photograph the progress of deformation in sample during testing. A large magnifying lens and lights were also used to visually observe the deformation bands and slip lines as they approached the phase boundary in the alpha phase. The rates of cross-head movement used were in the range 0.005 to 5.0 cm/min.

Once the slip lines were observed to be very close to the phase boundary, the cross-head was stopped to record the stress-relaxation at that point and the specimen was unloaded and removed from the testing machine. Initially all specimens were marked with a gauge length measured in each phase from the phase boundary. Upon removal from the testing machine the percent of elongation in each phase was measured.

All four sides of each specimen were then photographed using a research metallograph at relatively low magnification. This was done to obtain a record of the angle of the slip lines on each face and to observe and record

the slip pattern near the phase boundary. Before putting the specimens back in the testing machine for further deformation, plastic single or two-stage replicas were made of regions near the phase boundary for observation with the transmission electron microscope. After completion of this procedure, the specimens were returned to the testing machine and were plastically deformed a small additional amount. The specimens were then unloaded once more, photographed, the elongation was measured, and replicas of the surfaces were again taken. This procedure was repeated on each specimen two or three times to obtain as much information as possible about the interaction of slip with the phase boundary. With each specimen, this repeated loading procedure was carried out until definite evidence of deformation in the beta phase was obtained, at which point testing of that specimen was stopped. In some specimens slip did not cross the phase boundary and fracture occurred in the alpha region.

After all photographs, replicas and measurements were made on each completely tested specimen. A section 10 mm. long containing equal lengths of each phase near the phase boundary was carefully cut from each specimen with a fine jewelers saw. These specimen sections were studied with an Applied Research Laboratories scanning electron microscope.

CHAPTER V

TEST RESULTS

A. INDENTATION TESTS

Indentation tests were carried out on specimens having three interfacial geometries; Oriented duplex, equiaxed duplex and flat boundary.

(Shown in Fig. 7)

For all of the micrographs presented in this section of indentation test results, the alpha single crystal portion of the specimens is shown at the left and is designated by "A". The interface region and the beta phase appear to the right and are designated by "B".

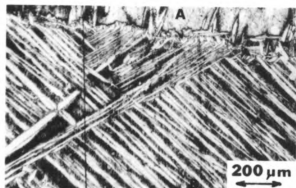
Oriented Duplex Boundary

The effect of the rate of indentation is shown in the micrographs presented in Fig. 8a - 8d. In this series the indentation load was 25 Kg and the indentation distance was 1.5 mm from the boundary in the alpha region. The rate of load application for indentation was varied by using the cross-head speeds from 0.005 cm/min. to 5.0 cm/min. At lower strain-rates, for 25 Kg load and a distance of 1.5 mm, the deformation produced by the stress concentration consists of fine slip lines. Such slip lines interact less with the boundary structure than slip lines produced by higher rates of load application. The high loading rates produced much coarser slip lines which propagate further from the indentation into the oriented duplex boundary structure. However, the oriented duplex interface

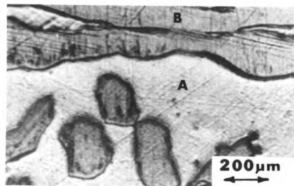
Fig. 7 Four Types of Interfaces Studied.

- (a) Oriented duplex interface.
- (b) Equiaxed duplex interface.
- (c) Corrugated bicrystal interface.
- (d) Flat bicrystal interface.

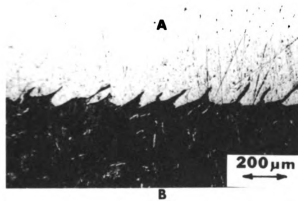
a



b



c



d

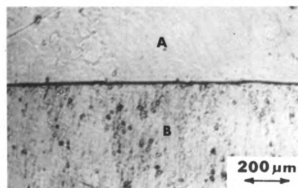


Fig. 7

Fig. 8 Slip Interactions With Oriented Duplex Interface.
25 Kg. load, indentation at a distance of 1.5mm from
interface at various rates of loading.
(a) 0.005 cm/min. cross-head speed.
(b) 0.05 cm/min. cross-head speed.

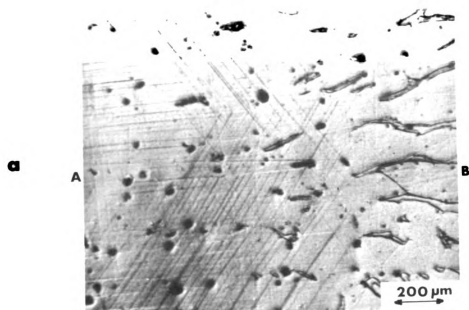


Fig. 8a

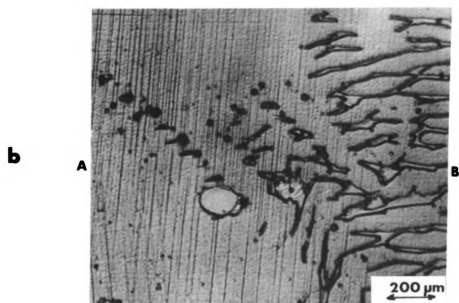


Fig. 8b

Fig. 8 (Continued)

(c) 0.5 cm/min. cross-head speed.

(d) 5.0 cm/min. cross-head speed.

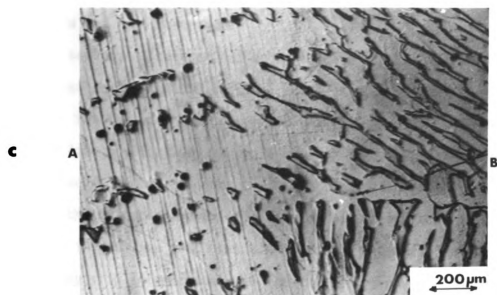


Fig. 8c

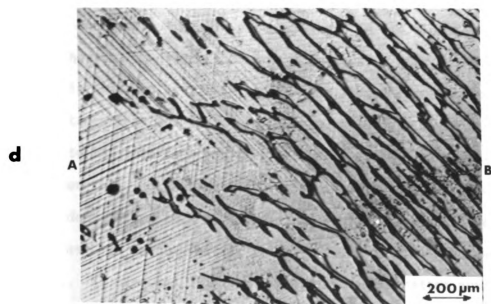


Fig. 8d

structure seems to be an effective barrier to slip under these test conditions, and no interaction of slip with the oriented beta phase in the structure has been observed.

A test series was carried out using a 25 Kg load, and a constant, low cross-head speed of 0.005 cm/min. The distances of indentation from the boundary for the indentation were 0.5 and 1.5 mm. At this load and low rate of load application, as would be expected, the indentation closer to the boundary (0.5 mm) produces more slip interaction with the nearby portions of the oriented duplex interface structure as shown in Fig. 9a and 9b. The indentation which was closer to the boundary, however, failed to produce any slip interaction into the duplex region or with the beta phase at this load and rate. Indentations using 25 Kg and higher cross-head speeds also failed to produce any propagation of slip into the duplex region of the interface when the indentations were made at 0.5 mm and 1.5 mm away from the boundary. The slip patterns shown in Fig. 10a and 10b indicate that for an indentation distance of 0.5 mm heavy slip with a higher slip line density is produced at the interface than in the specimen indentation at 1.5 mm distance from the interface. Although in both cases the propagation of slip to the interface was more effective at this rate of loading than at a lower rate, no propagation of slip into the duplex region was observed. Indentation with a 25 Kg load and a high cross-head speed of 5.0 cm/min. was also carried out at 1.5 mm and 0.5 mm distances away from the interface. As expected, the highest stress concentration near the interface for this load was achieved using the 0.5 mm indentation distance. Once again, as shown in Fig. 11a and 11b, the oriented duplex interface structure acted as an effective barrier to slip propagation at this load value of 25 Kg.

Fig. 9 Slip Interactions With Oriented Duplex Interface.

25 Kg. load, 0.005 cm/min. cross-head speed indentation at:

(a) 1.5 mm

(b) 0.5 mm

a

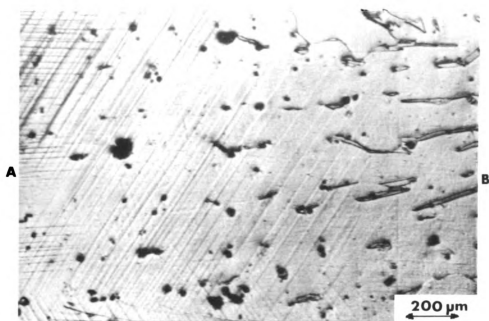


Fig. 9a

b

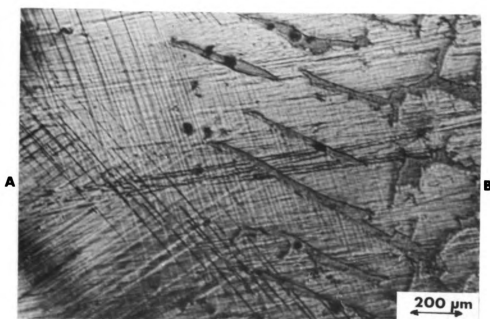


Fig. 9b

Fig. 10 Slip Interactions With A Oriented Duplex Interface.
25 Kg. load, 0.5 cm/min. cross-head speed indentation at:
(a) 1.5 mm
(b) 0.5 mm

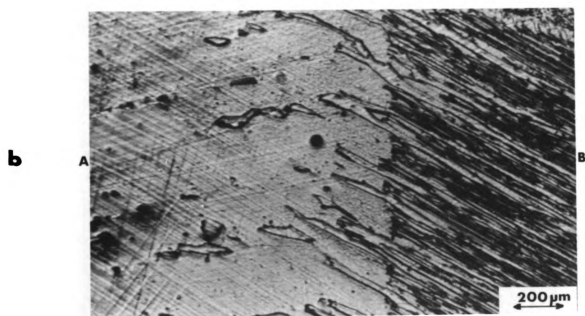
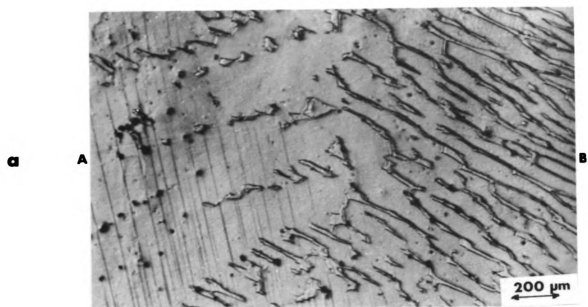


Fig. 10

Fig. 11 Slip Interactions With Oriented Duplex Interface.

25 Kg. load, 5.0 cm/min. cross-head speed indentation at:

(a) 1.5 mm

(b) 0.5 mm

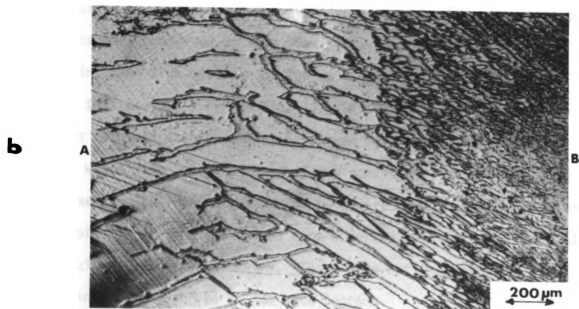
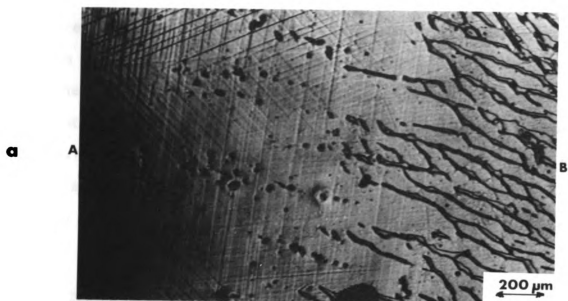


Fig. 11

For a comparison of the effect of varying the load, tests were performed using a 40 Kg load at a low indentation rate of 0.005 cm/min. and a distance to the interface of 1.5 mm. The results of this test are presented in Fig. 12. The 40 Kg load was more effective at this distance of indentation and loading rate in producing a much higher slip line density at the interface structure, than 25 Kg load. This can be seen by comparing Fig. 12 with Fig. 8a. Extensive cross-slip observed in the slip line pattern produced by the 40 Kg load, attests to the fact that the oriented duplex interface geometry is an effective barrier to slip propagation in indentation tests.

Equiaxed Duplex Boundary

In order to investigate the effects of the type of interface structure on the progress of slip into an interface region, tests were performed on samples having an equiaxed duplex interface geometry. For comparison purposes tests were conducted using a load of 25 Kg, a cross-head speed of 0.05 cm/min., and at a distance of 1.5 mm from the interfacial region. The result of this test is shown in Fig. 13. This test result may be compared to results obtained with specimens having an oriented duplex interface geometry, which were tested under the same conditions, shown in Fig. 8b. The equiaxed duplex interface seems to be a more effective barrier to the progress of slip as fine slip lines were observed in the alpha phase islands in the equiaxed interface geometry. These were not extensive, however, and no slip lines were observed in the beta regions.

To investigate the effect of stress concentration on the equiaxed interface geometry, series of tests were conducted using a 40 Kg load, a close distance of indentation to the boundary of 0.5 mm and various rates of indentation ranging from 0.005 to 5.0 cm/min. As anticipated from the results

Fig. 12 Slip Interactions With Oriented Duplex Interface.

40 Kg. load, 0.005 cm/min. cross-head speed indentation at 1.5 mm

Compare with Fig. 8 a

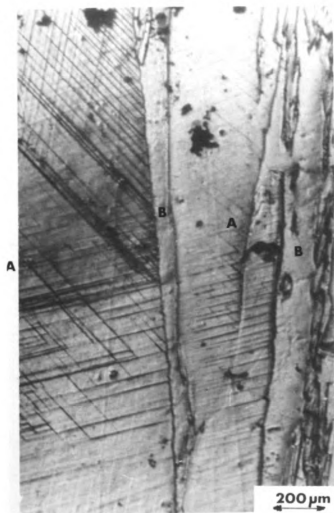


Fig. 12

Fig. 13 Slip Interactions With Equiaxed Duplex Interface.

25 Kg. load, 0.05 cm/min. cross-head speed indentation at 1.5 mm

Compare with Fig. 8 b.

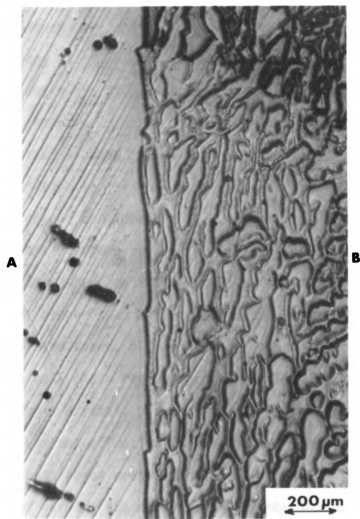


Fig. 13

of the previous test series for this load and distance of indentation to the interface, the higher rates of load application were more effective in generating a higher slip line density near the interface region. The effect of the various loading rates is shown in Fig. 14a - 14d; the slip line density in the interface region increases with increasing rates of load application. As found in the tests using the oriented duplex interface samples, a higher load coupled with a close distance of indentation to the interface, along with a high rate of load application produces more slip interactions with the interface structure. However, the equiaxed duplex interface geometry is not as effective a barrier to block the progress of slip as the oriented duplex interface geometry. This loading and distance of indentation to the boundary, even at a low cross-head speed of 0.005 cm/min., produced considerable slip interaction with the portions of the equiaxed duplex interface regions near the alpha single region. This is shown in Fig. 14a, where extensive cross-slip is observed in the alpha phase regions. At higher load application rates, and particularly at the 5.0 cm/min. cross-head speed, slip lines were observed to interact and progress through the beta phase regions present in the interface structure near the alpha single crystal. This most extreme stress concentration condition, however, was not effective in propagating slip through the interface structure to the beta phase present on the other side of the boundary.

The effect of varying the distance of indentation in the alpha phase from the interface is evident by comparing Fig. 15 to Fig. 14d. Both tests were conducted using 40 Kg load, and a cross-head speed of 5.0 cm/min. but in one an indentation distance of 1.5 mm was used and in the other 0.5 mm was used. As shown by the comparison of these figures, when the indentation is made farther away from the interface, the extent of slip interaction at the boundary is considerably less, and yet it is still capable of propagating

Fig. 14 Slip Interactions With Equiaxed Duplex Interface.

40 Kg. load, indentation at 0.5 mm from interface at various cross-head speeds.

- (a) 0.005 cm/min. cross-head speed.**
- (b) 0.05 cm/min. cross-head speed.**

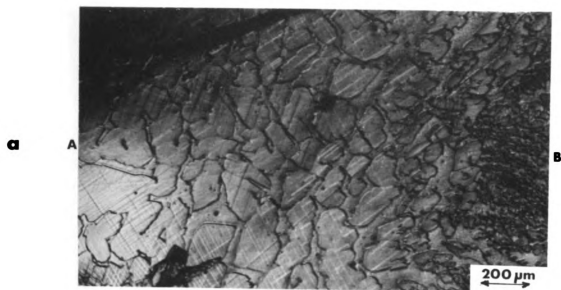


Fig. 14a

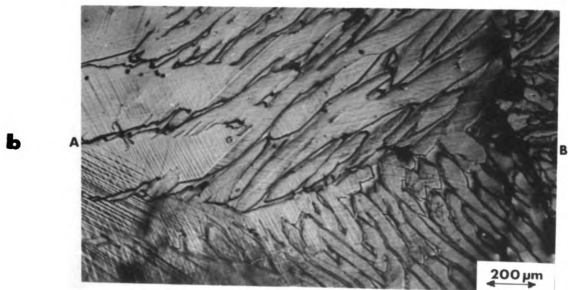


Fig. 14b

Fig. 14 (Continued)

(c) 0.5 cm/min. cross-head speed.

(d) 5.0 cm/min. cross-head speed.

c

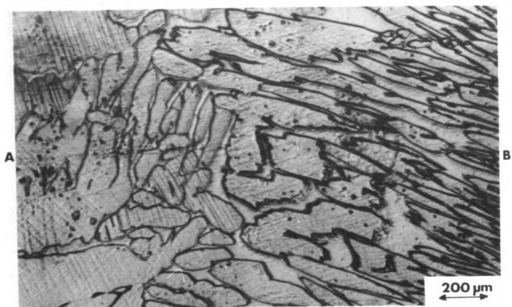


Fig. 14c

d

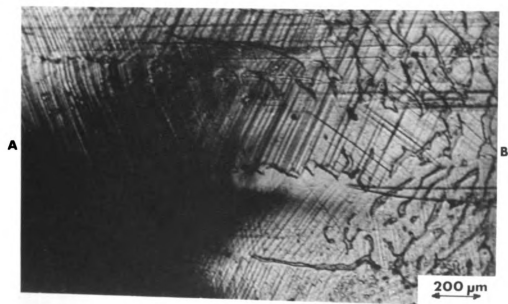


Fig. 14d

Fig. 15 Slip Interactions With Equiaxed Duplex Interface.
40 Kg. load, 5.0 cm/min. cross-head speed indentation at
1.5 mm from Interface.
Compare with Fig. 14 d.

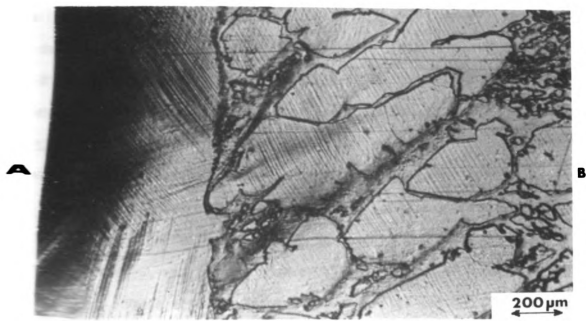


Fig. 15

7/19

1

slip partially through the interface structure. This effect is shown in Fig. 15, where the slip lines in the equiaxed alpha phase islands exist in regions farther away from the alpha single crystal.

Flat Boundary

The effect of stress concentration and slip interaction on flat bicrystal phase boundaries was also of interest in this study. The results of tests conducted using a 25 Kg load, indentation distances of 1.0 mm from the boundary, and cross-head speeds of 0.005 cm/min. and 5.0 cm/min., are shown in Figs. 16a and 16b. Once again, as observed in other tests, the higher cross-head speed is more effective in generating more slip lines closer to the boundary than are low rates. As may be seen in Fig. 16b where a high cross-head speed of 5.0 cm/min. was used, the slip lines are both closer to the boundary and have a higher density compared to Fig. 16 (a).

Test conditions with a more severe stress concentration at the flat boundary were created by using a 40 Kg load, indentation distance of 1 mm to the boundary, and low and high cross-head speeds of 0.005 and 5.0 cm/min. were used. These test results are shown in Fig. 17a and 17b and may be compared to Fig. 16 a and 16b where all conditions were the same except for the load. The higher 40 Kg load, even at a low cross-head speed of 0.005 cm/min., as shown in Fig. 17a, produces considerable cross-slip as well as multiple slip near the flat boundary. This condition is more severe as shown in Fig. 17b for a high cross-head speed of 5.0 cm/min. These test results show that the flat bicrystal boundary is a very effective barrier to the progress of slip lines produced by indentation.

Fig. 16 Slip Interactions With Bicrystal Flat Interface.
25 Kg. load, indentation at 1.0 mm from interface at
different rates of loading.
(a) 0.005 cm/min. cross-head speed.
(b) 5.0 cm/min. cross-head speed.

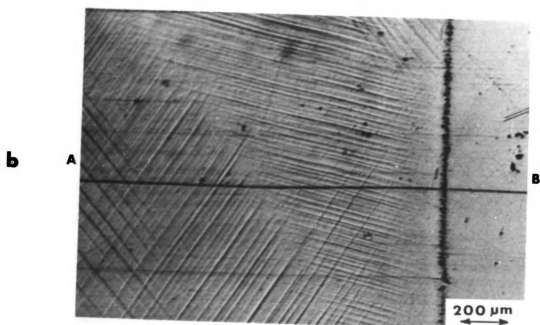
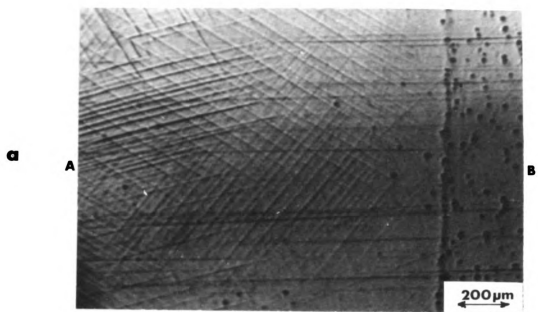


Fig. 16

Fig. 17 Slip Interactions With Bicrystal Flat Interface.
40 Kg. load, indentation at 1.0 mm from interface at
different rates of loading.
(a) 0.005 cm/min. cross-head speed.
(b) 5.0 cm/min. cross-head speed.

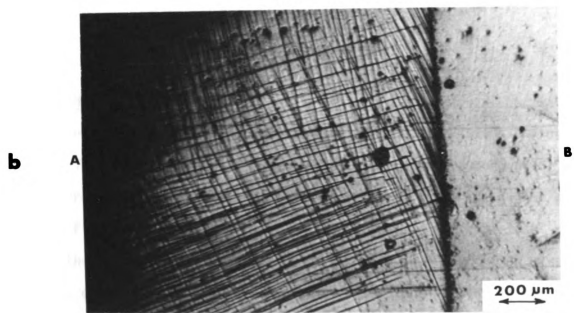
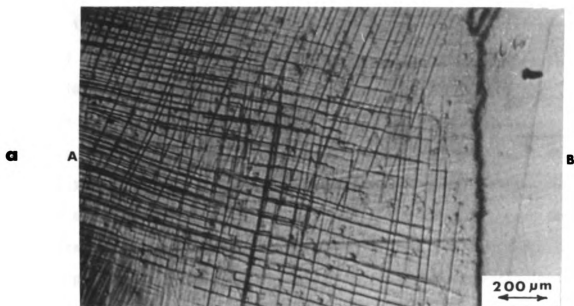


Fig. 17

Indentation in the Interface Region

Final indentation tests were conducted by placing the indentation directly in the equiaxed duplex interface region, which tests have shown to be the least effective type of interface geometry for preventing slip propagation. Extensive cross-slip in the alpha phase regions of the structure was observed and is shown in Fig. 18a and 18b at points Y. Some fine slip was observed to propagate into the beta phase adjacent to the alpha phase island, or through the phase boundaries. This is shown in Fig. 18a at points ZZ. This fine slip which is more prominent near the alpha-beta interface becomes very fine and diffuse at short distances away from the phase boundary in the beta phase. By indenting directly into the duplex interface, beta regions deformed slightly due to the very high local stress concentration. However, slip did not progress far enough in the beta regions to reach the beta grain in contact with the interface region.

B. STRAIN-RATE TESTS

Tensile strain-rate testing was carried out on specimens having four types of interface geometries; oriented duplex, equiaxed (unoriented) duplex, corrugated, and flat boundaries. Examples of these boundaries are shown in Fig. 7. In some specimens after a very little cyclic local annealing the duplex interface region tended to retain the original crystallographic orientations of the Widmanstätten structure present in the as joined condition. Such a structure is termed an oriented duplex interface and an example is shown in Fig. 7a. Other specimens experienced a rearrangement of the interface structure after moderate amounts of heat treatment to produce a structure composed of rather equiaxed regions of alpha phase generally connected and continuous with the alpha single crystal

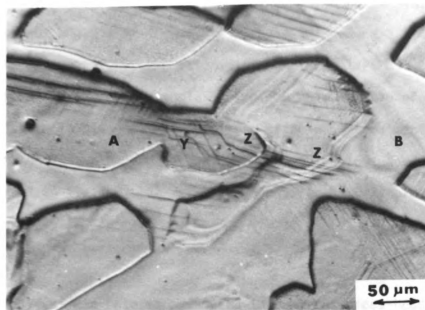
Fig. 18 Slip Interactions with Equiaxed Duplex Interface.

25 Kg load, indentation into the duplex interface

0.05 cm/min. cross-head speed

- (a) Cross-slip and slip propagation through the boundaries. Slip in the beta phase regions at Z, and cross-slip in the alpha region at Y.
- (b) Extensive cross-slip in the alpha phase region at Y.

a



b

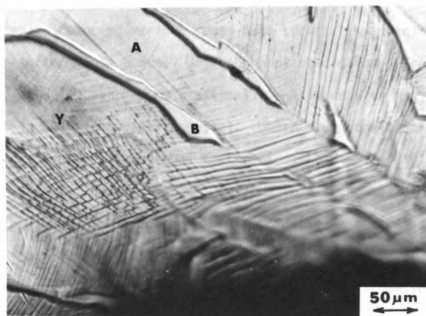


Fig. 18

phase. This type of boundary has been termed an equiaxed duplex interface structure and is shown in Fig. 7b.

Other specimens whose heat-treatment schedule to produce a flat boundary is interrupted before completion yield an irregular, but continuous boundary termed a corrugated duplex interface. An example of this type of boundary is shown in Fig. 7c. In specimens whose heat-treatment after joining was completed, the two-phase duplex interface regions could be completely eliminated to yield a flat interface boundary. An example of this boundary is presented in Fig. 7d.

Stress-Strain Data

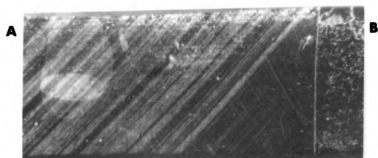
In this study, strain-rate is presented in terms of cross-head speed. The reason for this is the following: although the alpha-beta series bi-crystals (having different interface geometries) were deformed at selected deformation rates by choosing various cross-head speeds, the specimen deformed first in the softer alpha phase. Unless the plastic deformation of alpha was very heavy, beta did not deform plastically. As a result, most of the deformation was in the alpha single crystal. Under such conditions the strain-rate can be assumed to be equal to the cross-head speed divided by the alpha gage length. The gage length of alpha in all the test specimens was 1.58 cm (5/8"). An alternate approach is to define a nominal strain-rate, which is equal to the cross-head speed divided by the actual gage length of the specimen (including both alpha and beta). All the specimens had a 1.58 cm (5/8") gage length in beta, so the total gage length is twice the gage length of alpha. This will make strain-rate values one half of those obtained by assuming that alpha alone deforms. In order to avoid any uncertainty, strain rate is expressed as cross-head speed throughout this work.

Since beta deformed very little, strain is expressed assuming that alpha alone deformed. This assumption is reasonable since beta does not deform until alpha deforms very heavily. Further, in the test data, the maximum stress and strain that each specimen withstood is presented. Except for two of the specimens (No. 37 and No. 46) tested during the course of this study the rest of the specimens either fractured or the test was stopped as soon as alpha necked heavily just before failure.

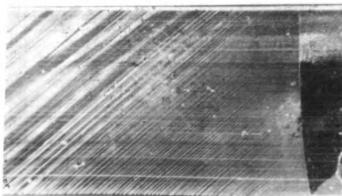
In Fig. 19, the four faces of a representative tensile strain-rate test specimen which has undergone slight deformation are presented. The crystallographic orientations of the alpha single crystal and the single beta crystal contacting it at the phase boundary for each test specimen are given in Table I. In Figs. 20, 21, 22, and 23 are presented the tensile stress-strain curves of the specimens having the four types of interfaces utilized in this portion of the study. Fig. 20 shows the results of tests using oriented duplex interface samples; Fig. 21 is for the unoriented or equiaxed duplex boundary samples; Fig. 22 presents the results of the corrugated bicrystal boundary specimens; and Fig. 23, presents the results of the flat bicrystal boundary specimens. The tabulated results of the strain-rate tests are presented in Tables II, III, IV and V, where each table is for one of the types of boundary geometries. Shown in these tables are the cross-head speeds at which each specimen was tested, the resolved shear stress values at which slip was observed to propagate through the interface, the maximum resolved shear stress values experienced by each specimen, and the specimen condition at the maximum stress level achieved in each.

All of the micrographs presented in this section of test results for tensile strain-rate specimens have been identified uniformly in the following manner. The tensile axis is shown where ever appropriate by arrows and the abbreviation "T.A.". The micrographs presented have all been oriented so

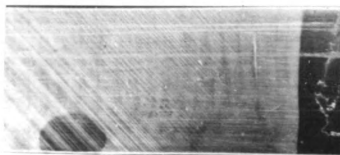
Fig. 19 Four Faces of a Slightly Deformed Strain-rate Tensile Specimen.
Specimen No. 13. Cross-head speed 3.0 cm/min.
Stress - 5.616 Kg/mm^2 , Strain - 17.48%
Picture magnification - 13 X



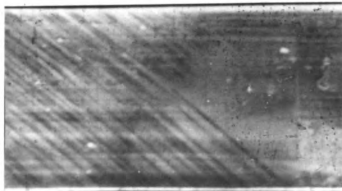
rt. side



back



left side



front

Fig. 19

Table Ia
CRYSTALLOGRAPHIC ORIENTATIONS OF
ORIENTED DUPLEX BOUNDARY SPECIMENS


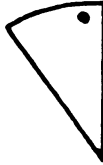
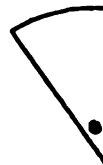

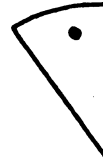

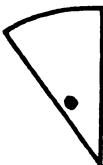




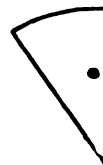

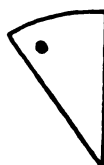




SPECIMEN NO.	<u>ALPHA ORIENTATION</u>		<u>TENSILE AXIS</u>	SCHMIDT FACTOR	<u>BETA ORIENTATION</u>		<u>TENSILE AXIS</u>	SCHMIDT FACTOR
	<u>FRONT FACE</u>	<u>SIDE FACE</u>			<u>FRONT FACE</u>	<u>SIDE FACE</u>		
48				.4545				.4924
50				.4996				.4988
36				.4785				.4997

Table Ib
CRYSTALLOGRAPHIC ORIENTATIONS OF
EQUIAXED DUPLEX BOUNDARY SPECIMENS

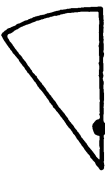

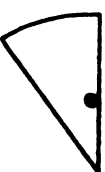
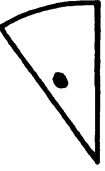
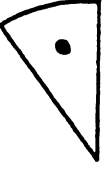


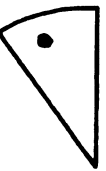
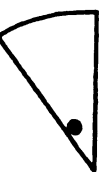



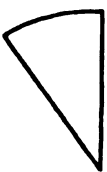
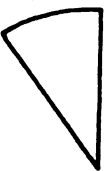




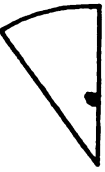
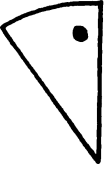
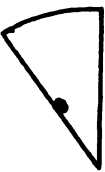
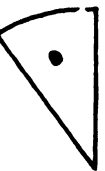


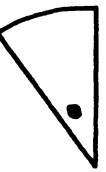













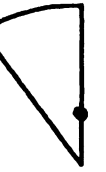
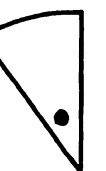
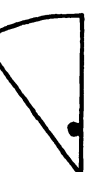

SPECIMEN NO.	ALPHA ORIENTATION		TENSILE AXIS	SCHMIDT FACTOR	BETA ORIENTATION		TENSILE AXIS	SCHMIDT FACTOR
	FRONT FACE	SIDE FACE			FRONT FACE	SIDE FACE		
40				.4749				.4891
39				.4851				.4738
24				--				--
42				.4635				.4875
38				.4755				.4542
45				.4851				.4851
46				.4999				.4988

Table Ic

CRYSTALLOGRAPHIC ORIENTATIONS OF
CORRUGATED BOUNDARY SPECIMENS

SPECIMEN NO.	ALPHA ORIENTATION		BETA ORIENTATION		TENSILE AXIS	SCHMIDT FACTOR	BETA ORIENTATION		TENSILE AXIS	SCHMIDT FACTOR
	FRONT FACE	SIDE FACE	FRONT FACE	SIDE FACE			FRONT FACE	SIDE FACE		
12						.4972				.4698
43						.4755				.4997
23						.4823				.4973
31						.4755				.4987

Table Id
CRYSTALLOGRAPHIC ORIENTATIONS OF
FLAT BOUNDARY SPECIMENS

SPECIMEN NO.	ALPHA ORIENTATION			TENSILE AXIS	SCHMIDT FACTOR	BETA ORIENTATION			TENSILE AXIS	SCHMIDT FACTOR
	FRONT FACE	SIDE FACE	FRONT FACE			FRONT FACE	SIDE FACE	FRONT FACE		
37					.4610					.4368
35					.4640					.4663
22					.4906					.4999
21					.4098					.4674
44					.4988					.4996
13					.3313					.4777
14					.4698					.4891

Fig. 20 Stress-Strain Curves for Specimens Having an Oriented Duplex Interface Structure.

Specimen No. 48, Cross-head speed 0.2 cm/min.

Specimen No. 50, Cross-head speed 0.3 cm/min.

Specimen No. 36, Cross-head speed 2.0 cm/min.

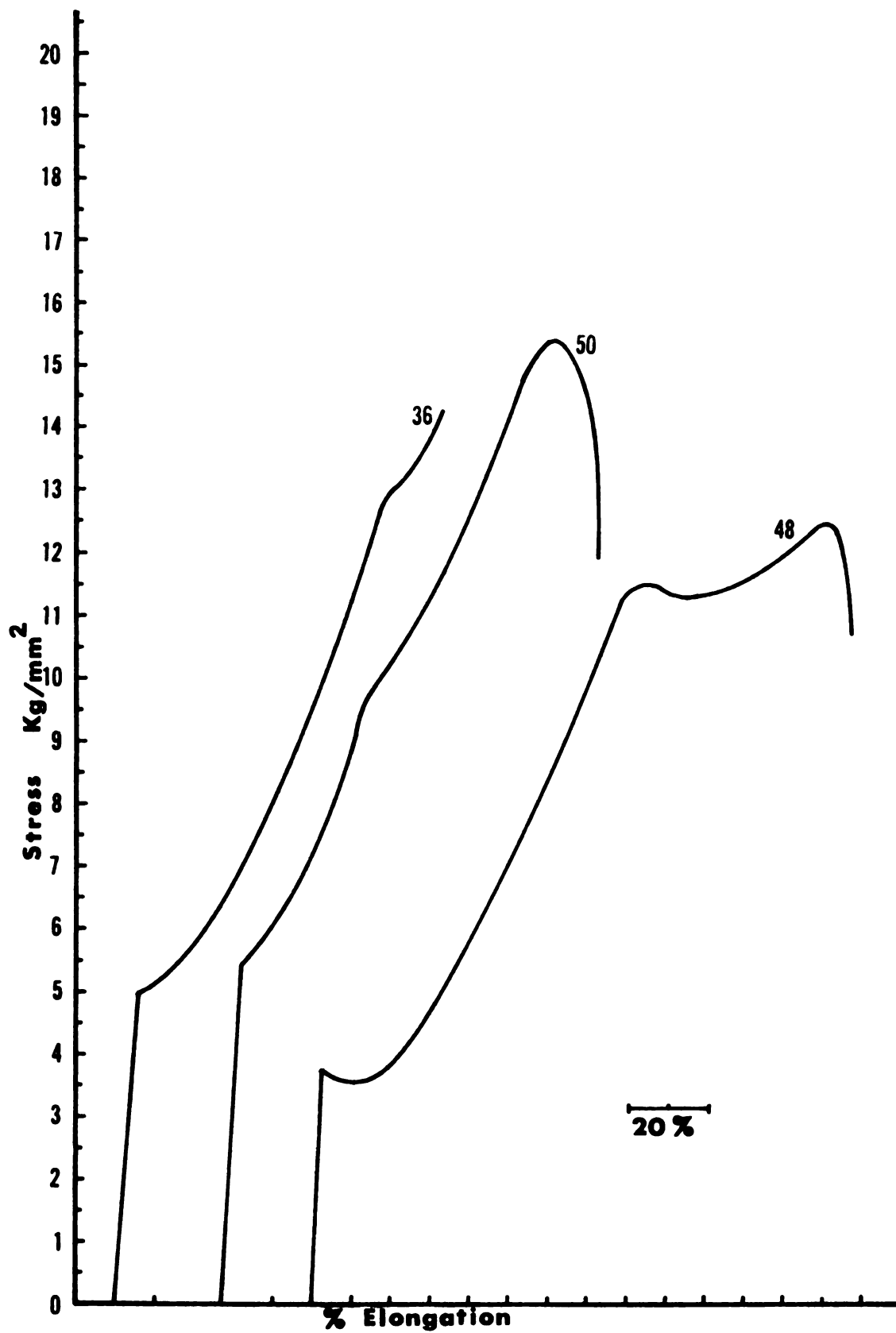


Fig. 20

Fig. 21 Stress-Strain Curves for Specimens Having an Equiaxed Interface Structure.

Specimen No. 40, Cross-head speed 0.1 cm/min.

Specimen No. 42, Cross-head speed 0.5 cm/min.

Specimen No. 39, Cross-head speed 0.5 cm/min.

Specimen No. 24, Cross-head speed 0.5 cm/min.

Specimen No. 38, Cross-head speed 1.0 cm/min.

Specimen No. 45, Cross-head speed 2.0 cm/min.

Specimen No. 46, Cross-head speed 3.0 cm/min.

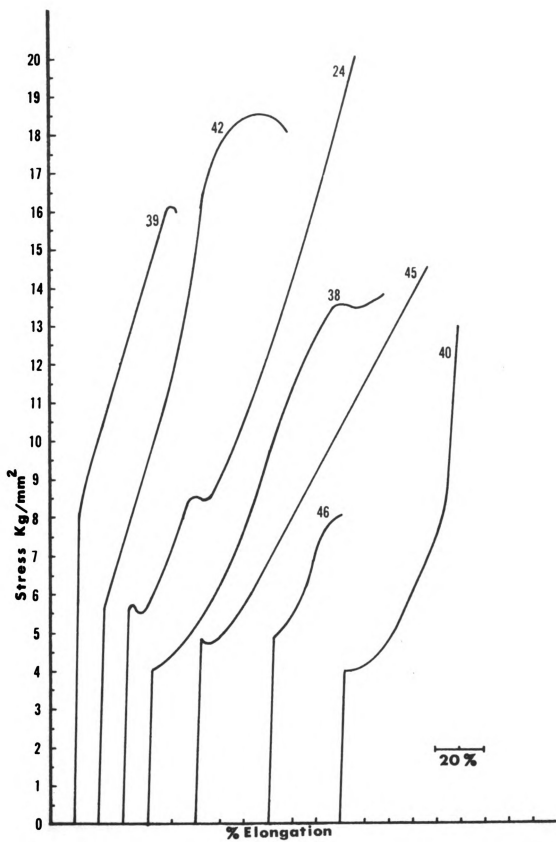


Fig. 21

Fig. 22 Stress-Strain Curves for Bicrystal Specimens Having a Corrugated Interface Structure.

Specimen No. 12, Cross-head speed .01 cm/min.

Specimen No. 43, Cross-head speed .05 cm/min.

Specimen No. 23, Cross-head speed 0.50 cm/min.

Specimen No. 31, Cross-head speed 1.0 cm/min.

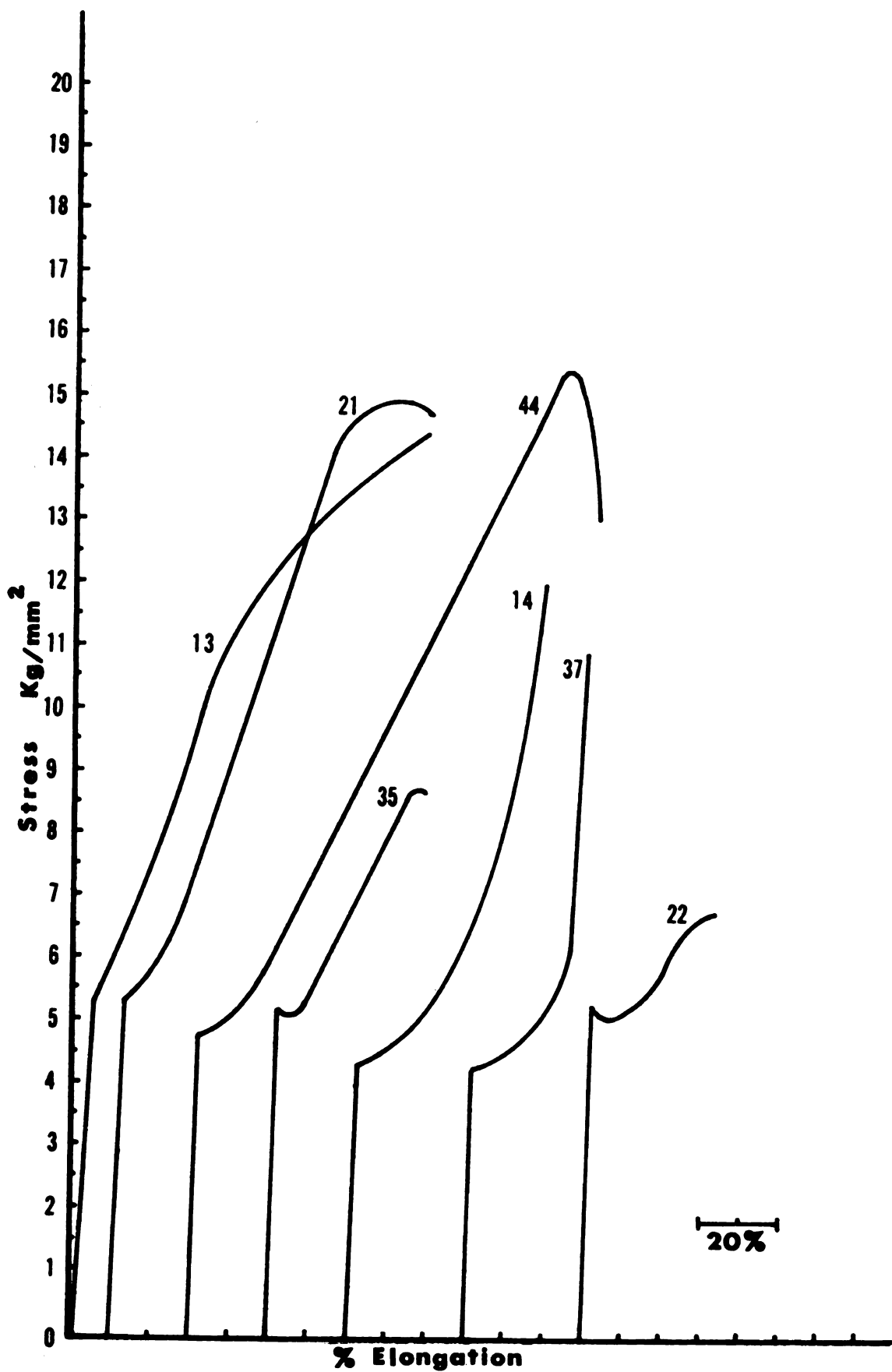


Fig. 23

5

Fig. 23 Stress-Strain Curves for Bicrystal Specimens Having a Flat Interface Structure.

Specimen No. 37, Cross-head speed .005 cm/min.

Specimen No. 35, Cross-head speed 0.1 cm/min.

Specimen No. 22, Cross-head speed 0.2 cm/min.

Specimen No. 21, Cross-head speed 0.3 cm/min.

Specimen No. 44, Cross-head speed 0.5 cm/min.

Specimen No. 13, Cross-head speed 3.0 cm/min.

Specimen No. 14, Cross-head speed 5.0 cm/min.

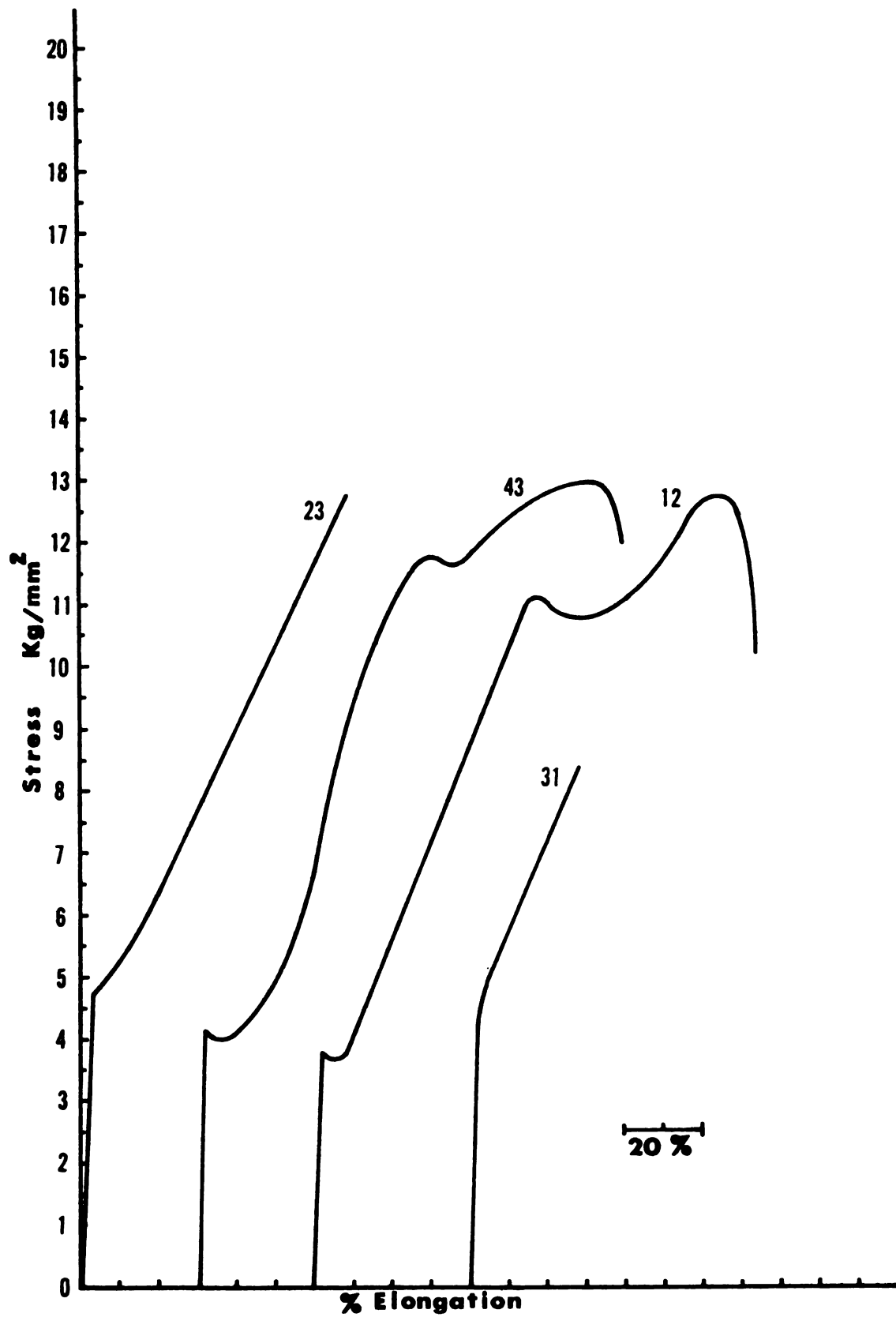


Fig. 22

Table II

STRAIN-RATE TEST RESULTS FOR SPECIMENS
HAVING AN ORIENTED DUPLEX TYPE OF INTERFACE

SPECIMEN NO.	CROSS-HEAD SPEED CM/MIN.	STRESS(σ), STRAIN(ϵ) AT WHICH SLIP PROGRESSED THROUGH THE INTERFACE	MAXIMUM STRESS AND STRAIN EXPERIENCED BY THE SPECIMENS DURING TESTING	SPECIMEN CONDITION AT MAXIMUM STRESS
48	0.2	Stress = 4.308 Kg/mm ² Strain = 28%	Stress = 12.35 Kg/mm ² Strain = 132.3%	Failed in Alpha
50	0.3	Stress = 9.65 Kg/mm ² Strain = 37.2%	Stress = 11.44 Kg/mm ² Strain = 95.4%	Failed in Alpha
36	2.0	Stress = 12.15 Kg/mm ² Strain = 64.07%	Stress = 14.2 Kg/mm ² Strain = 82.82%	No Fracture

Strain values are based on the maximum strain in the alpha phase.

Table II (continued)

SPEC. NO.	CROSS-HEAD SPEED CM/MIN.	RESOLVED SHEAR STRESS FOR SLIP TO PROPAGATE THROUGH THE BOUNDARY KILOGRAMS/mm ²		RESOLVED SHEAR STRAIN FOR SLIP TO PROPAGATE THROUGH THE BOUNDARY % ELONGATION	
		ALPHA	BETA	ALPHA	BETA
48	0.2	1.958	2.121	0.1273	0.1379
50	0.3	4.821	4.813	0.1859	0.1856
36	2.0	5.814	6.071	0.3066	0.3201

Strain values are based on the maximum strain in the alpha phase.

Table III

STRAIN-RATE TEST RESULTS FOR SPECIMENS

HAVING AN EQUIAXED (UNORIENTED) DUPLEX TYPE OF INTERFACE

SPECIMEN NO.	CROSS-HEAD SPEED CM/MIN.	STRESS(σ), STRAIN(ϵ) AT WHICH SLIP PROGRESSED THROUGH THE INTERFACE	MAXIMUM STRESS AND STRAIN EXPERIENCED BY THE SPECIMEN DURING TESTING	SPECIMEN CONDITION AT MAXIMUM STRESS
40	0.1 last load at 1.0	Stress = 7.84 Kg/mm ² Strain = 44.1%	Stress = 12.96 Kg/mm ² Strain = 48.9%	Failed in Alpha
39	0.5	Slip did not go through the interface	Stress = 7.37 Kg/mm ² Strain = 41.46%	Failed in Beta at nut
24	0.5	Slip into alpha islands Stress = 5.31 Kg/mm ² Strain = 15.12%	Stress = 20.06 Kg/mm ² Strain = 106.8%	No Fracture
42	0.5 last load rate 5.0	Stress = 14.37 Kg/mm ² Strain = 40.7%	Stress = 18.22 Kg/mm ² Strain = 77.9%	Failed in Alpha
38	1.0	Slip did not go through interface	Stress = 13.78 Kg/mm ² Strain = 98.7%	No Fracture
45	2.0	Slip did not go through interface	Stress = 14.56 Kg/mm ² Strain = 96.2%	Failed in Beta at nut
46	3.0	Slip did not go through interface	Stress = 7.95 Kg/mm ² Strain = 29.1%	No Fracture

Strain values are based on the maximum strain in the alpha phase.

Table III (continued)

SPEC. NO.	CROSS-HEAD SPEED CM/MIN.	RESOLVED SHEAR STRESS FOR SLIP TO PROPAGATE THROUGH THE BOUNDARY KILOGRAMS/mm ²	BETA	RESOLVED SHEAR STRAIN FOR SLIP TO PROPAGATE THROUGH THE BOUNDARY % ELONGATION	ALPHA	BETA
40	0.1 last load at 1.0	3.723	3.835	0.2094	0.2157	
39	0.5	Did not go through interface		--	--	
24	0.5	Data not available		--	--	
42	0.5 last load at 5.0	6.660	7.005	0.1886	0.1984	
38	1.0	Slip did not go through boundary		--	--	
45	2.0	Slip did not go through boundary		--	--	
46	3.0	Slip did not go through boundary		--	--	

Strain values are based on the maximum strain in the alpha phase.

Table IV

STRAIN-RATE TEST RESULTS FOR BICRYSTAL SPECIMENS
HAVING A CORRUGATED ALPHA-BETA INTERFACE

SPECIMEN NO.	CROSS-HEAD SPEED CM/MIN.	STRESS (σ), STRAIN (ϵ) AT WHICH SLIP PROGRESSED THROUGH THE INTERFACE	MAXIMUM STRESS AND STRAIN EXPERIENCED BY THE SPECIMEN DURING TESTING	SPECIMEN CONDITION AT MAXIMUM STRESS
12	0.01	Stress = 12.74 Kg/mm ² Strain = 10.85%	12.74 10.85%	No Fracture
43	0.05	Slip did not go through the interface. Slip in beta phase - away from boundary at Stress = 11.77 Kg/mm ² Strain = 60.4%	Stress = 14.3 Kg/mm ² Strain = 12.35%	No Fracture
23	0.5	Stress = 12.55 Kg/mm ² Strain = 81.3%	Stress = 12.55 Kg/mm ² Strain = 81.3%	No Fracture
31	1.0	Slip did not go through interface	Stress = 9.289 Kg/mm ² Strain = 42.5%	No Fracture

Strain values are based on the maximum strain in the alpha phase.

Table IV (continued)

SPEC. NO.	CROSS-HEAD SPEED CM/MIN.	RESOLVED SHEAR STRESS FOR SLIP TO PROPAGATE THROUGH THE BOUNDARY KILOGRAMS/mm ²	RESOLVED SHEAR STRAIN FOR SLIP TO PROPAGATE THROUGH THE BOUNDARY % ELONGATION
		ALPHA	BETA
12	0.01	6.334	5.985
			0.0539
			0.0509
43	0.05	Slip did not go through boundary	--
			--
23	0.5	6.053	6.241
			0.3921
			0.4043
31	1.0	Slip did not go through boundary	--
			--

Strain values are based on the maximum strain in the alpha phase.

TABLE V

STRAIN-RATE TEST RESULTS FOR BICRYSTAL SPECIMENS

HAVING A FLAT ALPHA-BETA INTERFACE

SPECIMEN NO.	CROSS-HEAD SPEED CM/MIN.	STRESS (σ), STRAIN (ϵ) AT WHICH SLIP PROGRESSED THROUGH THE INTERFACE	MAXIMUM STRESS AND STRAIN EXPERIENCED BY THE SPECIMEN DURING TESTING	SPECIMEN CONDITION AT MAXIMUM STRESS
37	0.005 1st load at 0.5	Stress = 5.361 Kg/mm ² Strain = 20.06%	Stress = 10.9 Kg/mm ² Strain = 30.9%	No Fracture
35	0.1	Stress = 5.15 Kg/mm ² Strain = 2.63%	Stress = 11.14 Kg/mm ² Strain = 35.13%	No Fracture
22	0.2	Stress = 6.67 Kg/mm ² Strain = 32.81%	Stress = 6.67 Kg/mm ² Strain = 32.81%	No Fracture
21	0.3	Slip did not go through interface	Stress = 14.7 Kg/mm ² Strain = 82.21%	No Fracture
44	0.5	Slip did not go through interface	Stress = 15.43 Kg/mm ² Strain = 96.7%	Failed in Alpha
13	3.0	Slip did not go through interface	Stress = 14.3 Kg/mm ² Strain = 123.5%	Failed in Alpha
14	5.0	Slip did not go through interface	Stress = 12.08 Kg/mm ² Strain = 120.37%	No Fracture

Strain values are based on the maximum strain in the alpha phase.

Table V (continued)

SPEC. NO.	CROSS-HEAD SPEED CM/MIN.	RESOLVED SHEAR STRESS FOR SLIP TO PROPAGATE THROUGH THE BOUNDARY KILOGRAMS/mm ²	RESOLVED SHEAR STRAIN FOR SLIP TO PROPAGATE THROUGH THE BOUNDARY % ELONGATION
		ALPHA	BETA
37	0.005	2.471	2.342
	last load at 0.5		
35	0.1	2.390	2.298
22	0.2	3.272	3.334
21	0.3	Slip did not go through boundary	
44	0.5	Slip did not go through boundary	
13	3.0	Slip did not go through boundary	
14	5.0	Slip did not go through boundary	

Strain values are based on the maximum strain in the alpha phase.

that the alpha single crystal portion of the specimen is to the left and is designated by "A". The adjacent interface region and the beta phase is at the right and is designated by "B".

Oriented Duplex Boundary

In oriented duplex specimens, slip progressed through the interface region at the lowest stress levels. Shown in Fig. 24(a) is the multiple slip build-up at the oriented duplex interface of a specimen tested at 0.2 cm/min. cross-head speed. Some fine cross-slip may be observed in the region marked X away from the interface. Slip progressed through the boundary at a moderate stress level and at a fairly low strain value. Another specimen also having the same type of boundary geometry was tested at a higher cross-head speed (0.3 cm/min.) and is shown in Fig. 24b. Because of the higher strain-rate and the particular orientation of the slip lines in this specimen, slip did not progress through the interface region until the stress level increased to twice that required for the specimen shown in Fig. 24(a). Another specimen of the same boundary geometry tested at a relatively high cross-head speed of 2.0 cm/min. did not evidence slip through the interface region until the stress level had increased an additional one-third beyond that required for the specimen deformed with a cross-head speed of 0.3 cm/min. This trend seems to indicate that the stress level necessary to propagate slip through the interface region increases with increasing strain-rate. Generally in the oriented duplex interface samples, no appreciable amount of cross-slip build-up was observed at the interface on any of the faces of test specimens.

Equiaxed Duplex Boundary

Specimens tested having an equiaxed (unoriented) duplex interface structure are shown in Fig. 25a and 25b. The specimen shown in Fig. 25a

Fig. 24 Slip Interactions With Oriented Duplex Interface. Tests Performed using Cross-head speed of 0.2 and 0.3 cm/min.

- (a) Specimen No. 48, Cross-head speed 0.2 cm/min.
Condition for progress of slip through the interface:
Stress-4.308 Kg/mm², Strain-28%
Micrograph was taken after subjecting the specimen to
Stress-12.35 Kg/mm², Strain-132.3%
- (b) Specimen No. 50, Cross-head speed 0.3 cm/min.
Condition for progress of slip through the interface:
Stress-9.65 Kg/mm², Strain-37.2%
Micrograph was taken after subjecting the specimen to
Stress-11.44 Kg/mm², Strain-95.4%

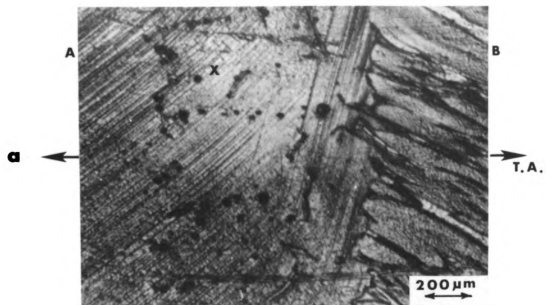


Fig. 24a

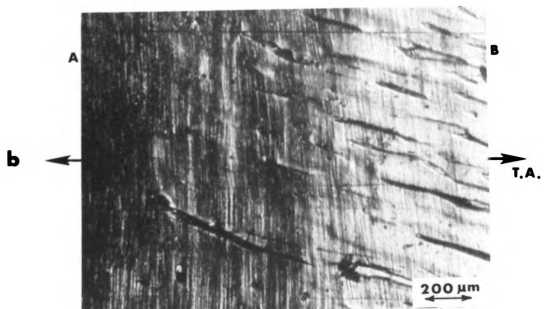


Fig. 24 b

Fig. 25 Slip Interactions With Equiaxed Interface Structure.

(Unoriented duplex interface structure) Tests performed using Cross-head speeds of 0.1 and 0.5 cm/min.

- (a) Specimen No. 40, Cross-head speed 0.1 cm/min.
Condition for progress of slip through the interface:
Stress- 7.84 Kg/mm^2 , Strain-44.1%
Micrograph was taken after subjecting the specimen to
Stress- 11.44 Kg/mm^2 , Strain-48.9%
- (b) Specimen No. 42, Cross-head speed 0.5 cm/min.
Condition for progress of slip through the interface:
Stress- 14.37 Kg/mm^2 , Strain-40.7%
Micrograph was taken after subjecting the specimen to
Stress- 18.22 Kg/mm^2 , Strain 77.9%

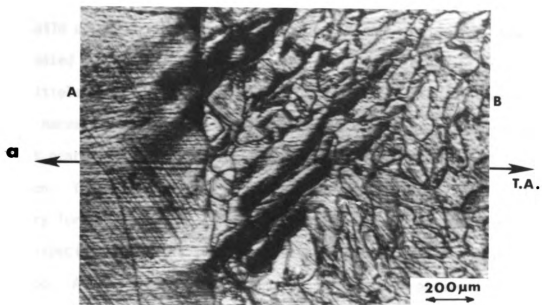


Fig. 25a

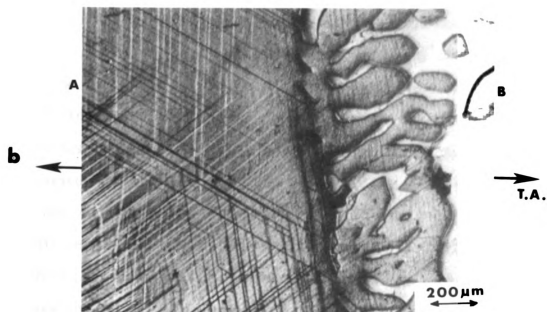


Fig. 25b

was tested with a cross-head speed of 0.1 cm/min. and slip progressed through the interface at a moderate stress level without appreciable cross-slip build up at the boundary. The specimen shown in Fig. 25b, however, when tested at a strain-rate of 0.5 cm/min. shows evidence of cross-slip and multiple slip systems operating and building up at the interface. The stress necessary to initiate slip through the interface region in this specimen was nearly twice that of the stress level needed for the 0.1 cm/min. specimen. To investigate the strain-rate effect upon this type of interface geometry further, other specimens were tested at still higher strain-rates.

A specimen tested at a cross-head speed of 1.0 cm/min. is shown in Fig. 25c. A fine slip pattern at the boundary may be observed and there is no evidence of multiple slip or cross-slip. Slip did not progress through the interface in this specimen, even after undergoing nearly 100% strain in alpha. Rather, slip was initiated in the beta phase in a region away from the interface. A specimen tested at yet a higher cross-head rate of 2.0 cm/min., shown in Fig. 25d, also failed to show any slip progressing through the interface. As in the 1.0 cm/min. cross-head speed sample, slip was again initiated in the beta phase away from the interface region. This specimen was also strained to nearly 100%. Note the extensive cross-slip in the equiaxed alpha regions designated by Z, and the very heavy slip in the alpha, and yet the absence of any form of slip in the beta.

This series of seven strain-rate tests utilizing cross-head speeds from 0.1 cm/min. to 3.0 cm/min. on specimens having an equiaxed duplex type of interface shows that with increasing strain-rate the stress level to propagate slip across the interface also increases.

Replicas of surfaces of deformed specimens were examined with a Hitachi HU-11A electron microscope. These replica studies could be made during the early stages of deformation of the alpha phase, however, at very high strains

Fig. 25 (Continued)

Tests Performed Using Cross-head Speeds of 1.0 and 2.0 cm/min.

(c) Specimen No. 38, Cross-head speed 1.0 cm/min.

Slip in beta phase away from the interface - slip did not go through the interface: Stress- 8.415 Kg/mm^2 , Strain-45%

Micrograph was taken after subjecting the specimen to Stress- 13.78 Kg/mm^2 , Strain-98.7%

(d) Specimen No. 45, Cross-head speed 2.0 cm/min.

Slip occurred in beta phase away from the interface - slip did not progress through the interface: Stress- 7.12 Kg/mm^2 , Strain-33.7%

Micrograph was taken after subjecting the specimen to Stress- 14.56 Kg/mm^2 , Strain-96.2%

Note extensive cross-slip at points Z.

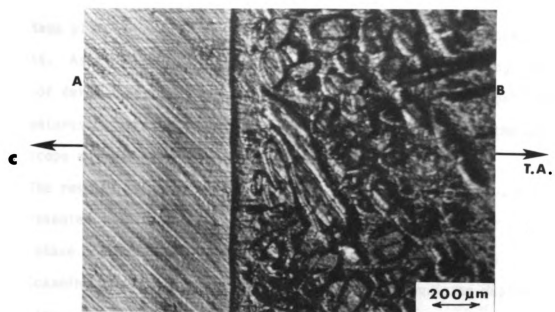


Fig. 25c

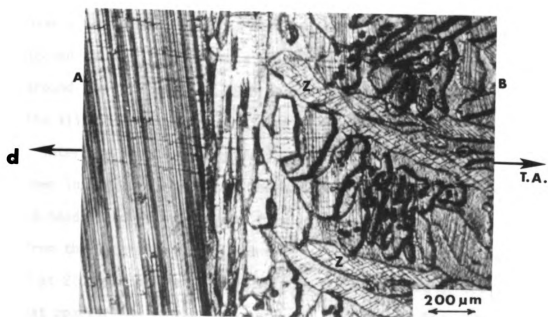


Fig. 25d

in alpha, when slip lines reach the alpha-beta interface, the surface becomes very rough. Single-stage plastic replicas could not be peeled off. Two-stage plastic-carbon replicas obtained did not yield any successful results. As a result, only single stage replicas obtained during the early stage of deformation were examined with the transmission electron microscope. The features observed were very similar to those observed with the optical microscope and the scanning electron microscope.

The results of the transmission electron microscopic observations are not presented in this section. However, some of the pictures of slip in alpha phase approaching the boundary are presented in Appendix A.

Scanning electron micrographs of an area in the equiaxed duplex interface structure after extensive deformation are shown in Fig. 26 at various magnifications. The important feature that these scanning electron micrographs show is the deviation of the slip lines in the alpha phase as they encounter a beta phase island as illustrated at point A. No slip lines can be observed to pass through these areas; instead the slip lines tend to flow around the obstacles as much as possible.

The slip lines that are initiated in the beta phase in the equiaxed duplex interface structure specimens, when high strain-rates are imposed, are shown in Fig. 27a and b. In the high strain-rate samples performed at a cross-head speed of 1.0 cm/min. fine slip appeared in the beta phase away from the interface region and is shown in Fig. 27a. In a specimen tested at 2.0 cm/min. the initial slip in the beta phase tended to be somewhat coarser and in the form of bands, as shown in Fig. 27b, where the slip in two adjacent beta phase grains meet at a grain boundary in the mid-length regions of the beta portion of the specimen.

The reluctance of the slip lines in the alpha phase regions in this type of interface structure to progress through the beta phase regions is

Fig. 26 Scanning Electron Micrographs of Specimen No. 36 Having an Oriented Duplex Interface. Tested using a Cross-head speed of 2.0 cm/min.

Cross-head speed - 2.0 cm/min. Slip blocked by alpha island at A.

Condition for progress of slip through the interface:
Stress-12.15 Kg/mm², Strain-14.2%

Micrograph was taken after subjecting the specimen to
Stress-6.507 Kg/mm², Strain-82%.

(a) 500 X

(b) 1000 X

a

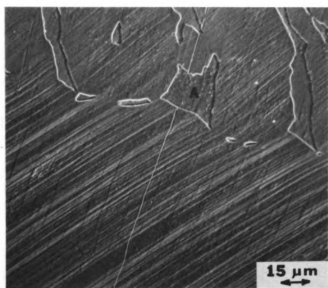


Fig. 26a

b

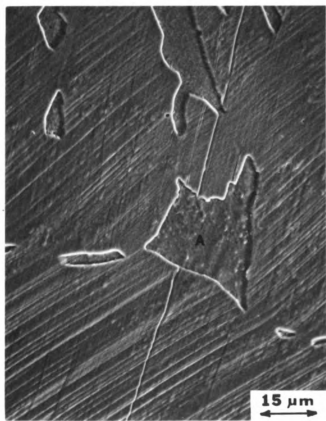


Fig. 26b

Fig. 26 (Continued)

Tested Using a Cross-head Speed of 2.0 cm/min.

(c) 2000 X

Note slip blocked by alpha island at A

C

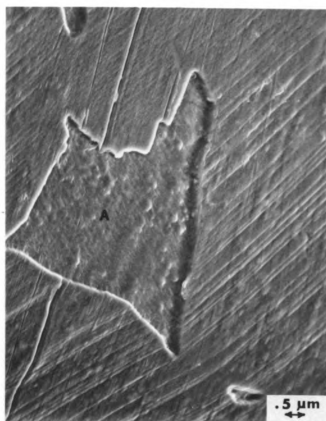


Fig. 26c

Fig. 27 Fine and Rumped Slip Occured In The Beta Phase In Regions Away From the Interface. Tests at Cross-head speeds of 1.0 and 2.0 cm/min.

- (a) Specimen No. 38, Cross-head speed 1.0 cm/min.
Slip occurred in beta phase in regions away from the interface: Slip did not go through the interface.
Stress- 8.415 Kg/mm^2 , Strain-45%
- (b) Specimen No. 45, Cross-head speed 2.0 cm/min.
Slip occurred in beta phase in regions away from the interface. Slip did not go through the interface.
Stress- 7.12 Kg/mm^2 , Strain-33.7%.

Note grain boundary in the beta phase at c

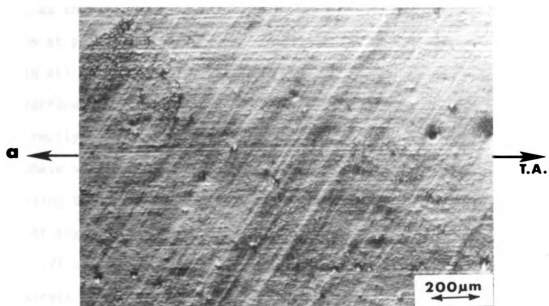


Fig. 27a

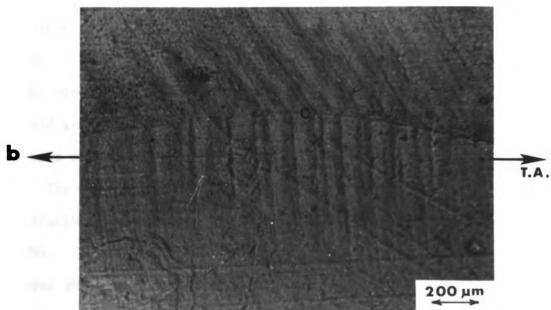


Fig. 27b

15-5.

further pointed out in Fig. 28. Here the slip in the alpha phase cross-slips, as shown along A-A, whenever it approaches too close to beta phase regions at points marked B.

In all of the examples cited thus far, for the equiaxed duplex type of interface structure, no evidence has been observed of the slip propagating directly from alpha phase regions, across phase boundaries, into the beta phase single crystal region in contact with the interface. One specimen having this type of boundary structure withstood the highest stress level of any of the specimens used in this study. The values for this specimen No. 24 are shown in Table IV. In this particular specimen, only at very high stress levels and amounts of deformation was any slip into the beta phase regions observed. Further, slipping occurred only in isolated areas in the interface structure. Two types of slip in the beta phase seemed to prevail in these regions, as shown in Fig. 29a and 29b. Fine slip (B) directly from the slip traces in the alpha phase regions (A) is shown in Fig. 29a. The slip is prominent at the crossing of the phase boundary, but does not continue into the beta phase very far before becoming very diffuse. It should also be observed that there is a deviation in the angle of the continuous slip traces as they pass from the alpha phase into the beta phase. The second type of slip found in more numerous areas of this specimen's structure was a banded or rumpled type of slip shown in region C of Fig. 29b. This slip did not appear to be in a direction of slip traces in the alpha phase regions in the vicinity of the duplex structure.

The scanning electron micrographs shown in Fig. 30 were also taken on this same specimen No. 24. These reveal that in some areas in the structure slip does progress from the alpha phase regions marked A, across the phase boundaries into the beta phase regions marked B. Once again the angular deviation of the slip line as it passes through the phase boundary into

Fig. 28 Cross-slip In Alpha Phase Regions Caused By Beta Island. Test run using a Cross-head speed of 0.5 cm/min.

Extensive cross-slip at AA caused by the beta islands at

Specimen No. 42, Cross-head speed 0.5 cm/min.

Condition for progress of slip through the interface: Stress-14.37

Stress-14.37 Kg/mm², Strain-40.7%

Micrograph was taken after subjecting the specimen to:

Stress-18.22 Kg/mm², Strain-77.9%



Fig. 28

Fig. 29 Optical Micrographs Showing Slip Propagation Through An Equiaxed Interface Structure.

Specimen No. 24, Cross-head speed 0.5 cm/min.

This specimen withstood the maximum stress observed in the course of this study.

Conditions for progress of slip through interface:

Stress- 5.31 Kg/mm^2 , Strain-15.12%

Micrograph was taken after subjecting the specimen to

Stress- 20.06 Kg/mm^2 , Strain-106.8%

(a) Fine slip in the beta phase at B. Alpha phase islands are at points A.

(b) Coarse slip in the beta phase in regions C.

a

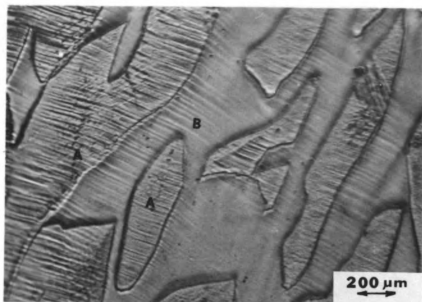


Fig. 29a

b

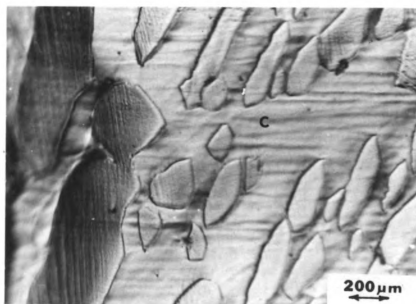


Fig. 29b

Fig. 30 Scanning Electron Micrographs Of An Equiaxed Interface Specimen Showing Fine Slip In The Beta Phase At B. Alpha Phase Islands Are At Points A.

Specimen No. 24, Cross-head speed 0.5 cm/min.

Micrograph was taken after subjecting the specimen to:

Stress-20.06 Kg/mm², Strain-106.8%

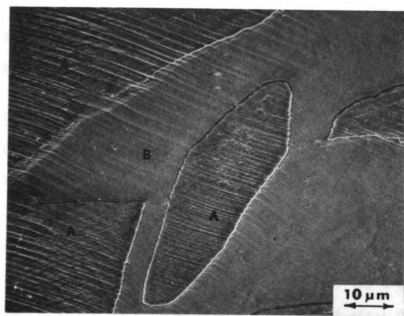


Fig. 30a

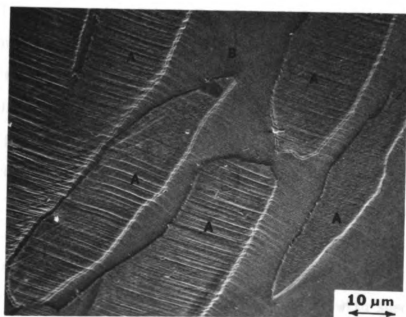


Fig. 30b

2

the beta phase can be clearly observed. In general, a comparison of the values tabulated in Tables III and IV shows that the equiaxed duplex type of interface structure specimens are stronger than the oriented duplex interface type specimens.

Corrugated Interface

Several specimens having a corrugated type of bicrystal boundary were tested to evaluate this type of boundary in comparison with the other three types. A typical example of this boundary geometry is shown in the scanning electron micrograph presented in Fig. 31. This specimen was tested with a cross-head speed of 0.5 cm/min. In the structure shown, the cross-slip build-up near the boundary is very evident. In selected areas of this specimen slip was observed to have passed through the phase boundary. A series of tests were performed using specimens having this type of boundary geometry at cross-head speeds varying from 0.01 cm/min. to 1.0 cm/min. The results of these tests are presented in Table II.

Optical micrographs of specimens tested at four different cross-head speeds from 0.01 to 1.0 cm/min. are presented in Fig. 32. In general, the nature of slip in the alpha phase was coarse and rather heavy at lower strain-rates, and considerably finer with an absence of cross-slip at high strain rates. The slip interaction with the corrugated type of boundary for a specimen tested at a strain-rate of 0.01 cm/min. is shown in Fig. 32a. Rather coarse slip is observed, and as shown in the micrograph multiple slip systems are operative near the boundary. As observed in tests with specimens having various types of boundaries, the slip when it does progress through the phase boundaries, is very fine or occurs in diffuse bands, and it continues only for short distances before becoming diffused.

The micrograph of a specimen tested at 0.05 cm/min., given in Fig. 32b,

Fig. 31 Scanning Electron Micrograph Of A Deformed Specimen With A Corrugated Interface.

Specimen No. 23, Cross-head speed 0.5 cm/min.

Micrograph was taken after subjecting the specimen to:
Stress- 12.55 Kg/mm^2 , Strain-81.3%

Note cross-slip in alpha phase at C.

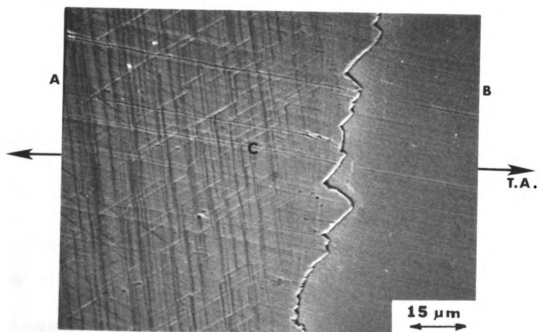


Fig. 31

Fig. 32 Slip Interactions With A Corrugated Interface At Various Strain-Rates. Tests performed using Cross-head speeds of 0.01 and 0.05 cm/min.

(a) Specimen No. 12, Cross-head speed 0.01 cm/min.

Condition for progress of slip through interface near edges:

Stress-10.87 Kg/mm², Strain-53.1%

Micrograph was taken after subjecting the specimen to:

Stress-12.74 Kg/mm², Strain-108.5%

(b) Specimen No. 43, Cross-head speed 0.05 cm/min.

Deformed in beta phase away from the interface:

Stress-11.7 Kg/mm². Strain-60.4%

Micrograph was taken after subjecting the specimen to:

Stress-14.3 Kg/mm², Strain 123.5%

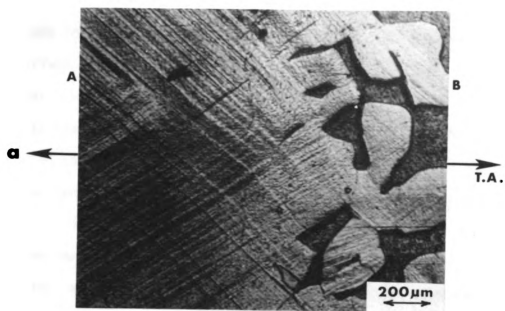


Fig. 32a

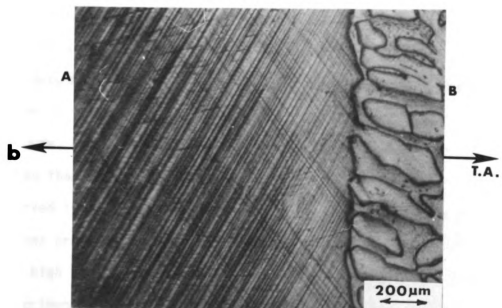


Fig. 32b

shows some fine scale cross-slip build-up at some finite distance from the boundary. Some very fine slip features may also be observed in the corrugated alpha phase regions of the boundary, but no slip progressed through the interface on this specimen. Rather, slip was initiated in the beta phase away from the boundary. This occurred at a stress level that was lower than the stress level at which slip went through the phase boundary in the 0.01 cm/min. specimen. A corrugated boundary specimen tested at a cross-head speed of 0.5 cm/min. did show progress of slip through the phase boundary. This result occurred at approximately the same stress level as in the specimen tested with a cross-head speed of 0.01 cm/min., but at a strain level nearly a magnitude larger than that of the previous specimen. The microstructure is presented in Fig. 32c. With the higher strain-rate, the slip in the alpha phase, as mentioned before, is finer; and there is little evidence of any cross-slip build-up in the vicinity of the boundary. The slip interaction with the corrugated type of boundary in a specimen tested with a cross-head speed of 1.0 cm/min. is shown in Fig. 32d. Slip did not propagate through the boundary in this specimen; rather, slip was initiated in the beta phase away from the phase boundary. As shown in this figure, the slip interactions in the alpha phase at the boundary is much less than that experienced at lower strain-rates. Very fine slip may be observed in the extended portions of the corrugated boundary, but no slip lines progress across phase boundaries into the beta phase.

At high strain-rates, the alpha single crystal portion of the bicrystal test specimen is subjected to large, heavy deformations. The side and front faces of the alpha phase, away from the boundary, are shown in Fig. 33 and the heavy rumpled appearance of the deformed surface is evident in these optical micrographs. For specimens in which slip was initiated in the beta phase in a region away from the boundary, two types of slip lines were

Fig. 32 (Continued)

Tests performed using Cross-head speeds of 0.5 and 1.0 cm/min.

(c) Specimen No. 23, Cross-head speed 0.5 cm/min.

Slip through interface at final loading

Micrograph was taken after subjecting the specimen to:

Stress- 12.55 Kg/mm^2 , Strain-81.3%

(d) Specimen No. 31, Cross-head speed 1.0 cm/min.

No slip through the interface. Slip did occur in the beta phase away from the interface:

Stress- 5.67 Kg/mm^2 , Strain-25.5%

Micrograph was taken after subjecting specimen to:

Stress- 9.289 Kg/mm^2 , Strain-42.5%

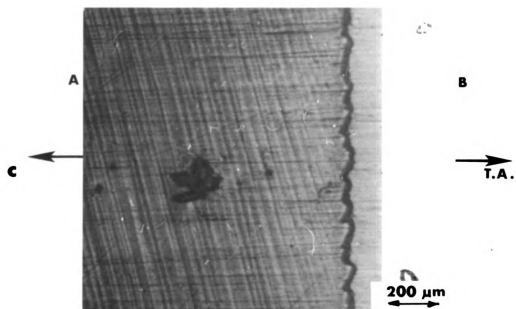


Fig. 32c

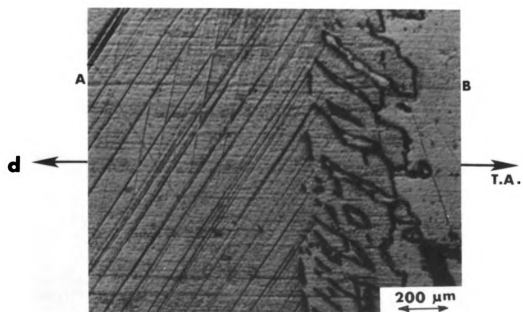


Fig. 32d

Fig. 33 Very Heavy Slip In The Alpha Crystal At Regions Away From
The Corrugated Duplex Interface.

Specimen No. 31, Cross-head speed 1.0 cm/min.

Micrograph was taken after subjecting the specimen to:
Stress- 9.289 Kg/mm^2 , Strain-42.5%

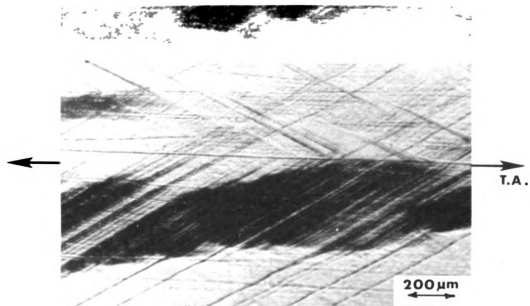


Fig. 33a

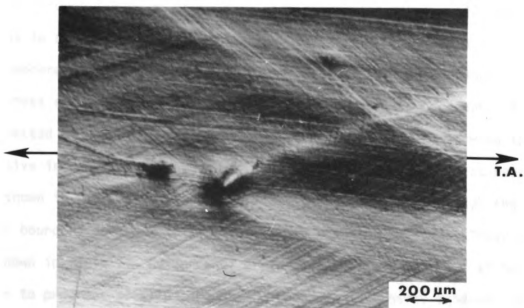


Fig. 33b

observed to occur in the beta phase. At low strain-rates this slip in the beta phase is fine and may be in fine diffuse slip bands as shown in Fig. 34a for a specimen tested with a cross-head speed of 0.05 cm/min. The slip initiated in the beta phase in high strain-rate specimens tends to be somewhat coarser and in wider more pronounced bands, as shown in Fig. 34b for a specimen tested with a cross-head speed of 1.0 cm/min.

Flat Boundary

Extensive testing was carried out using flat boundary bicrystal specimens, as this geometry seemed to be an ideal model. Strain-rate tests were performed with cross-head speeds in the range from 0.005 to 5.0 cm/min. The same strain-rate dependency of slip progressing through the boundary as observed in other types of boundary tests may be noted in Table V. At low strain-rates, a correspondingly low stress level is required for slip propagation through the phase boundary. With increasing strain-rate the level of stress to achieve slip propagation through the flat boundary also increases. At a moderate cross-head speed of 0.3 cm/min. as well as at higher rates, slip does not progress through the boundary. Optical micrographs of a specimen tested at a very low cross-head speed of 0.005 cm/min. showing the progressive increase in the amount of slip passing through the flat boundary are shown in Figs. 35a, b, c. The first passage of slip through the flat phase boundary is shown in Fig. 35a. This occurred at a low stress level, as shown in Table V. Evidence of cross-slip build-up at the flat boundary prior to progress of slip through the boundary is clearly evident. At a higher stress level, more deformation has propagated across the boundary, and the cross-slip build-up is more extensive as shown in Fig. 35b. At still higher stress levels, coarse slip in the alpha phase occurs, the cross-slip build-up closer to the flat boundary is more intense and slip

Fig. 34 Fine Slip In The Beta Phase Away From The Corrugated Duplex Interface. Tests performed using Cross-head speeds of 0.05 and 1.0 cm/min.

(a) Specimen No. 43, Cross-head speed 0.05 cm/min.

Micrographs taken after subjecting the specimen to:
Stress-14.3 Kg/mm², Strain-123.5%

(b) Specimen No. 31, Cross-head speed 1.0 cm/min.

Micrograph was taken after subjecting the specimen to:
Stress-9.289 Kg/mm², Strain-42.5%

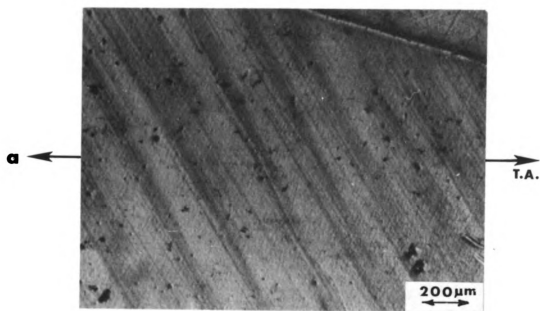


Fig. 34a

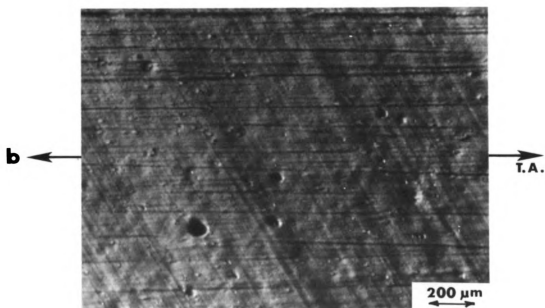


Fig. 34b

1/2

Fig. 35 Slip Propagation Through A Flat Bicrystal Boundary Loaded
At A Cross-head Speed of 0.005 cm/min.

Specimen No. 37

(a) Progress of slip through the boundary

Stress-5.361 Kg/mm², Strain 20.065%

(b) More extensive slip through the boundary

Stress-6.165 Kg/mm², Strain-26.86%

(c) Coarsening of slip in beta.

Stress-10.9 Kg/mm², Strain-30.9%

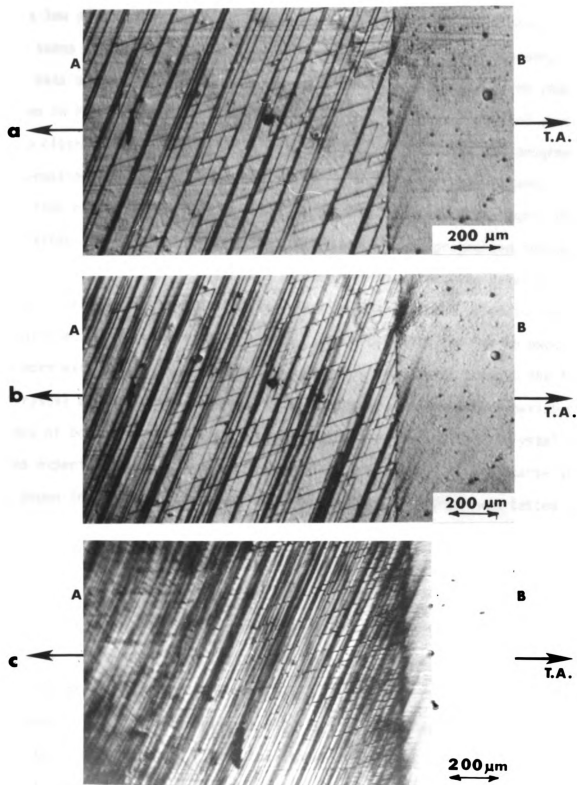


Fig. 35

progresses through the interface extensively as shown in Fig. 35c. At this low strain-rate the slip that progresses through the flat phase boundary seems to form deformation zones on the other side of the boundary in the beta phase. The increase in the size of these slip initiation zones is shown in Fig. 36a and b. Features such as the increased amount of cross-slip close to the boundary which is closely associated with the progress of deformation through the interface, is clearly shown in these figures. Inspection of these two figures, especially Fig. 36a, shows once again the deviation in the angle of the slip trace after having progressed through the boundary. Fig. 37 shows, at a higher magnification, the details of the initial cross-slip formation at the phase boundary as the slip initially progresses through the flat interface. The cross-slip, as may be expected, is more extensive in the region where the slip progresses through the flat bicrystal boundary. As observed in prior tests using specimens having other types of boundaries, the alpha single crystal portion of the bicrystal specimens experiences heavy, coarse slip at low strain-rates. This coarse slip is shown in Fig. 38. The specimen shown in this micrograph was tested using a cross-head speed of 0.005 cm/min., and the micrographic region is away from the boundary by approximately 1 cm. The heavy multiple-slip pattern is clearly evident.

At higher strain-rates, the slip in the alpha portion is finer, and there is less evidence of multiple-slip systems and cross-slip in regions near the phase boundary. The difference in the behavior of the alpha phase is shown by comparing the slip in Fig. 39 for a specimen tested with a cross-head speed of 0.1 cm/min. With that shown in Fig. 38 for a specimen tested with a cross-head speed of 0.005 cm/min. Slip that has progressed through the phase boundary is shown in Fig. 39. This is generally of the same character as the low strain-rate sample, except for the fact that the extent

Fig. 36 Coarse Slip Lines In The Beta Phase Initiated By Slip Interactions With The Flat Bicrystal Boundary. Tested using a Cross-head speed of 0.005 cm/min.

(a) Specimen No. 37 Cross-head speed 0.005 cm/min.

Stress- 5.361 Kg/mm^2 , Strain-20.065%

(b) Specimen No. 37, Cross-head speed 0.005 cm/min.

Stress- 6.165 Kg/mm^2 , Strain-26.86%

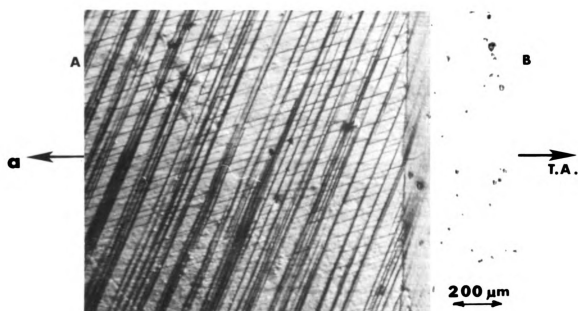


Fig. 36a

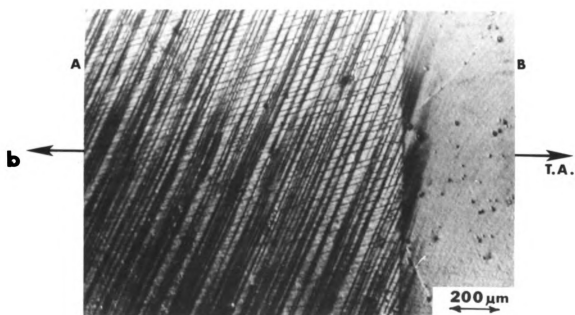


Fig. 36b

Fig. 37 Cross-slip In The Alpha Phase Occurring Very Near The
Phase Boundary.

Specimen No. 37, Cross-head speed 0.005 cm/min.

Stress-5.361 Kg/mm², Strain-20.065%

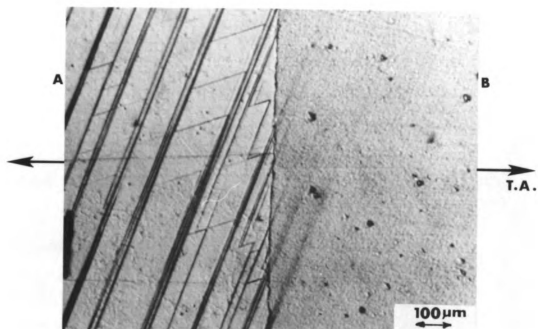


Fig. 37

Fig. 38 Multiple Slip In The Alpha Crystal In A Region Away From
The Phase Boundary.

Specimen No. 37, Cross-head speed 0.005 cm/min.

Stress-5.361 Kg/mm², Strain-20.065%

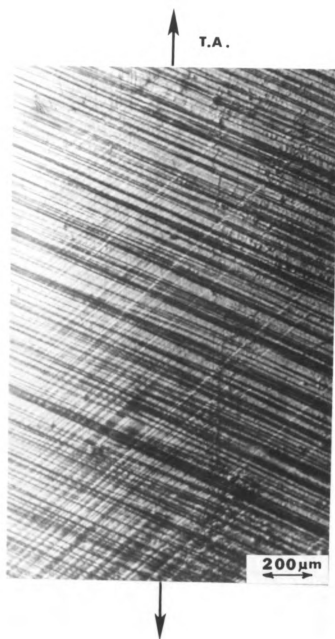


Fig. 38

Fig. 39 Slip Interactions In A Flat Boundary Specimen Tested At
0.1 cm/min. Cross-head Speed.

Specimen No. 35, Stress- 5.15 Kg/mm^2 , Strain-2.63%

Note that slip lines in the beta phase deviate slightly in
direction from the primary slip line direction in the alpha
phase.

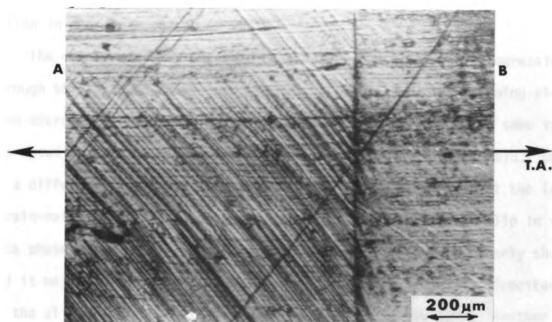


Fig. 39

to which the slip in the beta phase has propagated is considerably less than for the specimen tested at the 0.005 cm/min. cross-head speed.

Fig. 40 shows an interesting feature observed in a specimen tested at a strain-rate of 0.1 cm/min. The primary slip in the alpha phase approaches the flat boundary at a shallow angle. Heavy slip and deformation in the beta phase adjacent to the boundary makes an angle with the boundary that is equal to that of the slip in the alpha phase with the boundary, but in the opposite direction. Aligned with the direction of the slip trace in beta, there seems to be a heavy rumpled type of deformation in the alpha phase.

The more frequently observed behavior of the slip after progressing through the phase boundary into the beta phase is shown by scanning electron micrographs presented in Fig. 41. These were taken on the same specimen shown in Fig. 40, tested with a cross-head speed of 0.1 cm/min., but on a different face of the sample. Once again the heavy slip at the low strain-rate in the alpha phase is evident. The bands of fine slip in the beta phase after penetrating through the phase boundary are clearly shown and it may be noted that there is an angular deviation in the direction of the slip trace on passing through the flat phase boundary. Another fine feature that is evident in these, as well as in many of the other figures shown, is the "saw-tooth" effect created at the flat boundary by slip bands interacting with the flat bicrystal phase boundary. Results of a test with a higher cross-head speed of 0.2 cm/min. on a flat boundary bicrystal is shown in Fig. 42. Fine, closely spaced slip lines in bands initiate slip through the flat boundary as shown in Fig. 42b. At a later stage of deformation, the slip in the alpha phase is much heavier, but still predominately in bands, and it is accompanied by cross-slip within the bands. Directly opposite these heavy slip bands in the alpha phase

Fig. 40 Coarse Slip In The Beta Phase Near The Boundary Initiated In
A Direction Drastically Different From The Trace Of The
Primary Slip System In The Alpha Phase.

Specimen No. 35, Cross-head speed 0.1 cm/min.

Stress-7.194 Kg/mm², Strain-22.25%

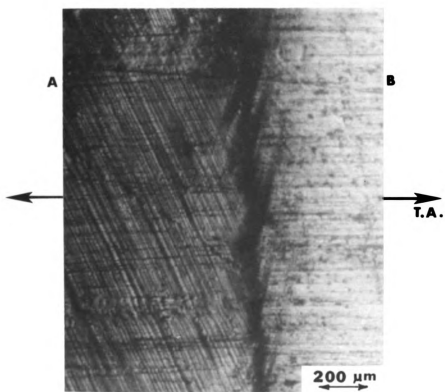
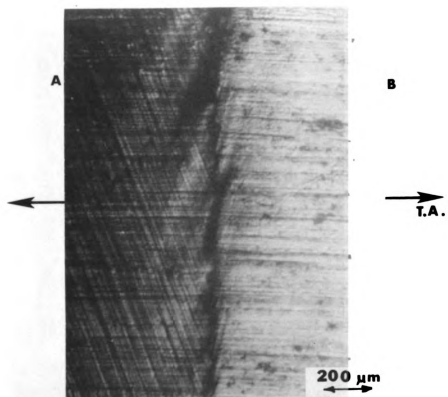


Fig. 40

Fig. 41 Scanning Electron Micrographs Showing Coarse Slip In The Beta Phase Initiated By Interaction Of The Slip In The Alpha Phase With The Interface In A Flat Boundary Bicrystal.

Specimen No. 35, Cross-head speed 0.1 cm/min.

Stress-11.14 Kg/mm², Strain-35.13%

Note that the direction of the slip lines in the beta phase are not parallel to the primary slip direction in the alpha phase.

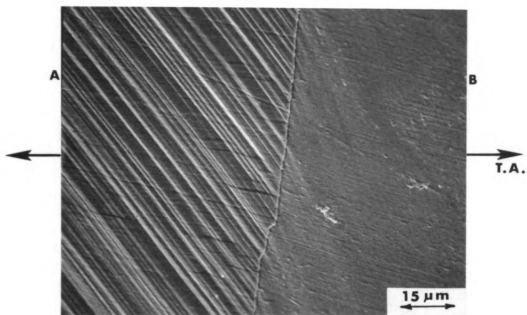


Fig. 41a

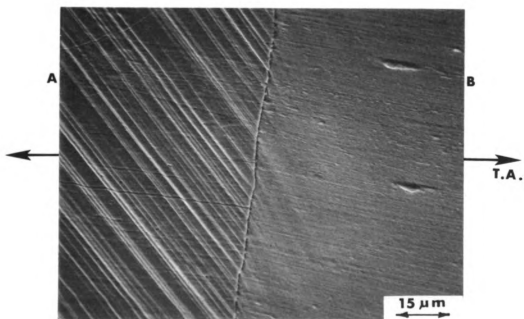


Fig. 41b

Fig. 42 Slip Propagation Through A Flat Interface.

Specimen No. 22, Cross-head speed 0.2 cm/min.

Slip through the boundary: Stress- 6.67 Kg/mm^2 , Strain-32.81%

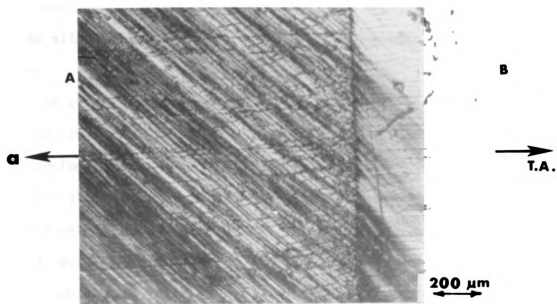


Fig. 42a

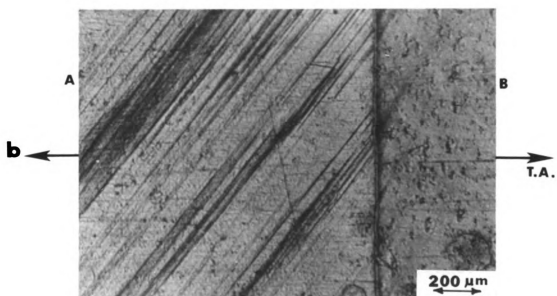


Fig. 42b

are the bands of fine slip lines. Scanning electron micrographs of this same specimen are shown in Fig. 43, where once again the angular deviation of the slip line after progressing through the phase boundary is clearly shown.

The slip interaction at flat bicrystal boundaries in specimens tested at high strain-rates are shown in the optical micrographs in Fig. 44a and b. The specimen shown in Fig. 44a was tested at a cross-head speed of 3.0 cm/min. The fine slip in the alpha phase, even after heavy deformation, that seems to be a characteristic of the alpha phase behavior at high strain rates is clearly evident. A comparison of this micrograph with that shown in Fig. 42a or 36c, which were taken at lower stress levels, emphasized the difference in the slip behavior in the alpha phase. Some evidence of multiple slip is present in these high strain-rate specimens, but little or no cross-slip in the boundary regions has been observed. In the region labeled X in the beta phase, fine slip was observed. This slip was initiated in the beta phase and propagated towards the phase boundary at higher stress levels. No slip was observed to progress through the flat boundary from the alpha phase.

A specimen having a flat boundary was tested with a cross-head speed of 5.0 cm/min., which was the highest rate available. The slip interaction with the boundary in this specimen is shown in Fig. 44b. The behavior of this specimen was similar to that of the 3.0 cm/min. rate specimen in that no slip progressed through the interface even at maximum stresses. Slip was initiated in the beta phase away from the boundary region. The type of fine slip initiated in the beta phase is shown in the optical micrograph presented in Fig. 45. The micrograph shown was taken on a specimen tested at a 3.0 cm/min. rate. Features observed in this micrograph are also representative of the fine slip observed in the specimen tested at a higher cross-head speed of 5.0 cm/min.

Fig. 43 Scanning Electron Micrographs Showing Slip Propagation
Through A Flat Boundary.

Specimen No. 22, Cross-head speed 0.2 cm/min.

Condition for progress of slip through the boundary:
Stress- 6.67 Kg/mm^2 , Strain-32.81%.

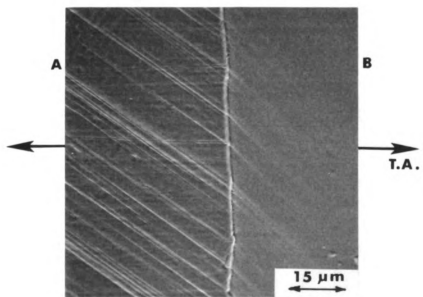
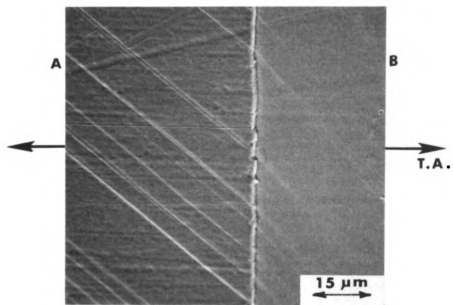


Fig. 43

152

Fig. 44 Slip Interactions With A Flat Boundary At High Strain-rates.

Cross-head speeds of 3.0 and 5.0 cm/min. used.

(a) Specimen No. 13, Cross-head speed 3.0 cm/min.

Fine slip in the beta phase occurred away from the boundary at:
Stress-12.4 Kg/mm², Strain-89.3%

No slip through the boundary at maximum stress.

Micrograph was taken after subjecting the specimen to:
Stress-13.7 Kg/mm², Strain-112.1%

(b) Specimen No. 14, Cross-head speed 5.0 cm/min.

Slip in the beta phase occurred in a region away from the
boundary at: Stress-9.35 Kg/mm², Strain-38.3%

No slip through the boundary at maximum stress

Micrograph was taken after subjecting the specimen to:
Stress-12.08 Kg/mm², Strain-120.37%

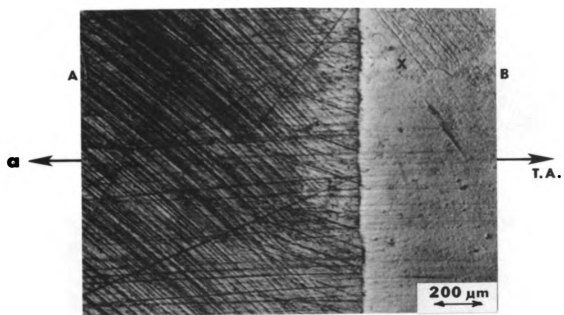


Fig. 44a

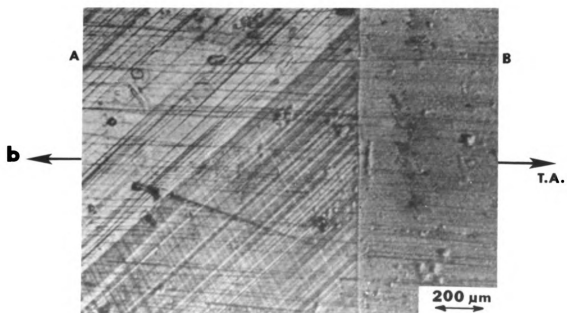


Fig. 44b

Fig. 45 Fine Slip In The Beta Phase.

Specimen No. 13, Cross-head speed 3.0 cm/min.

Stress-12.4 Kg/mm², Strain-89.3%

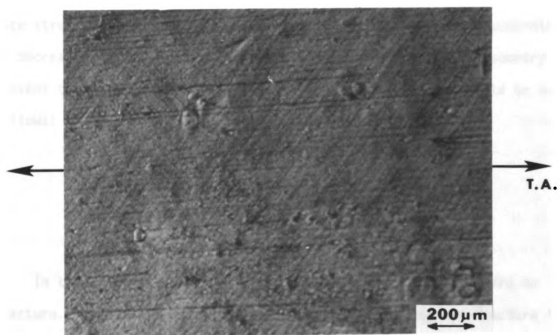


Fig. 45

A further example of the very fine nature of the slip in the alpha phase of these bicrystals when tested at high strain-rates is given in the scanning electron micrograph shown in Fig. 46. The specimen shown in this figure was tested with a cross-head speed of 3.0 cm/min. Two systems are observed to be operative which give rise to fine slip lines. No evidence of slip through the flat phase boundary or even any deformation of the boundary itself was observed.

As a general observation of the behavior of all four types of interface structures, it seems apparent that if these were ordered according to decreasing effectiveness, in possessing a strong boundary geometry to prevent the passage of slip through the boundary, the list would be as follows:

- a) Equiaxed (unoriented) duplex interface
- b) Corrugated bicrystal interface
- c) Flat bicrystal boundary
- d) Oriented duplex boundary.

In these strain-rate tests, six of the specimens were loaded to fracture. In all six cases failure occurred by necking and fracture in a region in the alpha single crystal approximately at its mid-length. Two samples failed unexpectedly due to small cracks or flaws that existed in the silver solder in the beta end of the bicrystals near the steel nuts. None of the samples tested showed any evidence of impending failure anywhere in the region of the boundary.

The progress of deformation was the same in all of the strain-rate tests carried out in this study. Slip and deformation was initiated somewhere in the mid-section or near the steel nut in the alpha single crystal. The slip progressed towards the interface and towards the grip end of the alpha crystal on continued loading. As the slip band progressed towards

the boundary, definite Lüders type bands were observed to move toward the interface. Most often the slip bands initially contacted the bicrystal phase boundary at an angle and therefore first reach a point where the boundary met the edge of the specimen. With continued loading the slip lines gradually moved across the boundary face and the previously formed slip-free triangular zone at the boundary became filled with slip. Continued stress application caused further elongation and produced heavy slip at low strain-rates, while creating fine slip in the alpha phase at high strain-rates. As the primary slip system became inactive owing to work hardening, a secondary slip system became activated somewhere in the alpha single crystal, and this system propagated to the boundary in much the same way that the primary system travelled to the boundary. Upon reaching the boundary, further work hardening of the material occurred and cross-slip became an active means of allowing further deformation to take place. As the cross-slip built up, a stress concentration was created at the boundary; and at low strain-rates, slip eventually progressed through the phase boundary into the beta phase where it was quickly dissipated.

Fig. 46 Scanning Electron Micrograph Showing The Fine Slip In The Alpha Crystal In High Strain-rate Flat Boundary Specimens. Specimen No. 13, Cross-head speed 3.0 cm/min. Micrograph was taken after subjecting the specimen to: Stress-13.7 Kg/mm², Strain-112.1%

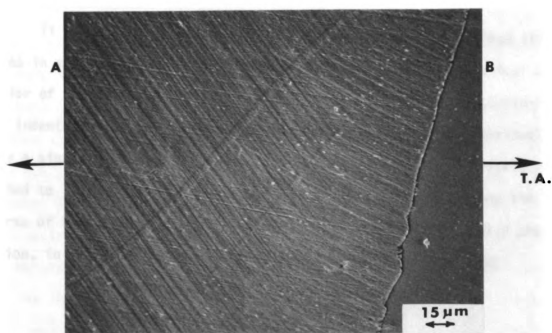


Fig. 46

CHAPTER VI

DISCUSSION AND ANALYSIS OF RESULTS

A. ROLE OF THE TYPE OF BOUNDARY

It was possible to create four different types of interface structures in samples by proper heat treatment schedules. The mechanical behavior of specimens having such boundaries were studied using strain-rate and indentation tests. The geometry features of the boundary obviously play a significant role in the mechanical behavior of the bicrystals subjected to loading, as noticeable differences were observed during the course of this study. The role of the boundary in preventing slip propagation, in order of decreasing effectiveness has been found to be:

- (a) Unoriented duplex region, termed equiaxed transition region
- (b) Corrugated type of boundary
- (c) Flat boundary,
- (d) Oriented duplex boundary.

Oriented Duplex Boundary

In the oriented duplex type of boundary there is an orientation relationship between the Widmanstätten alpha platelets and the beta matrix. Such crystallographic relationships have been observed by Greninger.⁵² This type of interface may result from having heat-treated a Widmanstätten type of interface structure which possesses a definite orientation

relationship between the alpha platelets and the beta phase matrix. In the model of this type of structure shown in Fig. 47, the $\langle 1\bar{1}0 \rangle$ slip direction in the alpha phase is nearly parallel to the $\langle 111 \rangle$ slip direction in the beta phase. Further, the close packed planes in alpha and beta phases are parallel. This immediately provides the condition for the slip plane $\{111\}_{\alpha}$ to be parallel to the slip plane $\{110\}_{\beta}$. This most favorable orientation facilitates the progression of slip through the phase boundary without much resistance. Honeycombe and Boas¹⁶ have observed this behavior in alpha-beta brass. Karashima,³⁸ using electron microscopic techniques has also observed slip through grain boundaries in alpha brass when the relative orientation relationship is satisfied. Propagation of slip in the beta phase is relatively difficult because it requires moving superlattice dislocations on the slip planes in the ordered beta phase, so slip does not propagate freely to great distances once it has overcome the phase boundary barrier. Observations of this behavior in the beta phase have been made by Brown.⁵¹ He has shown that a high stress is necessary to initiate and maintain the motion of superlattice dislocations in the beta phase.

As shown in Fig. 47, however, in the case of oriented duplex interface, slip need not propagate over large distances in the beta phase to progress through to the alpha regions. As a result of slip propagation through these beta platelets, a considerable relaxation of the stress and deformation built up at the interface can take place. As the deformation proceeds from one beta platelet, through an alpha region, and encounters another beta platelet, progressively more of the slip is blocked and retarded in its motion as shown in Fig. 47. This behavior further aids the relaxation of stresses at the interface region. With respect to the apparent effectiveness of the other three types of interfaces, the oriented duplex structure appears to be the least effective barrier to slip propagation at both low

Fig. 47 Model for the Interaction of Slip with an Oriented Duplex Type Boundary.

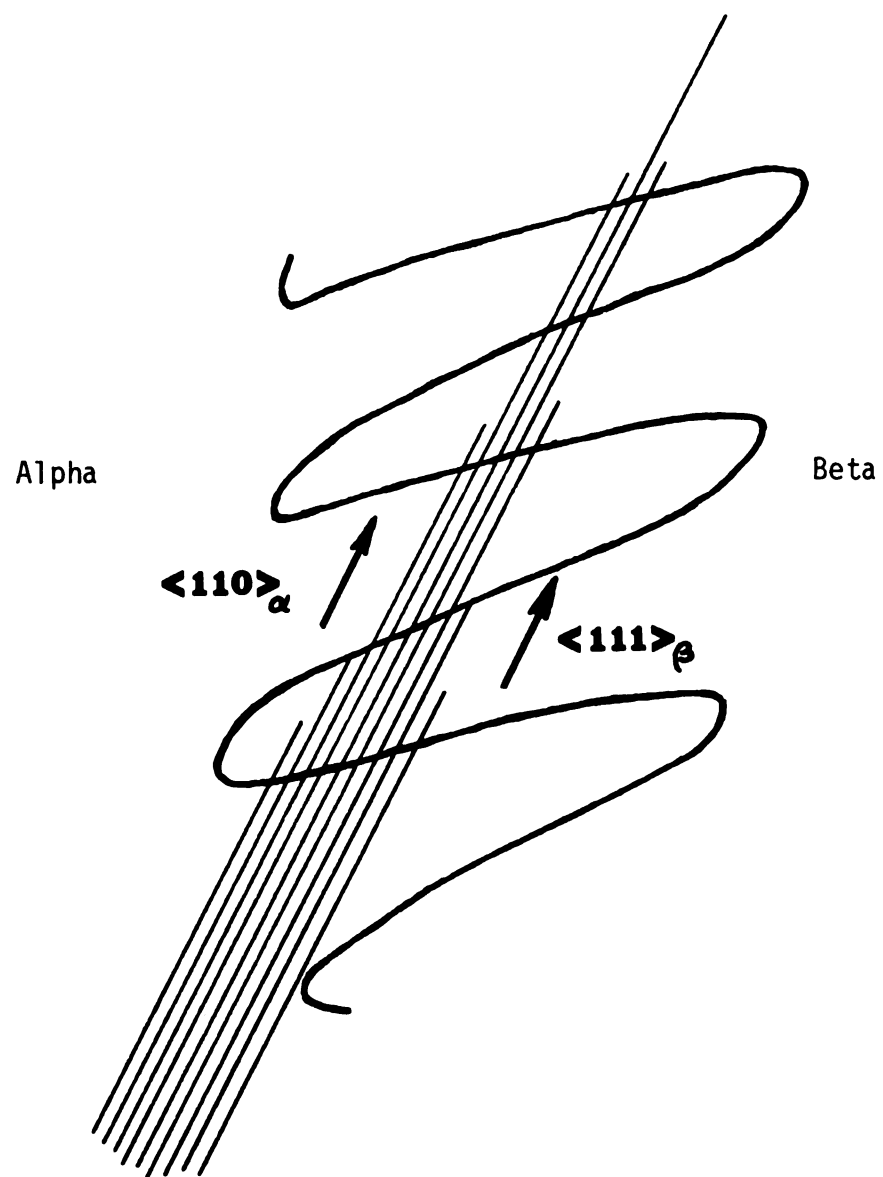


Fig. 47 Model for the Interaction of Slip with an Oriented Duplex Type Boundary.

2

and high strain-rates. Strain-rate sensitivity has been observed in testing specimens having this type of boundary. The stress level at which deformation progresses across the interface into the beta phase, however, was observed to be lower than for specimens tested under similar conditions that had other types of boundary geometries. The ineffectiveness of the oriented duplex interface as a barrier to slip propagation at all strain-rates relative to the other three boundary type is undoubtedly due to the existence of the orientation relationship between the alpha and beta phases. The model used to analyze the slip interaction with this types of interface is not suitable for use with other boundary geometries because the oriented duplex interface is the only case where this definite orientation relationship exists.

Flat Boundary

The flat boundary geometry has been observed to be a fairly effective barrier to the propagation of slip. It is more effective than the oriented duplex interface. As with the other types of boundary geometries investigated, the stress at which slip may be initiated in the beta phase across the boundary is strain-rate sensitive. At low strain-rates slip progressed across the boundary at a low stress value. This stress value increases as the strain-rate is increased until at a moderate strain-rate slip does not progress across the boundary; instead slip is initiated in the beta phase away from the interface. This indicates that the interface region is stronger than either alpha or beta alone because of geometrical constraints.

At low strain-rates, single or multiple slip interacting with the boundary cross-slips to accommodate the increasing stress concentration created by the dislocation pile-ups on the slip planes in the coarse slip bands. In the process of cross-slipping the dislocations multiply

and their density therefore increases, which serves to increase the stress concentration in the slip regions. The double cross-slip mechanisms of dislocation multiplication proposed by Gilman¹⁰² seems to be operating in alpha. This double cross-slip mechanism of dislocation multiplication was originally proposed to explain wide slip band formation in sodium chloride structure crystals. This mechanism facilitates the motion of dislocations in a slip plane to cross over to a parallel slip plane and multiply in that plane. Repeated operation of the double cross-slip process can give rise to closely packed slip lines and provide a slip band. In this model, cross-slip is believed to take place due to local stress conditions. In the present case, the stress concentration caused by the pile-up of dislocations at the boundary can create a suitable stress state to cause cross-slip. Such cross-slipping has been observed frequently in the micrographs of deformed specimens. After the initial cross-slipping takes place the stress concentration is sufficiently built-up again to propagate slip across the boundary. At higher stresses, further cross-slipping continues to occur. However, propagation of the deformation into the beta phase takes place because of the local stress concentration. At medium and particularly at high strain-rates, the increase in the yield stress of the beta phase⁵³ makes propagation of deformation across the boundary increasingly more difficult. If multiple slip systems interact with the boundary, the interacting dislocations will have a high density of jogs.⁴¹ The introduction of jogs in screw dislocations hampers their further movement. Such an occurrence near the boundary, therefore, as a result of the interacting multiple slip systems, immobilizes a large percentage of the dislocations. The drastically reduced quantity of mobile dislocations makes propagation of deformation across the boundary increasingly difficult. Further, the stress concentration produced by dislocation pile-ups in fine slip lines will not be as effective as the stress

concentration caused by the blocking of wide slip bands. The flat boundary in these bicrystals is a less effective barrier to the progress of deformation across the interface than the corrugated or equiaxed type of interfaces because of the boundary geometry. Slip interacts with the entire boundary surface in a flat geometry, whereas with the corrugated and equiaxed boundaries only a portion of the total boundary surface is oriented favorably for slip to interact effectively to propagate deformation into beta.

Corrugated Boundary

In formulating this study it was of interest to develop one type of specimen boundary geometry in which the boundary would be inclined to the tensile axis. Such specimens would be helpful in understanding the role of the relative orientation of the boundary with respect to the tensile axis. Since the attempts to obtain specimens with inclined boundaries were not successful, it was decided to use a non-uniform boundary such as a corrugated boundary. In such a boundary geometry, much of the boundary surface would be inclined to the tensile axis to various degrees, and thus any effect that an inclined boundary may have on the passage of deformation across the boundary could be observed.

Beta platelets present in a corrugated boundary are thicker and need not have any definite crystallographic relationship with the alpha single crystal. As a result slip propagation through such a boundary should be more difficult than in the case of oriented duplex boundary specimens. As shown in Fig. 48 owing to various possible boundary orientations, it is reasonable to expect that some of the regions of the boundary may be favorably oriented for slip to propagate through. Some of the regions may subtend angles with the active slip plane and slip direction in alpha which

Fig. 48 Model for the Interaction of Slip with a Corrugated Boundary.

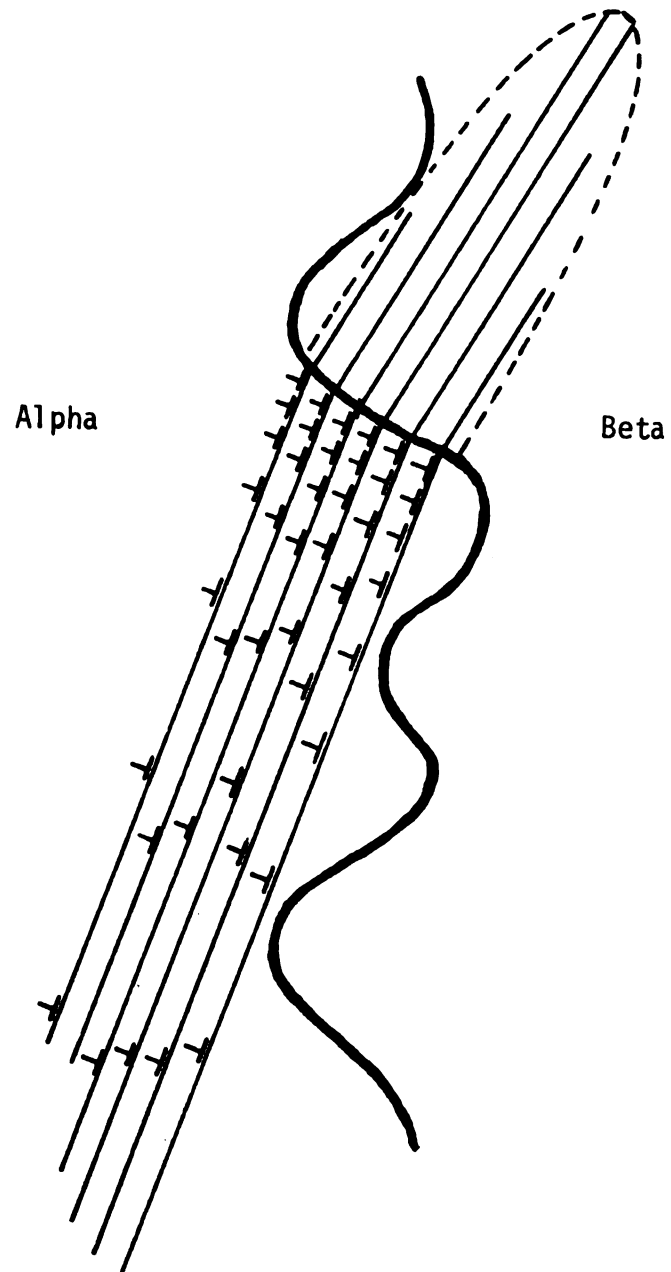


Fig. 48 Model for the Interaction of Slip with a Corrugated Boundary

are not favorable for initiating slip in the beta region.

The corrugated type of boundary may be obtained by cyclic heat-treating an oriented duplex interface structure for a longer time to reduce the extent of the alpha and beta phase interpretation. In doing so, however, the crystallographic orientation relationship between the phases meeting at the boundary may be modified. More often, it has been observed that the corrugated type of interface structure results from the reduction of structures other than the oriented duplex structure.

The passage of slip through the boundary for this case is caused by a high stress concentration created by dislocation pile-ups in the active slip planes near the boundary. These slip bands meeting the corrugated boundary will each encounter a somewhat different boundary geometry, - some being favorably oriented with respect to the slip band direction to withstand high stress concentration while others are less favorably oriented. The orientation of the slip traces and slip directions with respect to the boundary is certainly a consideration for the slip propagation. However, they are not the primary considerations since there are six possible slip planes, each having two possible slip directions in the beta phase. It is likely, therefore, that in most cases some system in the beta phase will be somewhat favorably oriented for slip to propagate through the boundary. The corrugated boundary geometry appears to be a more effective barrier to slip than the oriented duplex structure and the flat boundary. It also exhibits the same type of strain-rate sensitivity regarding the stress at which deformation progress through the boundary.

The corrugated boundary has been observed to be a stronger boundary than the oriented duplex type. This is undoubtedly because of the fact that the corrugated type of boundary lacks the crystallographic orientation relationship between the two phases meeting at the boundary. This lack of fully

favorably oriented slip systems makes the propagation of slip across the boundary more difficult. It is also observed that the corrugated boundary is stronger than the flat boundary geometry. The model in Fig. 49 shows two extreme conditions of how slip systems may interact with corrugated boundary geometry.

The model given in Fig. 49a can be used to explain why the corrugated boundary is stronger than the flat boundary. Because of the nature of the boundary geometry, slip systems approaching the boundary from one, or even two, directions for multiple slip encounter less boundary area at which effective dislocation pile-ups may build up. In the case of a flat boundary, the entire boundary surface is available for a particular slip system to interact effectively with it. The lack of favorable orientation relationship between the phases at this boundary makes a corrugated boundary stronger than the oriented duplex boundary.

The other extreme, where a slip system approaches the boundary on a shallow angle is given in the model illustrated in Fig. 49b. The initial interaction of the slip system with the boundary is effective in creating a favorable condition for initiating slip across the boundary. Once through the boundary, however, the further slip propagation is more difficult for two reasons. First, the motion of the superlattice dislocations in the beta phase is more difficult,⁵¹ and the stress concentration tends to decrease rapidly with distance from the boundary. As a result, there is a strong tendency for the slip propagation to stop.¹⁶ Secondly, as shown in the model, the slip is approaching another boundary ($A'B'$). Once slip is through this second boundary, ($A'B'$), at which some of the slip is blocked, fine slip continues in this new alpha phase area A' until another boundary $A'B'$ is encountered. At this boundary the fine slip may be totally blocked. The slip line length in the alpha phase to cause an effective dislocation pile-up has

Fig. 49 Model for Analysing the Effect of the Slip Orientation Relative to a Corrugated Boundary.

- (a) Slip band makes a steep angle with the boundary.
- (b) Slip band makes a shallow angle with the boundary.

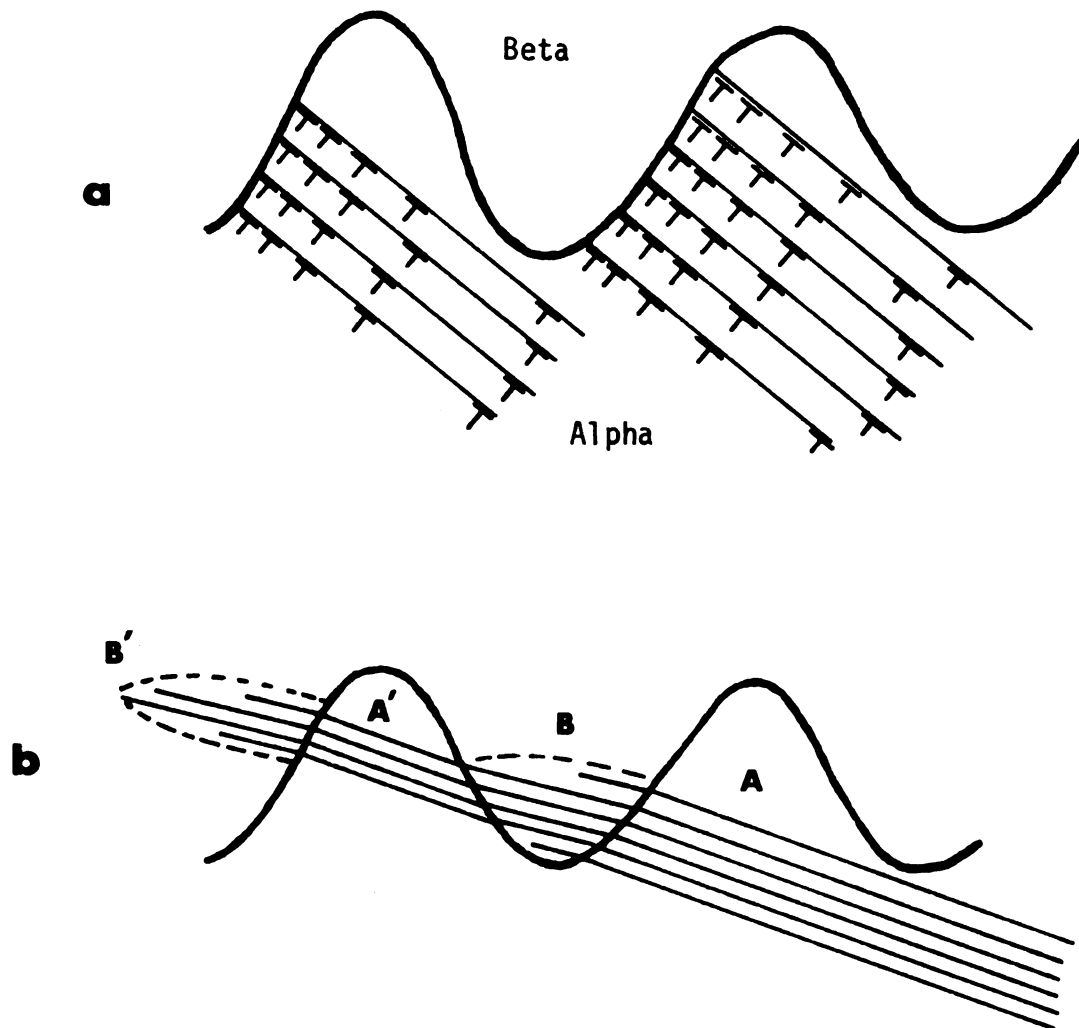


Fig. 49 Model for Analyzing the Effect of the Slip Orientation Relative to a Corrugated Boundary.

- (a) Slip band makes a steep angle with the boundary.
- (b) Slip band makes a shallow angle with the boundary.

decreased, and there will be a corresponding decrease in the severity of the stress concentration that may be developed. In the relative ordering of the boundary types, the corrugated boundary is weaker than the equiaxed duplex boundary. The primary difference between the corrugated boundary geometry and the equiaxed duplex, is the extent of the alpha-beta interpenetration. In the next section a detailed description is given concerning the behavior of the equiaxed duplex boundary, and why it is stronger than the other types of geometries.

Equiaxed Boundary

The equiaxed or unoriented duplex type of interface structure seems to be the most effective interface geometry to inhibit the progress of deformation across a boundary. While the geometry of this type of interface is somewhat similar to that of the oriented duplex structure, the orientation relationship between the alpha platelets and islands with respect to the beta phase is lacking. For all of the test specimens, the results indicate such an interface structure withstood higher stress levels before allowing deformation to propagate through the boundary into the beta phase. This behavior may be explained on the basis of greater total boundary surface area involved in this geometry compared with the other geometries. Optical and scanning electron micrograph observations give a clear indication of the behavior of the slip interaction with equiaxed boundaries.

Single or multiple slip reaching this unoriented type of interface encounters a large boundary surface area. Whenever a slip line interacts with an alpha-beta boundary, it is either turned away in another direction to continue in the alpha phase by multiple slip or cross-slips because of the stress concentration created at the boundary. This type of behavior is shown clearly in Figs. 25d and 28. As the deformation of alpha phase at the

boundary increases, existence of the large boundary surface area causes extensive multiple slip and cross-slip in adjacent alpha regions. In this way, a large amount of deformation can be accommodated in the alpha regions of the interface without the necessity of building large stress concentrations in some areas. Further, the length of the pile-ups at the interfaces will be short. This will make them relatively ineffective in causing the slip to propagate through the boundary. Microstructural studies show evidences for this analysis (Figs. 25a, b, c, d, 28). Once the continuous alpha phase regions in the boundary structure have been heavily deformed and reach a stage at which they cannot accommodate any further deformation, slip appears to progress across the boundary, especially at low strain-rates. The stress level to reach such a condition is higher than that needed for deformation to progress across the boundaries in any of the other three types of boundary geometries. As experienced in the case of specimens with other boundary types, the specimens with equiaxed interface also show rather strong strain-rate sensitivity. At low strain-rates slip, did eventually progress across the boundary but at a stress level higher than that required in other boundary types tested at the same strain-rate. With increasing strain-rate, this stress level also increased until, at a moderate rate, slip could not be propagated across the interface. Rather, slip was initiated in the beta phase in regions away from the boundary. This fact means that the stress level that the boundary withstood was higher than the critical resolved shear stress in the beta phase. This can partially be explained by the plastic constraints at the boundary and the multi-axial stress state developed by this constraints.

B. COARSE AND FINE SLIP IN ALPHA PHASE

During the course of testing the strain-rate specimens it was observed that in the alpha crystal coarse slip developed at low strain-rates and fine slip developed at high strain-rates. At low strain-rates a few dislocation sources are activated, and continue to operate until the alpha is very heavily deformed. Repeated operation of these sources give rise to very deep, coarse slip lines, usually in a band form. At high strain-rates, on the other hand, many sources are activated on many planes during the initial deformation. Although some of these sources become inoperative because of the back stress caused by the dislocation pile-up at the boundary, the stress level rises and activates the dislocation sources present in parallel slip planes. This process repeatedly takes place as the stress level continues to rise and the result, after considerable deformation has occurred, is very fine slip as observed in these tests. During high strain-rate tests, cross-slip was not observed to take place. As a result, most of the deformation occurred by fine slip. So dislocations did not move to parallel slip planes to create wide slip bands.

C. STRESS CONCENTRATION AND STRAIN-RATE EFFECTS

When slip approaches a boundary, it may do so in the form of single isolated slip lines having some average spacing. In this situation, the encounter of the slip with the barrier stops the progress of slip at least temporarily. When a single slip line encounters a barrier such as a phase boundary, the dislocations moving along this slip plane are blocked at the boundary, and the trailing dislocations pile up behind the leading dislocation as shown in Fig. 50. The stress at the boundary created by such a pile-up increases with increasing number of dislocations in the pile-up.

Fig. 50 Zone of Stress Concentration Caused by Dislocation
Pile-up in a Fine Slip Line.

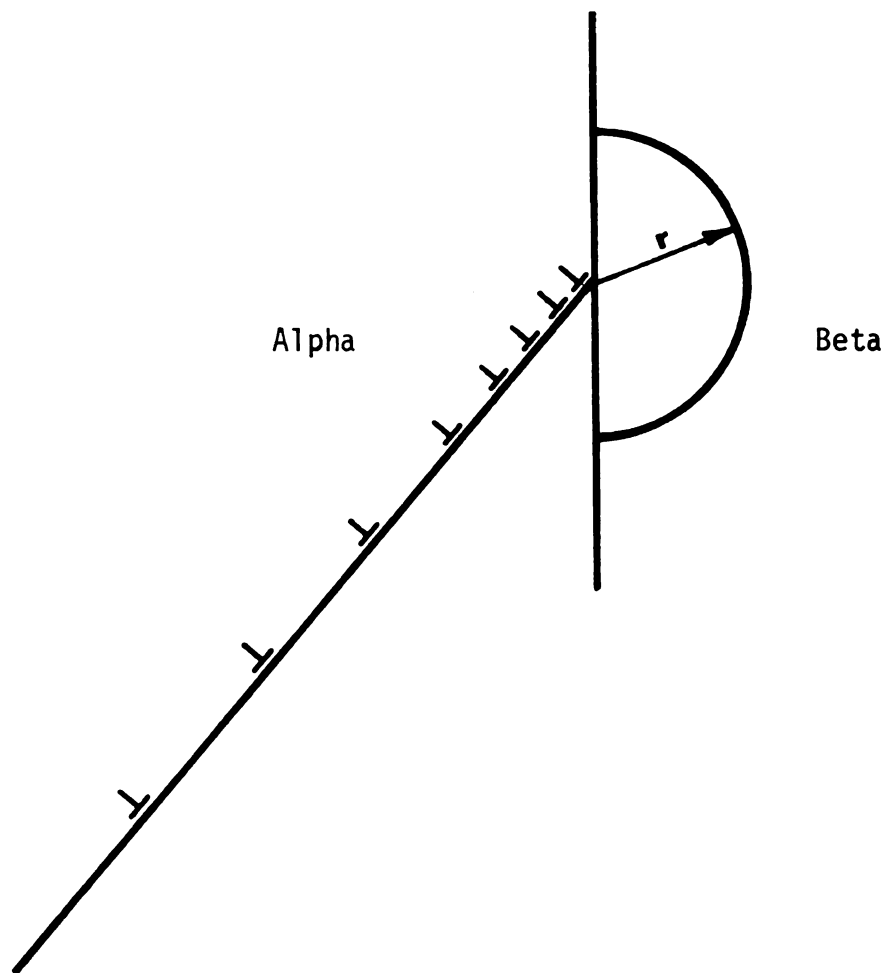


Fig. 50 Zone of Stress Concentration Caused by Dislocation
Pile-up in a Fine Slip Line.

270

This pile-up creates a localized region of higher stress concentration in nearby regions in the adjacent phase as shown in Fig. 50. If the applied stress does not increase sufficiently, the back-stress created by the dislocation pile-up may stop the operation of the dislocation source.

Karashima³⁸ has observed this type of stress concentration and work-hardening caused by dislocation pile-ups in alpha brass using electron microscopic techniques. When the stress concentration reaches a sufficiently high level, the dislocations present in the phase boundary may be forced into the adjacent grain and thereby propagate slip through the boundary.⁴⁷ In this way the high stress concentration can be relaxed. Another possibility is that the high stress concentration in this localized region may activate dislocation sources in regions on the other side of the phase boundary.^{43,45,46} Such a process will aid the stress relaxation at the boundary and in effect allow deformation to proceed across the interface into the adjacent grain.

If a large number of closely spaced slip lines are present in the slip band and are blocked at a boundary, a higher stress concentration will result. In all of the samples tested at low strain-rates, wide Lüders type slip bands were observed to initiate somewhere in the alpha phase and propagate to interact with the boundary. Samples tested at high strain-rates did not display this behavior. Fine single slip or multiple slip occurred in these specimens. Chalmers and co-workers^{94,95} have studied in detail this type of behavior of several different slip systems operating at a grain boundary when a polycrystal is deformed. Dislocations on the individual slip planes of a slip band can form pile-ups in their own slip planes. Stresses caused by such pile-ups will complement one another to cause a much higher stress concentration. Such stresses can be relaxed by cross-slipping in alpha. However, double cross-slip can cause dislocation multiplication in parallel slip planes. The double cross-slip mechanism of

dislocation multiplication proposed by Gilman¹⁰² can give rise to wide slip bands. Although cross-slipping can initially relax the stress concentration resulting from the pile-ups, activation of the newly created sources will produce a large number of dislocations piling up at the boundary in parallel slip planes as shown in Fig. 51. When the alpha has deformed sufficiently to prevent further cross-slip, relaxation by cross-slip becomes difficult, and the deformation must be accommodated in the beta region.

In a single phase material, the condition at which one grain will no longer accommodate the deformation by stress relaxation has been examined by Johnston.¹⁰³ Under such conditions the adjacent grain will be required to accommodate the deformation. The deformation rate \dot{D} may be expressed as

$$\dot{D} = \rho_1 b_1 v_1 \ell$$

where ρ_1 , b_1 , v_1 are the density, Burgers vector and velocity of the mobile dislocations in the primary slip plane and ℓ is a size parameter. During the initial stage of deformation in alpha, when cross-slip provides a means of stress relaxation as discussed previously, the relaxation rate \dot{R} , may be expressed as

$$\dot{R} = \rho_2 b_2 v_2 \ell$$

where ρ_2 , b_2 , v_2 are the density, Burgers vector and velocity of the mobile dislocations present in the cross-slipping plane of alpha. When the condition is reached whereby alpha can no longer relax the stress concentration by cross-slip alone, deformation has to take place in beta. Under such conditions the relaxation rate \dot{R} , will become

Fig. 51 Zone of Stress Concentration Caused by Dislocation
Pile-ups in a Slip Band.

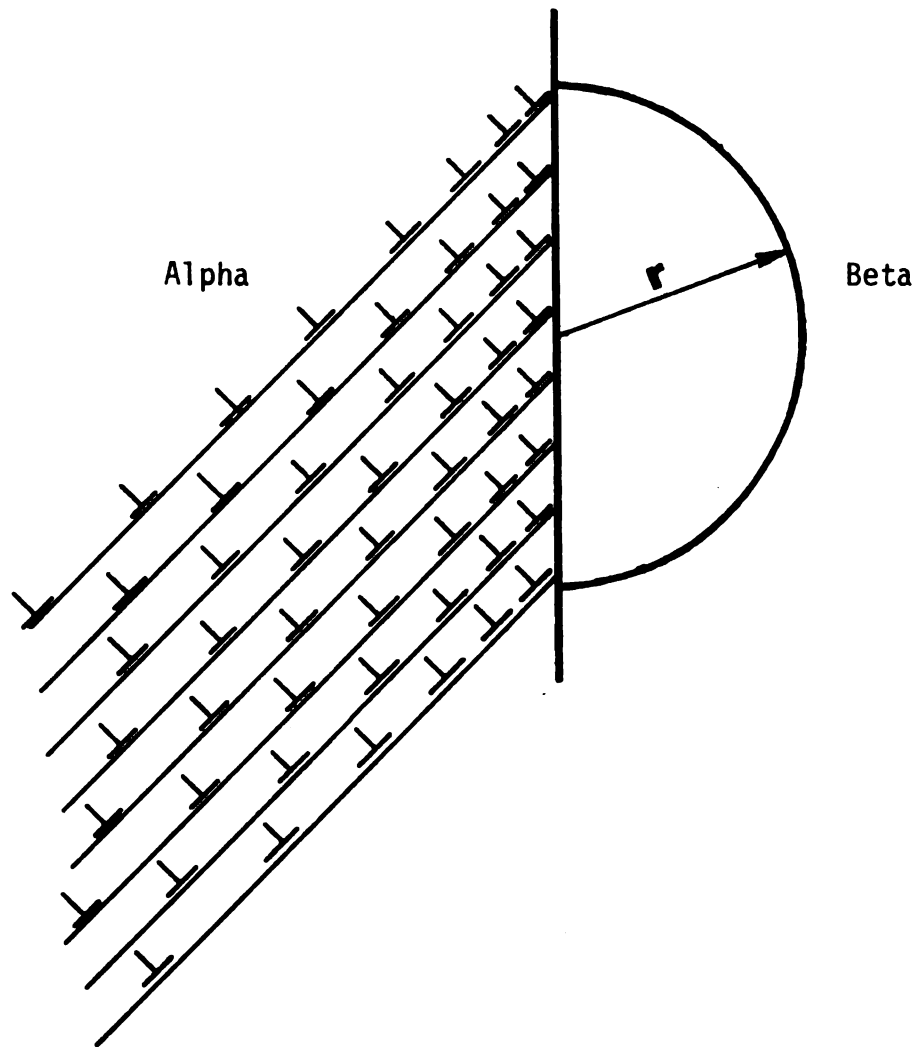


Fig.51 Zone of Stress Concentration Caused by Dislocation
Pile-ups in a Slip Band

$$\dot{R} = \rho_2 b_2 v_2 \ell + \frac{r}{m} [M \rho_{\beta_i} b_{\beta_i} v_{\beta_i}]$$

where r is the stress concentration region, m is the orientation factor, M is the dislocation multiplication factor, and ρ_{β_i} , b_{β_i} , v_{β_i} are the density, Burgers vector and velocity of the mobile dislocations respectively in beta. The importance of including an orientation term " m " was first emphasized by Armstrong.⁸⁶

Feltham and Spears⁵⁰ have studied the stress relaxation in solid solutions in detail. In single crystals there is a pronounced stress relaxation at large strains, while at low strains, especially in the linear stage of hardening, the stress relaxation is small.

In the present study, as indicated in the chapter on experimental procedures, the tensile loading of strain-rate specimens was periodically stopped during the tests to observe the stress relaxation behavior under different testing conditions. A general pattern of behavior followed by all the test specimens was observed. Tensile specimens tested using slow cross-head speeds evidenced very small stress relaxations when the load application was stopped. Samples tested using high cross-head speeds exhibited very large load drops in stress relaxations when the loading was stopped. The stress concentration built up at the boundary in the alpha phase during high strain-rate deformation relaxes very readily by what ever means it can, except by propagating deformation across the boundary. The stress concentration built up by slow strain-rate deformation in the alpha phase is more stable in nature, possibly owing to the extensive cross-slip and work-hardening that takes place, and the observed relaxation of stress is quite small.

In high strain-rate tests, slip in alpha progressed to the boundary as single slip. As explained in section B of this chapter, as the slip

lines become blocked at the boundary, dislocation sources present in parallel slip planes become active. However, multiple slip also takes place in high strain-rate samples. Dislocations moving in intersecting slip planes can interact with each other and cause jogs.⁴¹ When two dislocations moving in non-parallel slip planes intersect, then each acquires a jog equal to the component normal to its own slip plane of the other dislocation's Burgers vector.⁵⁷ Since the dislocations present in alpha near the interface will have a high density of jogs caused by the intersecting slip, most of them will be immobile. As a result, most of the dislocations present in alpha near the interface region will not be able to cause long-range stress fields because of dislocation pile-ups. Under such conditions, slip propagation through the interface cannot take place. Therefore, in specimens tested at high strain-rates there was no deformation across the boundary, regardless of boundary geometry. Rather, the applied stress level built up until the critical resolved shear stress of the beta phase was reached. Beta phase deforms because of the applied stress in a region away from the phase boundary. At high strain-rates, therefore, the phase boundary region seems to be the strongest part of the bicrystal specimens.

It has been observed that during low strain-rate testing, slip in alpha progressed to the boundary as single slip, as discussed in section B of this chapter. These slip lines undergo cross-slipping upon reaching a boundary. Such a cross-slipping process creates wide slip bands. Eventually the relaxation by cross-slip decreases, and the increased stress concentration causes deformation to progress across the boundary.

Another factor that has bearing on the high strain-rate behavior of these bicrystal test specimens is the behavior of the beta phase at high strain-rates. The yield stress of the beta phase increases when subjected

to dynamic loading conditions.⁵³ An interpretation for the lack of progress of slip through the boundary at high strain-rates can be attempted on the basis of higher critical resolved shear stress for beta at higher strain-rates. However, such an interpretation will have serious drawbacks. In specimens tested at high strain-rates, slipping had started in regions far away from the boundary indicating that the applied stress level was high enough to cause deformation in beta, although slip did not progress through the boundary in the interface region.

The stress concentration plays a major role in the process of creating conditions sufficient to propagate slip across a phase boundary. The response of the alpha phase to the type of stress-concentration imposed by the indentation test was similar to its response at high strain-rates. During indentation, the deformation was greatly accommodated in the alpha phase surrounding the indentation. The alpha phase region adjacent to the indentation can accommodate the deformation more easily than the boundary regions. Further, when the fine slip initiated by the indentation interacts with the boundary, cross-slip is facilitated as a means of relaxation. The ineffective stress concentration caused at the boundary structure, therefore, could not propagate deformation through the boundary. The fine slip that developed in the alpha phase during high strain-rate tensile testing also exhibited the same type of behavior as the fine slip from indentation. The alpha phase totally accommodated the deformation and the boundary region remained underformed until, at very high stress levels, deformation took place in the beta phase away from the boundary.

Higher indentation rates, higher indentation loads, and closeness of the indentation to the boundary were somewhat more effective in increasing the slip interactions with the boundary. However, even under these conditions the deformation could only proceed partially into the duplex boundary

structure. In corrugated and flat boundary specimens, slip completely stopped at the boundary. The relaxation of the deformation occurred in the alpha phase itself, and, as a result, there was no effective stress concentration at the boundary to facilitate the progress of slip through the boundary into the beta phase.

D. SLIP IN THE BETA PHASE

In regions where slip was observed to have progressed across the boundary, a zone of deformation was formed in regions of the beta phase adjacent to the boundary. This zone was especially apparent in specimens having a flat boundary as shown in many of the optical and scanning electron micrographs (Figs. 35,36,37,40, and 42). Once sufficient stress concentration was created owing to the dislocation pile-up at the barrier, slip proceeded into the beta phase. Observations made during the course of this study and by Honecombe and Boas,¹⁶ who studied the deformation of alpha-beta brass, show that the deformation does not proceed very far into the beta phase. It is stopped within a short distance of the boundary. Although slip lines in beta are prominent very near the boundary, they rapidly become very diffuse at points away from the boundary. The region of deformation within the beta phase near the boundary may be enclosed by a zone as shown in Fig. 52.

The slip propagation in the beta phase requires the movement of dislocations as in a typical cesium-chloride type of structure. These dislocations are superlattice dislocations which are composed of two partial dislocations joined to one another by an anti-phase boundary. Because of the geometry of this superlattice dislocation, it must move as a whole unit since the partial dislocations are connected to one another by the

Fig. 52 Model for the Deformation Zone in Beta

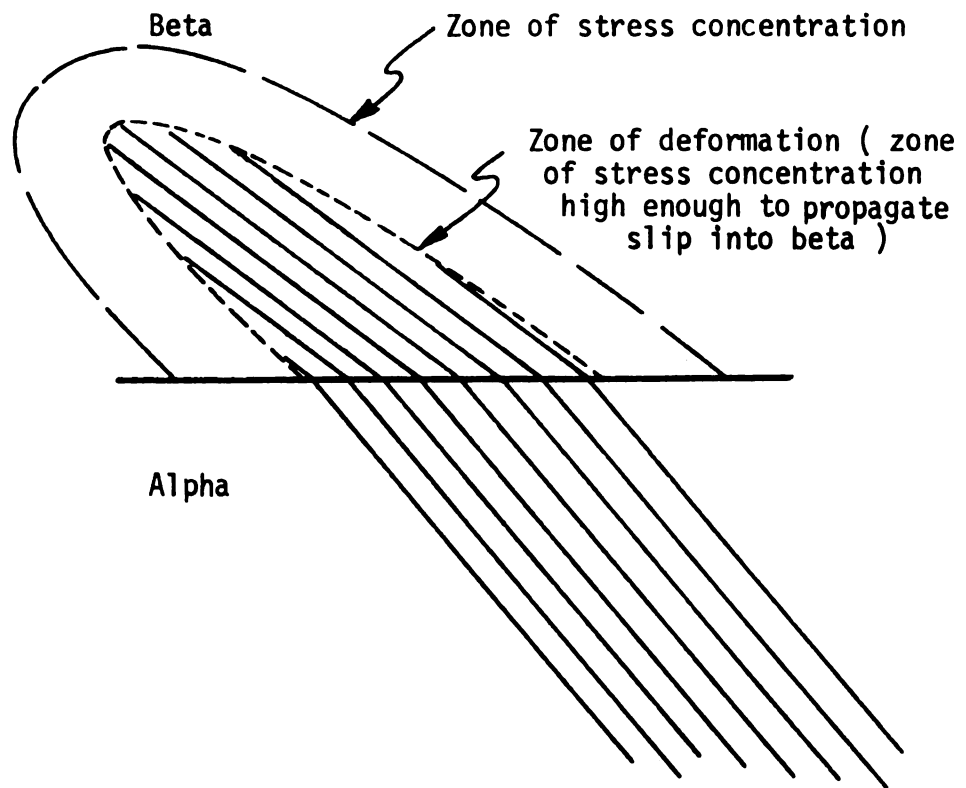


Fig. 52 Model for the Deformation Zone in Beta

anti-phase boundary. As a result, their motion is difficult and requires a high stress.⁵¹ The high stress concentration developed at the phase boundary which allows deformation to proceed through the boundary is quite limited in its extent into the beta region. Therefore, as any given slip line proceeds from alpha across the boundary and into beta, it will proceed only to a limited extent. The extent depends on the level of the stress concentration, which is a function of the distance from the boundary. When the slip line in beta reaches a position at which the stress concentration is insufficient to continue slip propagation, it will stop. The tips of the slip lines in beta, which are caused by any one of the stress concentrated regions, define a zone of deformation, as shown in Fig. 52. This feature can be observed in the optical and scanning electron micrographs of deformed specimens (Figs. 35,36,37,40,41,42 etc.). This zone does not define the entire region of stress concentration, but only the region where the stress concentration was high enough to propagate slip in beta.

The extent of this deformation zone in beta is affected by the change in strain-rate. As the strain-rate increases, the value of the yield stress in beta correspondingly increases. This increase results in a smaller deformation zone since a smaller portion of the stress concentration region will have stress high enough to move the superlattice dislocations in the beta phase. The two types of characteristic slip observed in the beta phase after deformation are shown in Fig. 29a and 29b. One type is a fine slip which is propagated across the phase boundary into the beta phase. At the boundary in the beta phase it is very prominent, but stops after travelling a short distance into the beta region. This slip consists of sets of fine parallel lines in the form of slip bands. The other type of slip in beta exhibits a corrugated relief and shows up as a light and dark

banding effect. Greninger⁵² has studied the plastic deformation behavior of beta brass and has observed this same behavior. He has also observed that neither slip lines nor deformation bands seem to continue across a grain boundary without changing direction, and feels that both are related in some way to the beta lattice.

CHAPTER VII

SUMMARY AND CONCLUSIONS

1. Among the four types of boundaries considered in this study, the equiaxed (unoriented) type of duplex interface structure is the most effective type of barrier to the progress of slip across the phase boundary. Among the four types of boundaries, the strength increases in the following order:
 1. Oriented duplex
 2. Flat boundary
 3. Corrugated boundary, and
 4. Equiaxed duplex.
2. All of the bicrystals, regardless of the type of boundary geometry, were found to be strain-rate sensitive.
3. Lower strain-rates tend to form wider slip bands and coarser slip lines in alpha phase, which creates a higher stress concentration at the boundary.
4. Higher strain-rates tend to form very fine slip by activating many dislocation sources on numerous planes. These are reflected at the boundary creating multiple slip which immobilizes a large portion of the dislocations and consequently makes the initiation of deformation across the boundary very difficult.
5. Lower strain-rate tests, especially those with flat interfaces exhibit

extensive cross-slip near the boundary. The cross-slip appears to help in creating wider slip bands in the alpha phase regions near the interface.

6. In specimens having equiaxed and corrugated boundaries, slip usually is initiated in the beta phase in a region away from the boundary, indicating that the interface regions are very effective barriers to slip in the absence of definite crystallographic orientation.
7. Indentation tests have shown that it is not easy to propagate slip through any of the four boundary geometries unless an indentation is placed right in the interface structure.
8. Irrespective of the nature of the boundary, no void formation was observed at the interface because of slip interaction in any of the boundaries during this study.
9. The results on flat boundary bicrystals do suggest that the dislocation sources in the beta phase become operative owing to dislocation pile-ups formed at the boundary in the alpha phase region. The slip lines observed in the beta regions lie at various crystallographic orientations and were not parallel to the trace of the primary slip directions operative in the alpha single crystal. This observation indicates that motion of dislocations through the boundary to initiate slip in the beta phase is not probable.
10. Phenomena such as initiation of slip at regions far away from the boundary, especially in equiaxed specimens, indicate that the activation of sources in beta region is more likely than the mechanism which will utilize grain boundary sources for initiation of slip.
11. There is definite correlation between the stresses at which slip propagates through the boundary and the relative crystallographic orientation of the two grains. Slip systems making shallower angles with the

boundary seem to be more effective in activating dislocation sources present in the beta phase than slip making steep angles with the boundary.

12. Deformation of the beta phase does not seem to be determined by the activation of the dislocation sources present. Propagation of slip in the beta phase as a result of its superlattice structure is more important than the activation of these sources.

CHAPTER VIII

SUGGESTED TOPICS FOR FURTHER INVESTIGATION

The alpha brass single crystals grown for this work, and those used in Hingwe and Subramanian's work were of random orientation. A suggested approach for further work would be to grow alpha brass single crystals of known orientations for making specimens for mechanical testing. The faces of the alpha phase portion of the specimen could be machined and polished to obtain desired crystallographic planes and directions.

A phase boundary inclined at various angles used in conjunction with oriented alpha brass single crystals would enable the resolved shear stress at the phase boundary and the stress at which deformation penetrated through the boundary to be studied. In the present work and in Hingwe and Subramanian's work, only phase boundaries normal to the tensile axis have been used.

Deformation studies on alpha-beta brass bicrystals at elevated temperatures would be of great interest. Oriented alpha brass single crystals as well as inclined and horizontal phase boundaries could be employed in this work. Possibly two temperatures below the beta prime order-disorder transformation temperature, one at the transformation temperature, and one temperature above could be used for testing the bicrystals. This would allow a study of the temperature effects on the slip interaction at the phase boundary. Further, the effect of the order-disorder transformation

of the beta prime phase and its role on the slip interaction with the phase boundary could be studied.

A further step towards an understanding of the bulk material deformation behavior could be taken by preparing and testing specimens having a few very large grains of each phase in a macro-sized specimen. The relative orientations of the adjacent alpha and beta phase regions in such a specimen could be determined by X-ray techniques. The testing and observation procedures employed could be similar to those used in bicrystal mechanical testing.

The mechanical behavior of alpha-beta brass bicrystals subjected to sudden dynamic axial loads would be an interesting area of further study. Successively larger dynamic tensile loads could be applied until deformation was propagated through the phase boundary. Oriented alpha brass single crystals with horizontal as well as inclined phase boundaries would be of interest in this work also.

It would be of great interest to conduct a study to determine what other two-phase systems could be used to make bicrystal model units for mechanical behavior studies. Possibly the procedures used to make alpha-beta brass bicrystals could be adapted to make bicrystals in other two-phase systems. This would greatly aid the whole field of two-phase materials research.

BIBLIOGRAPHY

1. J. D. Livingston, B. Chalmers; Acta Met., 1957, 5, p. 322.
2. R. L. Fleischer, B. Chalmers; Trans. A.I.M.E., 1958, 212, p. 265.
3. J. J. Hauser, B. Chalmers; Acta Met., 1961, 9, p. 802.
4. R. E. Hook, J. P. Hirth; Acta Met., 1967, 15, p. 535, 1099.
5. J. D. Meakin, H. G. F. Wilsdorf; Trans. A.I.M.E., 1960, 218, p.737.
6. J. H. Van der Merwe; "Single Crystal Films", Ed. M. Francombe and H. Sato, 1964, Pergamon Press, New York, p. 199.
7. A. K. Head; Phil. Mag., 1953, 44, p. 92.
8. G. H. Conners; Int. J. Engr. Sci., 1967, 5, p. 25.
9. E. H. Yoffe; Phil. Mag., 1961, 6, p. 1147.
10. J. D. Eshelby; Phil. Trans., 1957, A-244, p. 87.
11. H. Unckel; J. Inst. Metals, 1937, 61, p. 171.
12. D. Dew-Hughes, W. D. Robertson; Acta Met., 1960, 8, p. 147.
13. G. Thomas, J. Nutting; J. Inst. Metals, 1957-58, 86, p. 7.
14. H. C. Chao, L. H. Van Vlack; Trans. Met. Soc. A.I.M.E., 1965, 233, p. 1227.
15. H. C. Chao, L. H. Van Vlack; Mat. Res. Std., 1965, 5, p. 611.
16. R. W. K. Honeycombe, W. Boas; Aust. J. Sci. Res., 1948, [A], I, p. 70.
17. L. M. Clarebrough; ibid, 1950, [A], 3, p. 72.
18. L. M. Clarebrough, G. R. Perger; ibid, 1952, [A], 5, p. 114.
19. J. Gurland, J. T. Norton; Trans. A.I.M.M.E., 1952, 194, p. 1051.
20. J. Gurland; Trans. Met. Soc. A.I.M.E., 1961, 221, p. 407.
21. C. Nishimatsu, J. Gurland; Trans. A.S.M., 1960, 52, p. 469.

22. B. I. Edelson, W. M. Baldwin; Trans. A.S.M., 1962, 55, p. 230.
23. B. I. Edelson; *ibid*, 1963, 56, p. 82.
24. I. L. Mogford; Met. Reviews, 1967, 12, p. 57.
25. F. Felberbauer, E. P. Lautenschlager, J. O. Brittain; Trans. Met. Soc. A.I.M.E., 1964, 230, p. 1596.
26. G. T. Hahn; Acta Met., 1962, 10, p. 727.
27. H. Margolin, P. A. Farrar, M. A. Greenfield; "The Science, Technology, and Application of Titanium" ED. R. I. Jaffe, N. E. Promisel; 1970, Pergamon Press, New York, p. 795.
28. R. A. Wood, D. N. Williams, H. R. Ogden, R. I. Jaffe; Trans. A.I.M.E., 1959, 215, p. 308.
29. J. F. Bell; Phil. Mag., 1964, 10, p. 107.
30. J. F. Bell; *ibid*, 1965, 11, p. 1135.
31. W. F. Hartman; J. of Mat., JMLSA, 1969, 4, p. 104.
32. A. H. Cottrell; Phy. Soc. London, 1948, p. 30.
33. F. R. N. Nabarro; *ibid*, 1948, p. 38.
34. A. H. Cottrell, B. A. Bilby; Proc. Phys. Soc., 1949, [A], 62, p. 49.
35. R. D. Heidenreich, W. Shockley; Phy. Soc. London, 1948, p. 57.
36. G. W. Ardley, A. H. Cottrell; Proc. R. Soc., 1953, A219, p. 328.
37. S. Karashima; Trans. J.I.M., 1961, 2, p. 134.
38. D. A. Thomas, B. L. Averbach; Acta Met., 1959, 7, p. 69.
39. W. H. Lomer; Phil. Mag., 1951, 42, p. 1327.
40. A. H. Cottrell; *ibid*, 1952, 43, p. 645.
41. P. B. Hirsch: Cited by N. F. Mott; Trans. A.I.M.E., 1960, 218, p. 962.
42. G. J. Ogilvie; J. Inst. Met., 1952-53, 81, p. 491.
43. S. Karashima; Proc. 2nd. Japan Congr. Test. Mat., 1958, p. 59.
44. F. C. Frank, W. T. Read; Phys. Rev., 1950, 79, p. 722.
45. D. A. Thomas, B. L. Averbach; Acta Met., 1959, 7, p. 69.
46. T. Vreeland, D. S. Wood, D. S. Clark; Acta Met., 1953, 1, p. 414.

47. J. T. Fourie, H. G. F. Wilsdorf; J. Appl. Phys., 1960, 31, p. 2219.
48. T. E. Mitchell, P. R. Thornton; Phil. Mag., 1964, 10, p. 315.
49. P. R. Strutt, B. H. Kear, H. G. F. Wilsdorf; Acta Met., 1966, 14, p. 611.
50. P. Feltham, C. J. Spears; Met. Sci. J., 1968, 2, p. 183.
51. N. Brown; Phil. Mag., 1959, 4, p. 693.
52. A. B. Greninger; Trans. A.I.M.M.E., 1938, 128, p. 369.
53. A. L. Titchener, W. G. Ferguson; J. Inst. Metals, 1971, 99, p. 345.
54. M. J. Marcinkowski, N. Brown; Acta Met., 1961, 9, p. 764.
55. M. J. Marcinkowski, H. Chessin; Phil. Mag., 1964, 10, p. 837.
56. N. J. Petch; J. Iron Steel Inst., 1953, 174, p. 25.
57. A. H. Cottrell; "Dislocations and Plastic Flow in Crystals", 1953, Clarendon Press, Oxford, p. 117.
58. M. F. Ashby; Phil. Mag., 1970, 21, p. 399.
59. G. C. Weatherly; Met. Sci. J., 1968, 2, p. 237.
60. L. M. Brown, G. R. Woolhouse, U. Valdr ; Phil. Mag., 1968, 17, p. 781.
61. M. F. Ashby, S. H. Gelles, L. E. Tanner; *ibid*, 1969, 19, p. 757.
62. F. J. Humphries, J. W. Martin; *ibid*, 1967, 16, p. 927.
63. P. B. Hirsch, F. J. Humphries; "Physics of Strength and Plasticity", ED. A. Argon, 1969, M.I.T. Press, Cambridge Mass.; Op.sit., Ashby, Ref. 60.
64. W. M. Stobbs, L. M. Brown; Proc. 4th European Reg. Conf. on Elec. Microscopy, 1968: Op. sit., Ashby, Ref. 60.
65. E. Orowan; Proc. Phys. Soc., 1940, 52, p. 8.
66. W. G. Johnston, J. J. Gilman; "Dislocations and Mechanical Properties of Crystals", 1957, ED. Fisher, John Wiley and Son Inc., New York. p. 116.
67. J. J. Gilman; "Mechanical Behavior of Materials at Elevated Temperatures", 1961, McGraw-Hill, New York, p. 17.
68. D. F. Stein; Scripta Met., 1969, 3, p. 423.
69. J. J. Gilman; Adv. in Mat. Res., 1968, 2, p. 17.

70. J. W. Christian; Scripta Met., 1970, 4, p. 803.
71. H. L. Prekel, H. Conrad; "Dislocation Dynamics", ED. A. R. Rosenfield, et.al., 1967, McGraw-Hill, New York, p. 431.
72. H. Mecking, K. Lücke; Scripta Met., 1970, 4, p. 427.
73. A. Seeger; "Dislocation Dynamics", ED. A. R. Rosenfield, et.al., 1967, McGraw-Hill, New York, p. 751.
74. K. H. Adams, T. Vreeland Jr., D. S. Wood; Mat. Sci. Eng., 1967, 2, p. 37.
75. J. J. Gilman; Adv. In Mat. Sci. Res., 1968, 2, p. 217.
76. H. W. Schadler; Acta Met., 1964, 12, p. 861.
77. E. O. Hall; "Yield Point Phenomena in Metals and Alloys", 1970, Plenum Press, New York, p. 7.
78. I. R. Kramer, R. Maddin; J. Metals, 1952, 4, p. 197.
79. W. Sylwestrowicz, E. O. Hall; Proc. Phys. Soc., 1951, B64, p. 495.
80. E. O. Hall; "Yield Point Phenomena in Metals and Alloys," 1970, Plenum Press, New York, p. 59.
81. U. Heubner, V. Schumacher; Z. Metallkunde, 1968, 59, p. 337: Op. cit. Ardley and Cottrell, Ref. 35.
82. C. F. Elam; Proc. R. Soc., 1936, A153, p. 273.
83. L. M. Clarebrough; Acta Met., 1957, 5, p. 413.
84. H. Green, N. Brown; J. Metals, 1953, 5, p. 1240.
85. T. L. Johnston, C. E. Feltner; Met. Trans., 1960, 1, p. 1161.
86. R. Armstrong, I. Codd, R. M. Douthwaite, N. J. Petch; Phil. Mag., 1962, 7, p. 45.
87. J. D. Eshelby, F. C. Frank, F. R. N. Nabarro; *ibid*, 1951, 42, p. 351.
88. C. Zener; Phys. Rev., 1946, 69, p. 128.
89. E. O. Hall; Proc. Phys. Soc., London, 1951, B64, p. 747.
90. H. Conrad; "Electron Microscopy and Strength of Crystals" Ed. G. Thomas, J. Washburn, 1963, John Wiley and Sons, New York, p. 299.
91. J. C. M. Li; Trans. TMS-AIME, 1963 227, p. 239.
92. G. I. Taylor; J. Inst. Metals, 1938, 62, p. 307.

93. D. McLean; "Grain Boundaries in Metals", 1957, Clarendon Press, Oxford, p. 157.
94. B. Chalmers; Proc. Roy. Soc., 1937, A162, p. 120.
95. R. Clark, B. Chalmers; Acta Met., 1954, 2, p. 80.
96. R. von Mises, Z. Angew; Math. Mech., 1928, 8, p. 161, Op. cit., Johnston and Feltner, Ref. 87.
97. U. F. Kochs; Acta Met., 1958, 6, p. 85.
98. A. K. Hingwe, K. N. Subramanian; Mich. State Univ., Private Communication.
99. R. Maddin; Trans. AIME, 1948, 175, p. 86.
100. A. Greninger; ibid, 1937, 124, p. 379.
101. B. J. Brindley, D. J. H. Corderoy, R. W. K. Honeycombe; Acta Met., 1962, 10, p. 1043.
102. J.J. Gilman and W.G. Johnston; J. Appl. Phys., 1960, 31, p. 632.
103. T.L. Johnston and C.E. Feltner; Met. Trans., 1970, 1, p. 1161.

APPENDIX A

Presented in this appendix are some representative electron micrographs taken using a Hitachi HU-11A Transmission Electron Microscope. After the initial stage of tensile testing the strain-rate specimens, formvar plastic single-stage replicas were taken on all four of the deformed surfaces on each specimen and were examined in the electron microscope at 50 KV.

This procedure was used to determine, as closely as possible, when the initiation of slip across the boundary into the beta phase took place, so that closely correlated stress and strain values for this occurrence could be obtained. As stated in the test results, all attempts to obtain single stage plastic replicas and two-stage shadowed, plastic-carbon replicas of the specimens in their heavily deformed condition, were unsuccessful.

The electron micrographs were useful for correlation of observations made using optical microscopy techniques, but they did not increase the quality of these observations.

Fig. 53 Transmission Electron Micrographs of Deformed Alpha-Beta Bicrystals.

- (a) A flat boundary specimen deformed using a cross-head speed of 0.2 cm/min. Observations and replica of the specimen made at stress - 6.1481 kilograms/mm²
strain - 24.81%

Note the cross-slip build-up at the boundary, and the slip lines continuing into the beta phase at an angle deviating from the slip line in alpha.

- (b) A corrugated boundary specimen deformed using a cross-head speed of 0.5 cm/min. Observations and replica of the specimen made at stress - 12.55 kilograms/mm²
strain - 81.3%

Note the slip in the alpha phase near an isolated beta phase area.

a



b

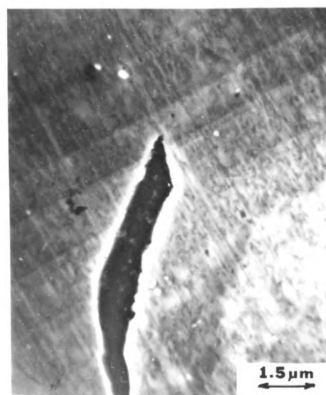


Fig. 53

2

MICHIGAN STATE UNIV. LIBRARIES



31293100923436